UNIVERSITÄT ROSTOCK

Faculty of Mechanical Engineering and Marine Technology
Chair of Modelling and Simulation

Lectures on ship manoeuvrability

Prof. Dr.-Ing. habil. Nikolai Kornev

Rostock
2013

Contents

List of Tables

List of Figures

Chapter 1

General differential equations of ship dynamics

Summary: The aim of this chapter is the derivation of the general body motion equations both in the inertial and body fixed referency system with and without principle axis. A special attention is paid to the forces and moments arising from acceleration through the water. They are expressed through the added mass using potential flow assumption.

1.1 Ship motion equations in the inertial reference system

The ship is assumed to be a rigid body with a constant mass m. The differential equations of the ship motion in the most general form are derived from the momentum theorem: *The rate of change of the momentum of a body is proportional to the resultant force acting on the body and is in the direction of that force.* Mathematically this theorem applied both for linear momentum and angular momentum can be expressed as

$$\begin{aligned} \frac{d}{dt}\vec{P} &= \vec{F}, \\ \frac{d}{dt}\vec{D} &= \vec{M} \end{aligned} \tag{1.1}$$

whereas $\frac{d}{dt}$ is the substantial time derivative, $\vec{P}$ and $\vec{D}$ are respectively linear and angular momentums of the ship, $\vec{F}$ and $\vec{M}$ are respectively total hydrodynamic force and total hydrodynamic torque acting on the ship. The equations (1.1) are written in the inertial system which is at the rest relatively to the earth (further referred as to the earth-fixed system). The forces acting on the ship comprise

- hydrostatic (buoyancy) forces,
- gravity forces,
- forces (thrust and transverse force) and moments supplied by the propulsion system,
- ship resistance including wave resistance and drag caused by viscosity,
- additional forces and moments caused by waves (wave-induced forces),
- control forces and moments exerted by rudders or other steering devices,
- transverse force, lift and corresponding moments caused by the viscosity,
- forces and moments caused by wind,
- forces and moments caused by currents,
- forces and moments arising from acceleration through the water (added mass).

(1.2)

The linear and angular momentums can be expressed through the kinetic energy of the rigid body by differentiation on velocity components:

$$\begin{aligned}\vec{P} =& \vec{i}\frac{\partial E_k}{\partial V_x} + \vec{j}\frac{\partial E_k}{\partial V_y} + \vec{k}\frac{\partial E_k}{\partial V_z},\\ \vec{D} =& \vec{i}\frac{\partial E_k}{\partial \omega_x} + \vec{j}\frac{\partial E_k}{\partial \omega_y} + \vec{k}\frac{\partial E_k}{\partial \omega_z}.\end{aligned} \tag{1.3}$$

where $\vec{V} = \vec{i}V_x + \vec{j}V_y + \vec{k}V_z$ and $\vec{\omega} = \vec{i}\omega_x + \vec{j}\omega_y + \vec{k}\omega_z$ are respectively linear and angular velocity of the origin. The kinetic energy of the body is obtained by the integration of the squared local velocity at each body point $\vec{r} = \vec{i}x + \vec{j}y + \vec{k}z$ multiplied with the elementary local mass dm:

$$2E_k = \int_m (\vec{V} + \vec{\omega} \times \vec{r})^2 dm = mV^2 + 2\vec{V}\int_m (\vec{\omega} \times \vec{r})dm + \int_m (\vec{\omega} \times \vec{r})^2 dm \tag{1.4}$$

Substituting the vector product

$$\vec{\omega} \times \vec{r} = \vec{i}(\omega_y z - \omega_z y) + \vec{j}(\omega_z x - \omega_x z) + \vec{k}(\omega_x y - \omega_y x) \tag{1.5}$$

into (1.4) one obtains

$$
\begin{aligned}
2E_k = (V_x^2 + &V_y^2 + V_z^2)m + \\
&2[V_x\omega_y \int\limits_m zdm - V_x\omega_z \int\limits_m ydm \\
&+V_y\omega_z \int\limits_m xdm - V_y\omega_x \int\limits_m zdm \\
&+V_z\omega_x \int\limits_m ydm - V_z\omega_y \int\limits_m xdm] \\
&\quad +\omega_y^2 \int\limits_m z^2dm - 2\omega_y\omega_z \int\limits_m yzdm + \omega_z^2 \int\limits_m y^2dm \\
&\quad +\omega_z^2 \int\limits_m x^2dm - 2\omega_z\omega_x \int\limits_m xzdm + \omega_x^2 \int\limits_m z^2dm \\
&\quad +\omega_x^2 \int\limits_m y^2dm - 2\omega_x\omega_y \int\limits_m xydm + \omega_y^2 \int\limits_m x^2dm
\end{aligned}
\tag{1.6}
$$

The coefficients $I_{xx} = \int\limits_m (y^2 + z^2)dm, I_{yy} = \int\limits_m (x^2 + z^2)dm$ and $I_{zz} = \int\limits_m (x^2 + y^2)dm$ are called the inertia moments , $I_{xy} = \int\limits_m xydm, I_{xz} = \int\limits_m xzdm$ and $I_{yz} = \int\limits_m yzdm$ are deviation moments or products of inertia, $S_x = \int\limits_m xdm, S_y = \int\limits_m ydm$ and $S_z = \int\limits_m zdm$ are static moments . With these designations the formula for the kinetic energy of the body takes the form:

$$
\begin{aligned}
&2E_k = ({V_x}^2 + {V_y}^2 + {V_z}^2)m \\
&+ 2[V_x\omega_y S_z - V_x\omega_z S_y + V_y\omega_z S_x - V_y\omega_x S_z + V_z\omega_x S_y - V_z\omega_y S_x] \\
&+ {\omega_x}^2 I_{xx} + {\omega_y}^2 I_{yy} + {\omega_z}^2 I_{zz} \\
&- 2\omega_x\omega_y I_{xy} - 2\omega_z\omega_x I_{xz} - 2\omega_y\omega_z I_{yz}
\end{aligned}
\tag{1.7}
$$

Substituting (1.7) into (1.3) and (1.1) one obtains the six coupled ordinary differential equations

$$
\begin{cases}
m\frac{dV_x}{dt} + S_z\frac{d\omega_y}{dt} - S_y\frac{d\omega_z}{dt} + \omega_y\frac{dS_z}{dt} - \omega_z\frac{dS_y}{dt} = F_x, \\
m\frac{dV_y}{dt} + S_x\frac{d\omega_z}{dt} - S_z\frac{d\omega_x}{dt} + \omega_z\frac{dS_x}{dt} - \omega_x\frac{dS_z}{dt} = F_y, \\
m\frac{dV_z}{dt} + S_y\frac{d\omega_x}{dt} - S_x\frac{d\omega_y}{dt} + \omega_x\frac{dS_y}{dt} - \omega_y\frac{dS_x}{dt} = F_z, \\
I_{xx}\frac{d\omega_x}{dt} + S_y\frac{dV_z}{dt} - S_z\frac{dV_y}{dt} - I_{xy}\frac{d\omega_y}{dt} - I_{xz}\frac{d\omega_z}{dt} + \\
\omega_x\frac{dI_{xx}}{dt} + V_z\frac{dS_y}{dt} - V_y\frac{dS_z}{dt} - \omega_y\frac{dI_{xy}}{dt} - \omega_z\frac{dI_{xz}}{dt} = M_x, \\
I_{yy}\frac{d\omega_y}{dt} + S_z\frac{dV_x}{dt} - S_x\frac{dV_z}{dt} - I_{xy}\frac{d\omega_x}{dt} - I_{yz}\frac{d\omega_z}{dt} + \\
\omega_y\frac{dI_{yy}}{dt} + V_x\frac{dS_z}{dt} - V_z\frac{dS_x}{dt} - \omega_x\frac{dI_{xy}}{dt} - \omega_z\frac{dI_{yz}}{dt} = M_y, \\
I_{zz}\frac{d\omega_z}{dt} + S_x\frac{dV_y}{dt} - S_y\frac{dV_x}{dt} - I_{xz}\frac{d\omega_x}{dt} - I_{yz}\frac{d\omega_y}{dt} + \\
\omega_z\frac{dI_{zz}}{dt} + V_y\frac{dS_x}{dt} - V_x\frac{dS_y}{dt} - \omega_x\frac{dI_{xz}}{dt} - \omega_y\frac{dI_{yz}}{dt} = M_z.
\end{cases}
\tag{1.8}
$$

The system (1.8) is the general system describing the six degree of freedom (6DOF) motion of the ship in earth connected reference system.

1.2 Ship motion equations in the ship-fixed reference system

The ship motion is sufficiently simplified when instead of the earth-fixed reference system the ship fixed reference system is used. The origin of the ship fixed reference system is moving with velocities $\vec{V} = \vec{i}V_x + \vec{j}V_y + \vec{k}V_z$ and $\vec{\omega} = \vec{i}\omega_x + \vec{j}\omega_y + \vec{k}\omega_z$. Advantage of the ship-fixed coordinates is that the inertia moments, products of inertia and static moments are constant in time, i.e. $dI_{ij}/dt = 0, dS_i/dt = 0$.

To rewrite the equations (1.1) in the ship-fixed reference system it is necessary to establish the relation between the linear and angular momentums written in different reference systems. This relation is found under condition that vectors of the linear and angular momentums are kept constant in the ship-fixed reference system.

Following to [21] let us consider consequently the translation with velocity $\vec{V} = \vec{i}V_x + \vec{j}V_y + \vec{k}V_z$ and rotation with angular velocity $\vec{\omega} = \vec{i}\omega_x + \vec{j}\omega_y + \vec{k}\omega_z$. At the time instant t both systems are coincided. At the time $t + \Delta t$ the body is located at the point $\vec{V}\Delta t$. Vectors $\vec{P}$ and $\vec{D}$ are also shifted from the point O to the point O' (see Figure 1.1).
As seen in Figure 1.1 the linear momentum vector transferred by the ship is not changed in the earth fixed system due to translation $\vec{P}_a(t+\Delta t) = \vec{P}_a(t) =$

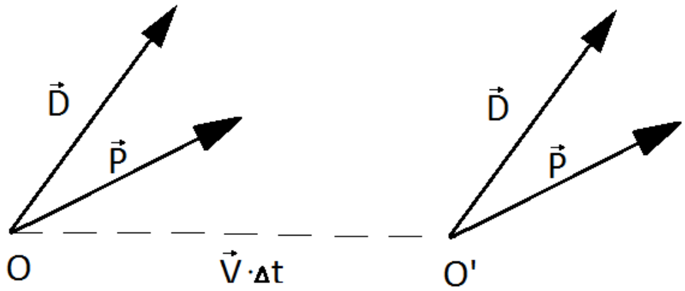

Figure 1.1: Change of the linear and angular momentums due to displacement of the origin of the ship fixed reference system from the point to the point.

$\vec{P}$. The angular momentum is changed due to change of the arm of the linear momentum $\vec{D}_a(t+\Delta t) = \vec{D}_a(t) + (\vec{V}\Delta t) \times \vec{P} = \vec{D} + (\vec{V} \times \vec{P})\Delta t$. Therefore, the contribution to rate of change of the momentums due to translation is:

$$\frac{d\vec{P}_{a\_tr}}{dt} = 0, \frac{d\vec{D}_{a\_tr}}{dt} = \vec{V} \times \vec{P} \tag{1.9}$$

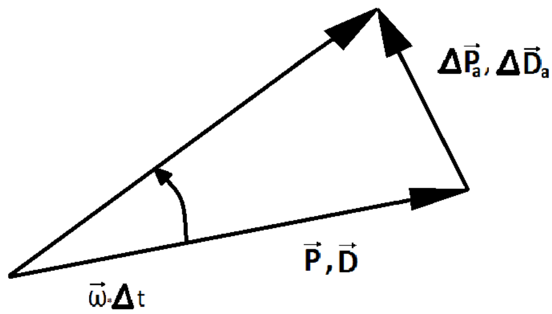

Figure 1.2: Change of the linear and angular momentums due to rotation at the angle $\vec{\omega}\Delta t$

In the second step, the momentums vectors are turned during the rotation of the ship fixed reference system with the angular velocity $\vec{\omega} = \vec{i}\omega_x + \vec{j}\omega_y + \vec{k}\omega_z$. The magnitudes of both vectors remain constant. Their change in the earth fixed system occurring in time Δt is

$$\vec{P}_a(t+\Delta t) = \vec{P}_a(t) + \Delta\vec{P}_a = \vec{P} + (\vec{\omega} \times \vec{P})\Delta t,$$
$$\vec{D}_a(t+\Delta t) = \vec{D}_a(t) + \Delta\vec{D}_a = \vec{D} + (\vec{\omega} \times \vec{D})\Delta t.$$

Therefore, the contribution to the rate of change of the momentums due to rotation is:

$$\frac{d\vec{P}_{a\_rot}}{dt} = \vec{\omega} \times \vec{P}, \frac{d\vec{D}_{a\_rot}}{dt} = \vec{\omega} \times \vec{D}. \tag{1.10}$$

Taking (1.9) and (1.10) into account the momentum theorem in ship fixed reference system is written in the form:

$$\begin{aligned} &\frac{d}{dt}\vec{P} + \vec{\omega} \times \vec{P} = \vec{F} \\ &\frac{d}{dt}\vec{D} + \vec{V} \times \vec{P} + \vec{\omega} \times \vec{D} = \vec{M} \end{aligned} \tag{1.11}$$

Here it should be noted that the forces $\vec{F}$ and moments $\vec{M}$ have to be determined also in the moving reference system. The second term in the first equation and second and third terms in the second equation describe the change of the linear and angular momentums due to translation and rotation of the ship fixed reference system. The right sides are responsible for momentum changes due to external forces.

The equations (1.11) were derived by Kirchhoff in 1869 .

The ship fixed reference system is the Cartesian right- handed coordinate system (xyz) with x and y lying in a horizontal plane and z vertical, positive upward. The x axis is the longitudinal coordinate, positive forward, y is the transverse coordinate, positive to the port side. The origin is in the plane of symmetry. The vertical location of the origin lies at the level of the undisturbed free surface when the ship is at the rest.

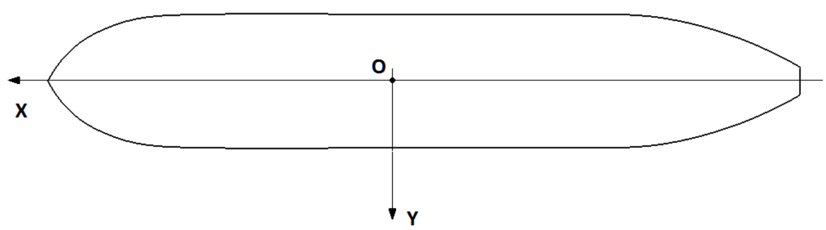

Figure 1.3: Sketch of the ship fixed coordinate system.

The ship mass distribution is symmetrical with respect to the plane xz. Therefore, the products of inertia I_{xy} and I_{yz} as well as the static moment

S_y are zero in the ship fixed system. This is the second advantage of the ship-fixed coordinates. Also, the third product I_{xz} is often assumed to be zero. With these simplifications the vector components are:

$$\begin{aligned}
&P_x = mV_x + \omega_y S_z, P_y = mV_y + \omega_z S_x - \omega_x S_z, P_z = mV_z - \omega_y S_x,\\
&D_x = \omega_x I_{xx} - V_y S_z - \omega_z I_{xz}, D_y = \omega_y I_{yy} + V_x S_z - V_z S_x,\\
&D_z = \omega_z I_{zz} + V_y S_x - \omega_x I_{xz}.
\end{aligned} \tag{1.12}$$

Substituting (1.12) into (1.11) results in the general system describing the six degree of freedom (6DOF) motion of the ship in the ship-fixed reference system:

$$\begin{cases}
m\frac{dV_x}{dt} + S_z\frac{d\omega_y}{dt} + \omega_y(mV_z - \omega_y S_x) - \omega_z(mV_y + \omega_z S_x - \omega_x S_z) = F_x,\\
m\frac{dV_y}{dt} + S_x\frac{d\omega_z}{dt} - S_z\frac{d\omega_x}{dt} + \omega_z(mV_x + \omega_y S_z) - \omega_x(mV_z - \omega_y S_x) = F_y,\\
m\frac{dV_z}{dt} - S_x\frac{d\omega_y}{dt} + \omega_x(mV_y + \omega_z S_x - \omega_x S_z) - \omega_y(mV_x + \omega_y S_z) = F_z,\\
I_{xx}\frac{d\omega_x}{dt} - S_z\frac{dV_y}{dt} - I_{xz}\frac{d\omega_z}{dt} - V_y\omega_y S_x - V_z(\omega_z S_x - \omega_x S_z) +\\
\omega_y(\omega_z I_{zz} + V_y S_x - \omega_x I_{xz}) - \omega_z(\omega_y I_{yy} + V_x S_z - V_z S_x) = M_x,\\
I_{yy}\frac{d\omega_y}{dt} + S_z\frac{dV_x}{dt} - S_x\frac{dV_z}{dt} + V_z\omega_y S_z + V_x\omega_y S_x +\\
\omega_z(\omega_x I_{xx} - V_y S_z - \omega_z I_{xz}) - \omega_x(\omega_z I_{zz} + V_y S_x - \omega_x I_{xz}) = M_y,\\
I_{zz}\frac{d\omega_z}{dt} + S_x\frac{dV_y}{dt} - I_{xz}\frac{d\omega_x}{dt} + V_x(\omega_z S_x - \omega_x S_z) - V_y\omega_y S_z +\\
\omega_x(\omega_y I_{yy} + V_x S_z - V_z S_x) - \omega_y(\omega_x I_{xx} - V_y S_z - \omega_z I_{xz}) = M_z.
\end{cases} \tag{1.13}$$

This system is integrated numerically using modern numerical 6DOF solvers (CFX, STAR CCM+, OpenFoam). In this case the hydrodynamic forces are calculated by direct integration of normal and shear stresses over the ship surface without the subdivision according to physical nature of forces (1.2).

1.3 Ship motion equations in the ship-fixed coordinates with principle axes

The principle axes coordinate system is chosen from the condition that all off-diagonal elements of the inertia matrix (products of inertia)

$$\begin{pmatrix} I_{xx} & I_{xy} & I_{xz}\\ I_{xy} & I_{yy} & I_{yz}\\ I_{xz} & I_{yz} & I_{zz} \end{pmatrix}$$

and the static moments are zero, i.e.,

$$I_{xy} = I_{xz} = I_{yz} = 0 \tag{1.14}$$

$$S_x = S_y = S_z = 0. \tag{1.15}$$

The conditions (1.14) and (1.15) can be satisfied by a special choice of the location of the origin and a special direction of the coordinate system axes. A sample of such a system for the case of manoeuvring will be shown later.

In the principle axes system the ship motion equations take the form:

$$\begin{cases} m(\frac{dV_x}{dt} + V_z\omega_y - V_y\omega_z) = F_x, \\ m(\frac{dV_y}{dt} + V_x\omega_z - V_z\omega_x) = F_y, \\ m(\frac{dV_z}{dt} + V_y\omega_x - V_x\omega_y) = F_z, \\ I_{xx}\frac{d\omega_x}{dt} + \omega_y\omega_z(I_{zz} - I_{yy}) = M_x, \\ I_{yy}\frac{d\omega_y}{dt} + \omega_x\omega_z(I_{xx} - I_{zz}) = M_y, \\ I_{zz}\frac{d\omega_z}{dt} + \omega_x\omega_y(I_{yy} - I_{xx}) = M_z. \end{cases} \tag{1.16}$$

The forces $\vec{F}$ and moments $\vec{M}$ have to be determined in the moving principle axes coordinate system.

1.4 Forces and moments arising from acceleration through the water

The physical nature of the forces and moments arising from acceleration through the water is the inertia of the medium which the body is moving in. Traditionally these forces are determined using the irrotational inviscid fluid model. This model is described in details in [23], Chapters 1, 2 and 3. For students who did not attend in the lecture course on Fluid Dynamics we give overview of basic principles of the theory of flows in the Appendix A.

1.4.1 Kinetic energy of the fluid surrounding the body

If the flow is incompressible, inviscid and irrotational ($\nabla \times \vec{V} = 0$) the kinetic energy of the fluid surrounding the moving body is

$$E_{Fl} = \frac{1}{2}\sum_{i=1}^{6}\sum_{k=1}^{6} V_i V_k m_{ik} \tag{1.17}$$

where $V_1 = V_x, V_2 = V_y, V_3 = V_z, V_4 = \omega_x, V_5 = \omega_y, V_6 = \omega_z$ are components of linear and angular velocities, whereas mik are added mass. Generally, the body has 36 added mass

$$\begin{vmatrix} m_{11} & m_{12} & m_{13} & m_{14} & m_{15} & m_{16} \\ m_{21} & m_{22} & m_{23} & m_{24} & m_{25} & m_{26} \\ m_{31} & m_{32} & m_{33} & m_{34} & m_{35} & m_{36} \\ m_{41} & m_{42} & m_{43} & m_{44} & m_{45} & m_{46} \\ m_{51} & m_{52} & m_{53} & m_{54} & m_{55} & m_{56} \\ m_{61} & m_{62} & m_{63} & m_{64} & m_{65} & m_{66} \end{vmatrix} \tag{1.18}$$

Due to symmetry condition $m_{ik} = m_{ki}$ the number of unknown mass is 21[1]. The added mass are determined from the formulae (see [23]):

$$m_{ik} = -\rho \oint_S \varphi_i \frac{\partial \varphi_k}{\partial n} dS \tag{1.19}$$

where S is the wetted ship area, ρ is the density, φ_i are potentials of the flow when the ship is moved in i-th direction with unit speed. The potentials φ_i satisfy the Laplace equation

$$\frac{\partial^2 \varphi_i}{\partial x^2} + \frac{\partial^2 \varphi_i}{\partial y^2} + \frac{\partial^2 \varphi_i}{\partial z^2} = 0 \tag{1.20}$$

the boundary condition of the decay of perturbations far from the moving body

$$\nabla \varphi_i \xrightarrow[r \to \infty]{} 0 \tag{1.21}$$

and no penetration boundary condition at each point (x,y,z) on the ship surface

$$\left.\begin{aligned} &\frac{\partial \varphi_1}{\partial n} = \cos(n, x); \\ &\frac{\partial \varphi_2}{\partial n} = \cos(n, y); \frac{\partial \varphi_3}{\partial n} = \cos(n, z); \\ &\frac{\partial \varphi_4}{\partial n} = y \cos(n, z) - z \cos(n, y); \\ &\frac{\partial \varphi_5}{\partial n} = z \cos(n, x) - x \cos(n, z); \\ &\frac{\partial \varphi_6}{\partial n} = x \cos(n, y) - y \cos(n, x). \end{aligned}\right\} \tag{1.22}$$

Here $\vec{n}$ is the normal vector to the ship surface at the point (x,y,z), $\cos(n, x) = \vec{n}\vec{i}, \cos(n, y) = \vec{n}\vec{j}, \cos(n, z) = \vec{n}\vec{k}$. When the ship moves arbitrarily the po-

[1] if the body is far from the flow boundaries

tential of the flow is the sum of particular potentials multiplied with corresponding components of linear and angular velocities:

$$\varphi = \sum_{k=1}^{6} V_k \varphi_k \tag{1.23}$$

1.4.2 Momentum of the fluid surrounding the body

Let us consider the amount of fluid between the surfaces S (wetted ship surface) and $\sum$ which is located far from the ship. The momentum of this fluid is

$$\vec{P}_{Fl} = \rho \int_U \vec{V} dU = \rho \int_U grad\varphi dU \tag{1.24}$$

According to the Gauss theorem

$$\vec{P}_{Fl} = \rho \int_U \vec{V} dU = \rho \int_U grad\varphi dU = \rho \int_\Sigma \varphi \vec{n} dS - \rho \int_S \varphi \vec{n} dS \tag{1.25}$$

Let us $\vec{F}_h$ and $\vec{F}_h'$ are respectively the forces acting on the surface S and $\sum$:

$$\vec{F}_h = -\int_S p\vec{n} dS \tag{1.26}$$

$$\vec{F}_h' = -\int_\Sigma p\vec{n} dS \tag{1.27}$$

Since the shear stresses are zero in the inviscid fluid, only normal stresses are present in formulae (1.26) and (1.27).
From the momentum theorem follows:

$$(\vec{F}_h' - \vec{F}_h)dt = d\vec{P}_{Fl} \tag{1.28}$$

The temporal change of the momentum reads:

$$d\vec{P}_{Fl} = d\int_\Sigma \rho\varphi\vec{n} dS - d\int_S \rho\varphi\vec{n} dS + \int_\Sigma \rho\vec{V}(\vec{V}\vec{n}) dS dt \tag{1.29}$$

The last term considers the fact that a part of the momentum $\rho\vec{V}(\vec{V}\vec{n})dSdt$ is transported from the fluid volume U through the surface $\sum$ by the mass

$\rho(\vec{V}\vec{n})dSdt$. From (1.29) follows:

$$\vec{F}'_h - \vec{F}_h = \frac{d\vec{P}_{Fl}}{dt} = \frac{d}{dt}\int\limits_{\Sigma} \rho\varphi\vec{n}dS - \frac{d}{dt}\int\limits_{S} \rho\varphi\vec{n}dS + \int\limits_{\Sigma} \rho\vec{V}(\vec{V}\vec{n})dS \qquad (1.30)$$

Since the surface $\sum$ is motionless the integral and differentiation are commutative operators:

$$\frac{d}{dt}\int\limits_{\Sigma} \varphi\vec{n}dS = \int\limits_{\Sigma} \frac{\partial\varphi}{\partial t}\vec{n}dS \qquad (1.31)$$

The pressure in inviscid irrotational fluid is determined from the general Bernoulli equation :

$$p = p_0 - \rho\frac{\partial\varphi}{\partial t} - \rho\frac{V^2}{2} \qquad (1.32)$$

Substitution of (1.32) into (1.27) brings:

$$\vec{F}'_h = -\int\limits_{\Sigma} p\vec{n}dS = -\int\limits_{\Sigma} \left(p_0 - \rho\frac{\partial\varphi}{\partial t} - \rho\frac{V^2}{2}\right)\vec{n}dS = \rho\int\limits_{\Sigma} \left(\frac{\partial\varphi}{\partial t} + \frac{V^2}{2}\right)\vec{n}dS \qquad (1.33)$$

With consideration of (1.31) and (1.33) the force acting on the surface S can be expressed from (1.30) in the following form

$$\begin{aligned}
\vec{F}_h &= -\frac{d}{dt}\int\limits_{\Sigma} \rho\varphi\vec{n}dS + \frac{d}{dt}\int\limits_{S} \rho\varphi\vec{n}dS - \int\limits_{\Sigma} \rho\vec{V}(\vec{V}\vec{n})dS + \vec{F}'_h = \\
&= -\frac{d}{dt}\int\limits_{\Sigma} \rho\varphi\vec{n}dS + \frac{d}{dt}\int\limits_{S} \rho\varphi\vec{n}dS - \int\limits_{\Sigma} \rho\vec{V}(\vec{V}\vec{n})dS + \rho\int\limits_{\Sigma} \left(\frac{\partial\varphi}{\partial t} + \frac{V^2}{2}\right)\vec{n}dS = \\
&= \frac{d}{dt}\int\limits_{S} \rho\varphi\vec{n}dS + \rho\int\limits_{\Sigma} \left(\frac{V^2}{2}\vec{n} - \vec{V}(\vec{V}\vec{n})\right)dS
\end{aligned} \qquad (1.34)$$

We choose the surface $\sum$ located very far from the body. All perturbations decay according to the condition (1.21) so quickly that the last integral in (1.34) is zero. Therefore, we have

$$\vec{F}_h = -\frac{d\vec{P}_{Fl}}{dt} = \frac{d}{dt}\int\limits_{S} \rho\varphi\vec{n}dS, \qquad (1.35)$$

where $\vec{P}_{Fl} = -\int\limits_S \rho\varphi\vec{n}dS$ is the linear momentum of the fluid. The components of the force are (see formulae (1.22) and (1.23))

$$\begin{aligned}
F_{hx} &= \frac{d}{dt}\int\limits_S \rho\varphi n_x dS = \frac{d}{dt}\int\limits_S \rho\varphi\cos(nx)dS = \frac{d}{dt}\int\limits_S \rho\sum_{k=1}^{6} V_k\varphi_k\frac{\partial\varphi_l}{\partial x}dS = \\
&\frac{d}{dt}\sum_{k=1}^{6}\rho\int\limits_S \varphi_k\frac{\partial\varphi_l}{\partial x}dS = -\frac{d}{dt}\sum_{k=1}^{6} m_{lk}V_k = -\frac{d}{dt}P_{Flx} \\
F_{hy} &= \frac{d}{dt}\int\limits_S \rho\varphi n_y dS = \frac{d}{dt}\int\limits_S \rho\varphi\cos(ny)dS = -\frac{d}{dt}\sum_{k=1}^{6} m_{2k}V_k = -\frac{d}{dt}P_{Fly} \\
F_{hz} &= \frac{d}{dt}\int\limits_S \rho\varphi n_z dS = \frac{d}{dt}\int\limits_S \rho\varphi\cos(nz)dS = -\frac{d}{dt}\sum_{k=1}^{6} m_{3k}V_k = -\frac{d}{dt}P_{Flz}
\end{aligned} \tag{1.36}$$

Similarly, the moment arising from acceleration through the water can be expressed through the angular momentum derivative:

$$\vec{M}_h = -\frac{d\vec{D}_{Fl}}{dt} = \frac{d}{dt}\int\limits_S \rho\varphi(\vec{r}\times\vec{n})dS \tag{1.37}$$

where $\vec{D}_{Fl} = -\int\limits_S \rho\varphi(\vec{r}\times\vec{n})dS$ is the angular momentum of the fluid. The components of moments are (see formulae (1.22) and (1.23)).

$$\begin{aligned}
M_{hx} &= \frac{d}{dt}\int\limits_S \rho\varphi(\vec{r}\times\vec{n})_x dS = \frac{d}{dt}\rho\int\limits_S \varphi(y\cos(nz) \\
&\quad - z\cos(ny))dS = -\frac{d}{dt}\sum_{k=1}^{6} m_{4k}V_k = -\frac{d}{dt}D_{Flx}, \\
M_{hy} &= \frac{d}{dt}\int\limits_S \rho\varphi(\vec{r}\times\vec{n})_y dS = \frac{d}{dt}\rho\int\limits_S \varphi(z\cos(nx) \\
&\quad - x\cos(nz))dS = -\frac{d}{dt}\sum_{k=1}^{6} m_{5k}V_k = -\frac{d}{dt}D_{Fly}, \\
M_{hz} &= \frac{d}{dt}\int\limits_S \rho\varphi(\vec{r}\times\vec{n})_z dS = \frac{d}{dt}\rho\int\limits_S \varphi(x\cos(ny) \\
&\quad - y\cos(nx))dS = -\frac{d}{dt}\sum_{k=1}^{6} m_{6k}V_k = -\frac{d}{dt}D_{Flz}.
\end{aligned} \tag{1.38}$$

The relation between the linear and angular momentums of the fluid and the kinetic energy can be found from formulae (1.36), (1.38) and (1.17).

$$\begin{aligned}\vec{P}_{Fl} =& \vec{i}\frac{\partial E_{Fl}}{\partial V_x} + \vec{j}\frac{\partial E_{Fl}}{\partial V_y} + \vec{k}\frac{\partial E_{Fl}}{\partial V_z},\\ \vec{D}_{Fl} =& \vec{i}\frac{\partial E_{Fl}}{\partial \omega_x} + \vec{j}\frac{\partial E_{Fl}}{\partial \omega_y} + \vec{k}\frac{\partial E_{Fl}}{\partial \omega_z}.\end{aligned} \tag{1.39}$$

This relation has exactly the same form as the relation between linear and angular momentums and kinetic energy of solid body (1.3).

1.4.3 Ship motion equations in the inertial reference system

The ship motion equations in the earth-fixed system (1.1) are rewritten in the form

$$\begin{aligned}&\frac{d}{dt}(\vec{P} + \vec{P}_{Fl}) = \vec{F}\\ &\frac{d}{dt}(\vec{D} + \vec{D}_{Fl}) = \vec{M}\end{aligned} \tag{1.40}$$

Where, in contrast to (1.1), the forces $\vec{F}$ and moments $\vec{M}$ don't account for forces and moments arising from acceleration through the water.

1.4.4 Ship motion equations in the ship-fixed reference system

$$\begin{aligned}&\frac{d}{dt}(\vec{P} + \vec{P}_{Fl}) + \vec{\omega} \times (\vec{P} + \vec{P}_{Fl}) = \vec{F}\\ &\frac{d}{dt}(\vec{D} + \vec{D}_{Fl}) + \vec{V} \times (\vec{P} + \vec{P}_{Fl}) + \vec{\omega} \times (\vec{D} + \vec{D}_{Fl}) = \vec{M}\end{aligned} \tag{1.41}$$

where the forces and moments don't account for forces and moments arising from acceleration through the water, since they are explicitly considered on the left hand side of the equation by terms with $\vec{P}_{Fl}$ and $\vec{D}_{Fl}$.
Substitution of (1.36) and (1.38) into (1.41) results in the following change

of equations (1.13)

$$
\begin{cases}
m\frac{dV_x}{dt}+S_z\frac{d\omega_y}{dt}+\omega_y(mV_z-\omega_yS_x)-\omega_z(mV_y+\omega_zS_x-\omega_xS_z)+\frac{d}{dt}\sum\limits_{k=1}^{6}m_{1k}V_k\\
\qquad+\omega_y\sum\limits_{k=1}^{6}m_{3k}V_k-\omega_z\sum\limits_{k=1}^{6}m_{2k}V_k=F_x,\\
m\frac{dV_y}{dt}+S_x\frac{d\omega_z}{dt}-S_z\frac{d\omega_x}{dt}+\omega_z(mV_x+\omega_yS_z)-\omega_x(mV_z-\omega_yS_x)+\frac{d}{dt}\sum\limits_{k=1}^{6}m_{2k}V_k\\
\qquad+\omega_z\sum\limits_{k=1}^{6}m_{1k}V_k-\omega_x\sum\limits_{k=1}m_{3k}V_k=F_y,\\
m\frac{dV_z}{dt}-S_x\frac{d\omega_y}{dt}+\omega_x(mV_y+\omega_zS_x-\omega_xS_z)-\omega_y(mV_x+\omega_yS_z)+\frac{d}{dt}\sum\limits_{k=1}^{6}m_{3k}V_k\\
\qquad+\omega_x\sum\limits_{k=1}^{6}m_{2k}V_k-\omega_y\sum\limits_{k=1}^{6}m_{1k}V_k=F_z,\\
\\
I_{xx}\frac{d\omega_x}{dt}-S_z\frac{dV_y}{dt}-I_{xz}\frac{d\omega_z}{dt}-V_y\omega_yS_x-V_z(\omega_zS_x-\omega_xS_z)+\\
\quad+\omega_y(\omega_zI_{zz}+V_yS_x-\omega_xI_{xz})-\omega_z(\omega_yI_{yy}+V_xS_z-V_zS_x)+\frac{d}{dt}\sum\limits_{k=1}^{6}m_{4k}V_k+\\
\quad+V_y\sum\limits_{k=1}^{6}m_{3k}V_k-V_z\sum\limits_{k=1}^{6}m_{2k}V_k+\omega_y\sum\limits_{k=1}^{6}m_{6k}V_k-\omega_z\sum\limits_{k=1}^{6}m_{5k}V_k=M_x,\\
\\
I_{yy}\frac{d\omega_y}{dt}+S_z\frac{dV_x}{dt}-S_x\frac{dV_z}{dt}+V_z\omega_yS_z+V_x\omega_yS_x+\omega_z\left(\omega_xI_{xx}-V_yS_z-\right.\\
\quad\left.-\,\omega_zI_{xz}\right)-\omega_x(\omega_zI_{zz}+V_yS_x-\omega_xI_{xz})+\frac{d}{dt}\sum\limits_{k=}^{6}m_{5k}V_k+V_z\sum\limits_{k=1}^{6}m_{1k}V_k-\\
\quad-V_x\sum\limits_{k=1}^{6}m_{3k}V_k+\omega_z\sum\limits_{k=1}^{6}m_{4k}V_k-\omega_x\sum\limits_{k=1}^{6}m_{6k}V_k=M_y,\\
\\
I_{zz}\frac{d\omega_z}{dt}+S_x\frac{dV_y}{dt}-I_{xx}\frac{d\omega_x}{dt}+V_x(\omega_zS_x-\omega_xS_z)-V_y\omega_yS_z+\omega_x\left(\omega_yI_{yy}+V_xS_z-\right.\\
\quad\left.-\,V_zS_x\right)-\omega_y(\omega_xI_{xx}-V_yS_z-\omega_zI_{xz})+\frac{d}{dt}\sum\limits_{k=1}^{6}m_{6k}V_k+V_x\sum\limits_{k=1}^{6}m_{2k}V_k-\\
\quad-V_y\sum\limits_{k=1}^{6}m_{1k}V_k+\omega_x\sum\limits_{k=1}^{6}m_{5k}V_k-\omega_y\sum\limits_{k=1}^{6}m_{4k}V_k=M_z.
\end{cases}
\tag{1.42}
$$

1.4.5 Ship motion equations in the ship-fixed reference system along the x-axis

The system (1.42) takes the simplest form for the case of the straight ship motion along the x-axis ($V_y = V_z = \omega_x = \omega_y = \omega_z = 0$):

$$(m + m_{11})\frac{dV_x}{dt} = F_x \tag{1.43}$$

As seen the fluid inertia results in the increase of the real mass m by the additional virtual mass m_{11}. The total mass is becoming larger due to inertia of the fluid. That is why the mass m_{11} is called as the additional or hydrodynamic mass. The effect of the fluid inertia makes the ship motion milder, i.e.

$$m\frac{dV_x}{dt} = F_x - m_{11}\frac{dV_x}{dt} \tag{1.44}$$

If the ship speed is growing $\frac{dV_x}{dt} > 0$ the fluid inertia effect decelerates the ship motion and, vice versa, if the ship speed becomes smaller $\frac{dV_x}{dt} < 0$ the fluid inertia effect accelerates the ship motion.

1.5 Exercises

1. **Equations of ship manoeuvring.**
   The ship manoeuvring theory is based on the following assumptions:

   - the ship motion is occurred only in the horizontal plane xy. Heave velocity, rolling and pitching are neglected ($V_z = 0, \omega_x = \omega_y = 0$).
   - The Froude number is small and the free surface deformation is neglected. The mirror principle is used to model the free surface effect. Hydrodynamically the ship is considered as a doubled body.

   Let us derive the equations of ship manoeuvring.

2. **Equations of ellipsoid motion in the vertical plane.**
   Derive the equations of ellipsoid motion in the vertical plane.

3. **Equations of rolling ellipsoid in longitudinal direction.**
   Derive the equations of ellipsoid motion when it rotates about the longitudinal axis and moves in longitudinal direction.

Chapter 2

Equations of ship manoeuvring with three degree of freedom

Summary: In this chapter we derive the equations of ship motion in the horizontal plane with three degree of freedom, the so called ship manoeuvring equations. The equations are presented both in dimensional and dimensionless forms. The Munk moment is introduced.

2.1 Coordinate system

The coordinate system used in ship manoeuvring is shown in Figure 2.1. The designations are

x_0, y_0	Coordinates in the inertial coordinate system,
x, y	Coordinates in ship-fixed coordinate system,
$V = \sqrt{V_x^2 + V_y^2}$	Ship speed,
β	Drift angle , positive if the flow incomes from the starboard side,
ψ	Heading angle , positive if the yawing against clockwise direction,
δ_R	Rudder angle , positive if the rudder causes increase of the heading angle.

2.2 Aims of the ship manoeuvring theory

The ship manoeuvring theory is intended to investigate the ability of ship:

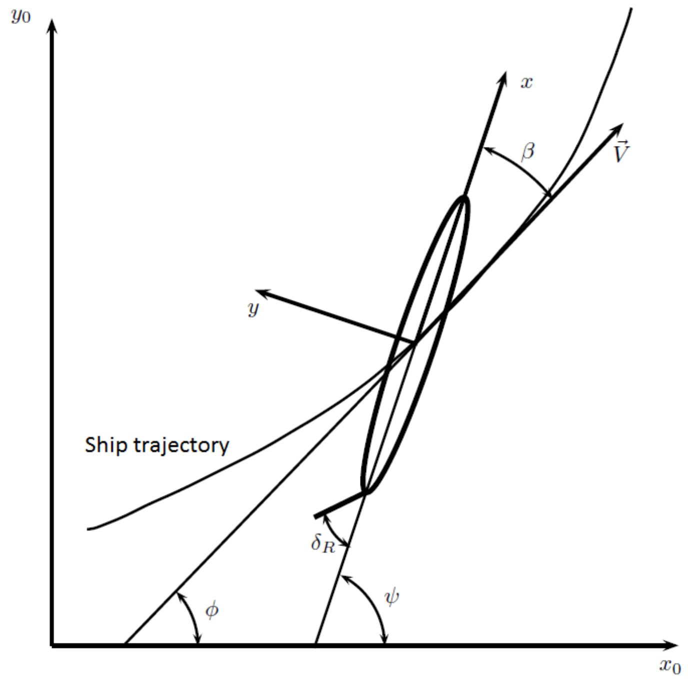

Figure 2.1: Coordinate system used in ship manoeuvring

- to keep the prescribed course,
- to change the course following a prescribed trajectory and to avoid obstacles,
- to change the speed.

Important questions for the specification of ship manoeuvrability may include [9]:

- Does the ship keep a reasonably straight course (in autopilot or manual mode),
- under what conditions (current, wind) can the ship berth without tug assistance?
- Up to what ratio of wind speed to ship speed can the ship still be kept on all courses?
- Can the ship lay rudder in acceptable time from one side to the other?

The characteristics usually used to regulate the manoeuvrability are discussed in the next sections.

2.3 Main assumptions of the theory

The ship manoeuvring theory is based on the following assumptions:

- The ship motion is occurred only in the horizontal plane xy. Heave velocity, rolling and pitching are neglected ($V_z = 0, \omega_x = \omega_y = 0$).
- The Froude number is small and the free surface deformation is neglected. The mirror principle (see Appendix B) is used to model the free surface effect. Hydrodynamically the ship is considered as a doubled body without any flow boundaries except the ship.

The doubled body has two symmetry planes that is why the ship has only eight added mass: $m_{11}, m_{22}, m_{33}, m_{44}, m_{55}, m_{66}, m_{26}, m_{35}$. The static moment of the doubled body and the product of inertia are zero, i.e. $S_z = 0$ and $I_{xz} = 0$. The system (1.42) is reduced to:

$$\begin{cases} (m + m_{11})\frac{dV_x}{dt} - (m + m_{22})V_y\omega_z - \omega_z^2(m_{26} + S_x) = F_x, \\ \\ (m + m_{22})\frac{dV_y}{dt} + (m + m_{11})V_x\omega_z + (m_{26} + S_x)\frac{d\omega_z}{dt} = F_y, \\ \\ (I_{zz} + m_{66})\frac{d\omega_z}{dt} + V_xV_y(m_{22} - m_{11}) + (m_{26} + S_x)(\frac{dV_y}{dt} + V_x\omega_z) = M_z. \end{cases} \tag{2.1}$$

2.4 Equations in the ship-fixed coordinates with principle axes

The principle axes coordinate system was chosen in Section 1.3 from the condition that all off-diagonal elements of the products of inertia and the static moments of body are zero. It simplifies the equation system. However, many terms proportional to off-diagonal elements of the added mass matrix remain. For example, the system (2.1) contains terms with m_{26}. The motion equations have the simplest form if the axes are principle axes of the $\underline{coupled\ system"body + fluid"}$. The system with principle axes can easily be found for the doubled body moving in the horizontal plane from the following conditions:

- the x axis is along the longitudinal axis of the doubled body,
- the xy and xz are symmetry planes,
- the position of the origin is found from the formula

$$m_{26} + S_x = 0 \tag{2.2}$$

Remember that the origin in the equation (1.67) was chosen from the condition that only body static moment is zero $S_x = 0$

Let us consider the sum $m_{26} + S_x = -\rho \int\limits_s \varphi_2(x\cos(n,y) - y\cos(n,x))dS + \int\limits_m xdm$. The ship can be considered as a slender body . The normal vector to the slender body has the following asymptotic estimations which are valid on the most part of the ship length:

$$\begin{aligned} x/L &\sim 0(1), \\ y/L &\sim 0(\epsilon), \\ \cos(n,x) &\sim 0(\epsilon), \\ \cos(n,y) &\sim 0(1), \\ \varphi_2 &\sim 0(1). \end{aligned} \tag{2.3}$$

where ϵ is a small parameter.
Therefore, the asymptotic estimation for the sum $m_{26} + S_x$ for the slender body reads

$$\begin{aligned} m_{26} + S_x =& -\rho \int\limits_S \varphi_2(x\cos(n,y) - y\cos(n,x))dS + \int\limits_m xdm \\ \approx& -\rho \int\limits_S \varphi_2 x\cos(n,y)dS + \int\limits_m xdm \end{aligned} \tag{2.4}$$

The condition (2.2) can be satisfied by shifting the origin by x_g:

$$-\rho \int\limits_S \varphi_2(x - x_g)\cos(n,y)dS + \int\limits_m (x - x_g)dm = 0$$

$$\Downarrow$$

$$-\rho \int\limits_S \varphi_2 x\cos(n,y)dS + \int\limits_m xdm + x_g \left[\rho \int\limits_S \varphi_2 \cos(n,y)dS - \int\limits_m dm\right] = 0$$

$$\Downarrow$$

$$x_g = \frac{\int\limits_m xdm - \rho \int\limits_S \varphi_2 x\cos(n,y)dS}{m - \rho \int\limits_S \varphi_2 \cos(n,y)dS}$$

Using the middle value rule $-\rho \int\limits_S \varphi_2 x \cos(n,y) dS = x''(-\rho \int\limits_S \varphi_2 \cos(n,y) dS) = x'' m_{22}$ and $\int\limits_m x dm = x' m$ the last formula is rewritten in the form

$$x_g = \frac{x'm + x''m_{22}}{m + m_{22}} \tag{2.5}$$

Here x' is the ship gravity center and x'' is the hydrodynamic center. If the origin lies at the point $x = x_g$ the system (2.1) takes the simplest form

$$\begin{cases} (m+m_{11})\dfrac{dV_x}{dt} - (m+m_{22})V_y\omega_z = F_x, \\ (m+m_{22})\dfrac{dV_y}{dt} + (m+m_{11})V_x\omega_z = F_y, \\ (I_{zz}+m_{66})\dfrac{d\omega_z}{dt} + V_xV_y(m_{22}-m_{11}) = M_z. \end{cases} \tag{2.6}$$

The aim of the ship trajectory calculation is also determination of the ship position in the earth- connected coordinates system $x_0 0 y_0$. Two following equations are used for this purpose (see Fig. 2.1):

$$\frac{dx_0}{dt} = V\cos(\psi - \beta), \frac{dy_0}{dt} = V\sin(\psi - \beta). \tag{2.7}$$

Here ψ is the heading angle calculated from the equation:

$$\omega_z = \frac{d\psi}{dt} \tag{2.8}$$

Combining (2.6), (2.7) and (2.8) we obtain the full system of ship equation in the horizontal plane:

$$
\begin{cases}
(m+m_{11})\dfrac{dV_x}{dt} - (m+m_{22})V_y\omega_z = F_x, \\
(m+m_{22})\dfrac{dV_y}{dt} + (m+m_{11})V_x\omega_z = F_y, \\
(I_{zz}+m_{66})\dfrac{d\omega_z}{dt} = M_z - V_xV_y(m_{22}-m_{11}), \\
x_0(t) = x_0(0) + \int\limits_0^t V\cos(\psi-\beta)dt, \\
y_0(t) = y_0(0) + \int\limits_0^t V\sin(\psi-\beta)dt, \\
\psi(t) = \psi(0) + \int\limits_0^t \omega_z dt.
\end{cases}
\tag{2.9}
$$

2.5 Munk moment

The second term $-V_xV_y(m_{22}-m_{11})$ on the r.h.s in the moment equation is referred as to the moment of Munk who investigated this moment for Zeppelins.

The Munk moment appears in the full form only in the inviscid fluid. In the inviscid potential fluid the flow around the ship hull is shown in Fig. 2.2. In the bow area on the lower side we have the deceleration of the flow and increase of the pressure. On the upper side the flow is accelerated and the pressure decreases. As a result a lift force appears in the bow region. An opposed flow process takes place in the stern area in the inviscid flow. Here the deceleration arises on the upper side whereas the flow acceleration appears on the lower one. The negative down force counterbalances the lift and the total force is zero according to the D'Alambert paradox . However, these two forces produce the moment which is exactly the Munk moment.

This moment is called also as the unstable moment. It can be explained at small drift angles β. The velocity components are expressed through the ship speed and the drift angle:

$$
V_x = V\cos\beta, V_y = -V\sin\beta \tag{2.10}
$$

Since m_{11} is much less than m_{22}, the Munk moment is $M_{Munk} = \frac{V^2}{2}(m_{22} - m_{11})\sin 2\beta \approx m_{22}\frac{V^2}{2}\sin 2\beta$. This moment is the moment which causes the instability. With the other words, if a small drift angle appears, this moment increases this angle. Indeed, the additional moments arising due to the presence of small drift angle $\beta > 0$ is positive, i.e. it causes further increase of the drift angle:

$$\Delta M_z = \beta \frac{dM_{Munk}}{d\beta} \approx m_{22} \beta V_0^2 \cos 2\beta > 0$$

In the real viscous fluid the flow in the stern area is changed. This change is taken into account in the wing theory by Kutta condition . The down force doesn't appear and the unstable moment is approximately only a half of the Munk moment (see Figure 2.2). Very often the yaw moment M_z is determined in measurements in real viscous fluids and capture the Munk's part of the moment automatically. That is why it is common to carry the Munk moment to the right hand side of the moment equation and to consider the combination $M_z - V_x V_y (m_{22} - m_{11})$ as a total yaw moment, i.e.

$$\begin{cases} (m + m_{11}) \dfrac{dV_x}{dt} - (m + m_{22}) V_y \omega_z = F_x, \\ (m + m_{22}) \dfrac{dV_y}{dt} + (m + m_{11}) V_x \omega_z = F_y, \\ (I_{zz} + m_{66}) \dfrac{d\omega_z}{dt} = M_z. \end{cases} \tag{2.11}$$

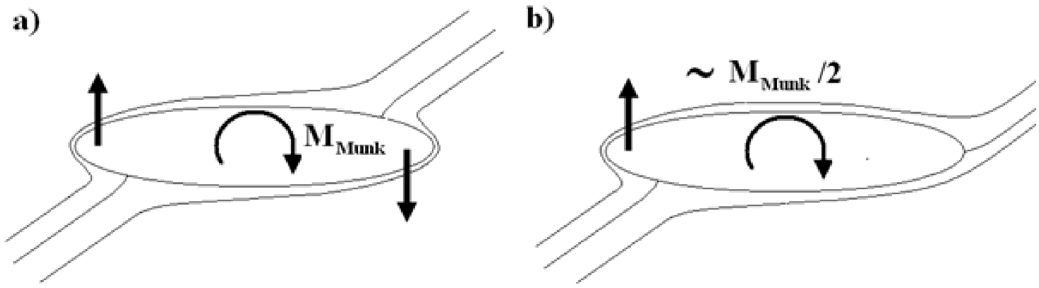

Figure 2.2: Illustration of the Munk moment. a)-inviscid fluid, b)-viscous fluid.

2.6 Equations in terms of the drift angle and trajectory curvature

Classical form of the manoeuvrability equations are written in non-dimensional form in terms of the drift angle and trajectory curvature. This form is very convenient to study the ship yaw stability. The time derivative of speed components (2.10) are:

$$\begin{aligned}\frac{dV_x}{dt} =& \frac{dV}{dt}\cos\beta - V\sin\beta\frac{d\beta}{dt} = \dot{V}\cos\beta - V\dot{\beta}\sin\beta,\\ \frac{dV_y}{dt} =& \frac{dV}{dt}\sin\beta - V\cos\beta\frac{d\beta}{dt} = -\dot{V}\sin\beta - V\dot{\beta}\cos\beta,\end{aligned} \tag{2.12}$$

where point over the quantity means the time derivative of this quantity, i.e. $\dot{V} = \frac{dV}{dt}, \dot{\beta} = \frac{d\beta}{dt}$.

To derive the non-dimensional equation form one uses the typical force representations:

$$F_x = C_x\frac{\rho V^2}{2}A_L, F_y = C_y\frac{\rho V^2}{2}A_L, M_z = m_z\frac{\rho V^2}{2}A_L L \tag{2.13}$$

Introducing the non-dimensional time t, non-dimensional angular velocity Ω and instantaneous trajectory radius R

$$\tau = tV/L, \quad \Omega = \omega_z L/V = \frac{V}{R}\frac{L}{V} = L/R, \tag{2.14}$$

the dimensional time derivatives $\dot{V}$ and $\dot{\beta}$ are expressed through the non-dimensional ones $\frac{V'}{V}$, β' and Ω' by:

$$\begin{aligned}\dot{V} =& \frac{dV}{dt} = \frac{V}{L}\frac{dV}{d\tau} = \frac{V^2}{L}\left(\frac{1}{V}\frac{dV}{d\tau}\right) = \frac{V^2}{L}\frac{V'}{V},\\ \dot{\beta} =& \frac{d\beta}{dt} = \frac{V}{L}\frac{d\beta}{d\tau} = \frac{V}{L}\beta',\\ \dot{\omega}_z =& \frac{d\omega_z}{dt} = \frac{V}{L}\frac{d}{d\tau}\left(\frac{V}{L}\Omega\right) = \left(\frac{V}{L}\right)^2\frac{d\Omega}{d\tau} + \left(\frac{V}{L}\right)^2\Omega\left(\frac{1}{V}\frac{dV}{d\tau}\right) =\\ &= \left(\frac{V}{L}\right)^2\left(\Omega' + \Omega\frac{V'}{V}\right).\end{aligned} \tag{2.15}$$

Here $V' = \frac{dV}{d\tau}, \beta' = \frac{d\beta}{d\tau}, \Omega' = \frac{d\Omega}{d\tau}$. From the second formula in (2.14) follows that dimensionless angular velocity is the dimensionless trajectory curvature.

Using dimensionless mass and inertia moments

$$\kappa_x = \frac{m + m_{11}}{\frac{\rho}{2}A_L L}, \qquad \kappa_y = \frac{m + m_{22}}{\frac{\rho}{2}A_L L}, \qquad \mu = \frac{I_{zz} + m_{66}}{\frac{\rho}{2}A_L L^3}. \tag{2.16}$$

and substituting (2.12), (2.13), (2.14) and (2.15) into (2.11) one obtains:

$$\begin{cases} \kappa_x \dfrac{V'}{V} \cos\beta - \kappa_x \beta' \sin\beta + \kappa_y \Omega \sin\beta = C_x, \\ -\kappa_y \dfrac{V'}{V} \sin\beta - \kappa_y \beta' \cos\beta + \kappa_x \Omega \cos\beta = C_y, \\ \mu\Omega \dfrac{V'}{V} + \mu\Omega' = m_z. \end{cases} \tag{2.17}$$

2.7 Exercises

1. Derive the motion equations for ship moving along the turning circle with the constant speed, drift angle and angular velocity, i.e. $V = const$, $\omega_z = const, \beta = const$.

2. A submarine with the length of 100 m and diameter of 10 m has the velocity of 1 m/s. Determine the added mass of the submarine. Calculate the submarine acceleration if thrust is 10 ton.

3. The thrust has been doubled. What is the increase of the ship motion speed?

4. A cylinder with the density $\varrho = 0,7\varrho_{water}$ and the diameter D is submerged at $h = 1000$ m under the free surface. There is no propulsor on the cylinder. Derive the motion equations of the cylinder if its resistance coefficient c_w referred to $\pi D^2/4$ is equal to 0,4.

5. Calculate the added mass of a cylinder with radius r_0.

6. Calculate the free fall of a steel sphere with the diameter $D = 0.2m$ in the vacuum and in the air.

Chapter 3

Determination of added mass

Summary: The aim of this chapter is the determination of added mass in general and particular cases. Slender body concept is used to get simplified expressions for ship added mass. The Lewis conformal mapping theory is discussed.

3.1 General solution

The basis for an exact determination of added mass is the formula

$$m_{ik} = -\rho \oint\limits_S \varphi_i \frac{\partial \varphi_k}{\partial n} dS \tag{3.1}$$

where φ_i are potentials of the flow when the ship is moved in i-th direction with unit speed. These potentials can be found from the solution of the integral equation (3.2) which was derived in [23] from the no penetration condition

$$-V_{\infty i} + \frac{1}{4\pi} \oint\limits_S q_i \frac{\cos(n, R_{MN})}{R_{MN}^2} dS + \frac{q_i}{2} = 0 \tag{3.2}$$

Here the component of the inflow velocity is calculated depending on i:

$$\begin{aligned} V_{\infty 1} =& \cos(n,x), V_{\infty 2} = \cos(n,y), V_{\infty 3} = \cos(n,z), \\ V_{\infty 4} =& y\cos(n,z) - z\cos(n,y), V_{\infty 5} = z\cos(n,x) - x\cos(n,z), \\ V_{\infty 6} =& x\cos(n,y) - y\cos(n,x) \end{aligned} \tag{3.3}$$

Once the source intensity is found from (3.3), the potential φ_i is calculated according to the definition

$$\varphi_i(x, y.z) = -\frac{1}{4\pi} \oint\limits_S \frac{q_i(\xi, \eta, \varsigma)}{\sqrt{(x-\xi)^2 + (y-\eta)^2 + (z-\varsigma)^2}} dS \tag{3.4}$$

Substituting (3.4) in (3.1) one calculates all added mass. Nowadays the numerical solution of the equation (3.2) presents no serious difficulties and can be performed by any code using panel methods.

For some simple bodies there are analytical solutions. For instance, for an elliptical cylinder the following analytic formulae are valid

$$m_{11} = \rho\pi b^2; \quad m_{22} = \rho\pi a^2; \quad m_{66} = \frac{\rho\pi}{8}\left(a^2 - b^2\right)^2 \tag{3.5}$$

where a and b are semi axis of the ellipse ($a > b$).

The analytic solution which is the most interesting for shipbuilding is the solution for rotational ellipsoid. Unfortunately, this solution is cumbersome and contains non elementary functions. The results of calculation using this solution are presented in Fig. 3.1 for added mass coefficients.

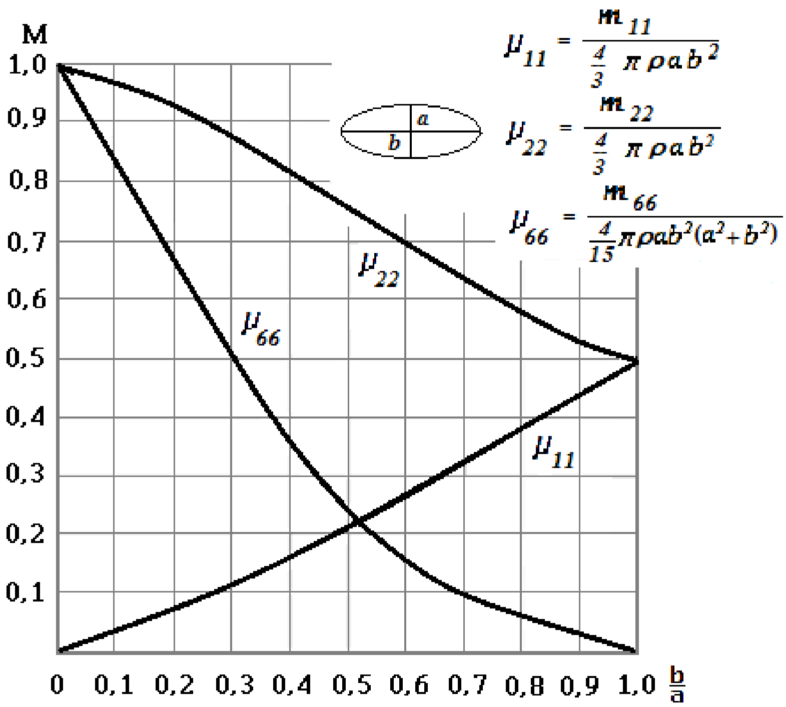

Figure 3.1: Dimensionless added mass of rotational ellipsoid

In the simplest approach, the largest axis 2a is the ship length, 2b is a middle value between the width B and the draught 2 T.

3.2 Added mass of the slender body

Another way of determination of added mass is the use of the slender body assumption. Let us consider the added mass $m_{22} = -\rho \int\limits_S \varphi_2 \cos(n, y) dS$. Using the slender body estimations (2.3) the formula for this mass can be written as follows:

$$m_{22} = -\rho \int\limits_S \varphi_2 \cos(n, y) dS \approx \int\limits_0^L -\rho \oint\limits_C \varphi_2 \cos(n, y) dC dL = \int\limits_0^L m'_{22} dL \quad (3.6)$$

where C is the ship frame contour and $m'_{22} = -\rho \oint\limits_C \varphi_2 \cos(n, y) dC$ is the added mass of this contour. The formula (3.6) is easier than the original one $m_{22} = -\rho \int\limits_S \varphi_2 \cos(n, y) dS$ since the contour added mass is calculated from 2D theory. Similar formulae can be written for the added mass m_{66}:

$$m_{66} = -\rho \int\limits_S \varphi_6 (x \cos(n, y) - y \cos(nx)) dS \approx \int\limits_0^L -\rho \oint\limits_C \varphi_6 x \cos(n, y) dC dL \quad (3.7)$$

Expression for φ_6 can be found from the following asymptotic analysis:

$$m_{26} = -\rho \int\limits_S \varphi_2 (x \cos(n, y) - y \cos(n, x)) dS \approx -\rho \int\limits_S \varphi_2 x \cos(n, y) dS,$$

$$m_{62} = m_{26} \Rightarrow -\rho \int\limits_S \varphi_6 \cos(n,y) dS \approx -\rho \int\limits_S \varphi_2 x \cos(n, y) dS \quad (3.8)$$

$$\Downarrow$$

$$\varphi_6 \approx \varphi_2 x$$

Substituting the last result in (3.7) gives

$$\begin{aligned} m_{66} &\approx \int\limits_0^L -\rho \int\limits_C \varphi_2 x^2 \cos(n, y) dC dL \approx \\ &\approx \int\limits_0^L x^2 \left(-\rho \oint\limits_C \varphi_2 \cos(n, y) dC \right) dL = \int\limits_0^L x^2 m'_{22} dL \end{aligned} \quad (3.9)$$

$$
\begin{aligned}
m_{26} &= -\rho \int\limits_S \varphi_2 (x \cos(n, y) - y \cos(n, x)) dS \approx \\
&\approx -\rho \int\limits_S \varphi_2 x \cos(n, y) dS \approx \int\limits_0^L x m'_{22} dx
\end{aligned} \tag{3.10}
$$

Similarly, added mass m_{33}, m_{35} and m_{55} can be found. Unfortunately, the slender body theory is not capable of simplifying the formulae for mass like m_{1k}, since the effect of the motion in x direction is assumed to be neglected. The mass m'_{22} can be found using 2D panel method which is much easier than 3D version of this method.

3.3 Added mass of the slender body at small Fn numbers

In what follows we use the concept of doubled body assuming the Froude number is small and water surface deformation effects can be neglected. An effective way to get m'_{22} is the use of the Lewis theory which became a classical way to determine the added mass in naval architecture. Lewis used theory of conformal mapping[1] which is applicable only for two dimensional flows. According to this theory (see also chapter 5.8.1 in [23]) the physical plane $z = x + iy$ is mapped into an auxiliary plane $\varsigma = \xi + i\eta$. The skill is to find such a mapping function $z(\varsigma)$ and inversion mapping function $\varsigma(z)$ so that the flow around the contour is mapped into the flow around a cylinder. Lewis succeeded in mapping of a special class of doubled ship frames, called further as Lewis frames, into cylinders. The Lewis frames (see Fig. 3.2) have the form typical for ship frames in the middle ship area. In the bow and stern regions Lewis frames are deviated significantly from the typical frames. Lewis inversion mapping function is written in general form

$$
\varsigma = z + \frac{a}{z} + \frac{b}{z^3}, \tag{3.11}
$$

where a and b are real coefficients. Changing a and b one gets a family of Lewis frames. Lewis performed a serial calculation for various frames and presented his results in a form of a resulting diagram shown in Fig. 3.3. He introduced the coefficient (referred as to the Lewis coefficient) which is the

[1] see, for instance, *en.wikipedia.org/wiki/Conformal_map*

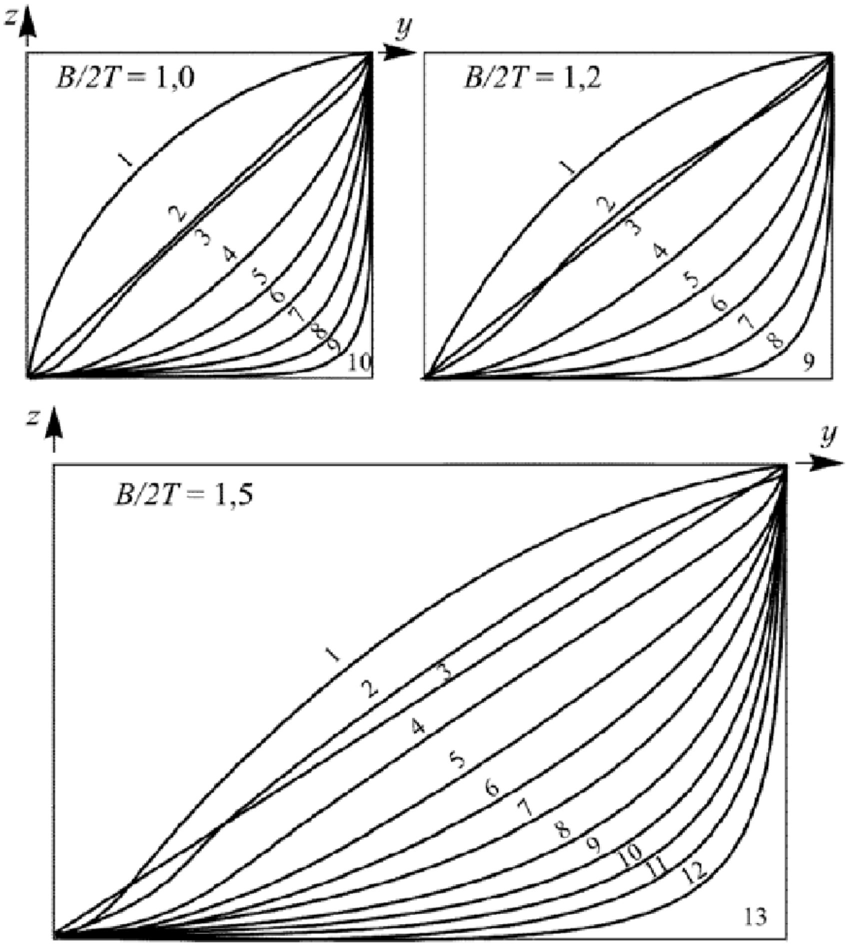

Figure 3.2: Sample of Lewis frames [26]

ratio of the added mass of the frame to that of the cylinder with radius T

$$C = \frac{m'_{22}}{\rho \pi T^2} \tag{3.12}$$

Therefore, $C = 1$ for the cylinder. C for different Lewis frames are presented in Fig. 3.3 depending on $H = 2T/B$ and $\sigma = A_{sp}/(BT)$, where A_{sp} is the frame area.

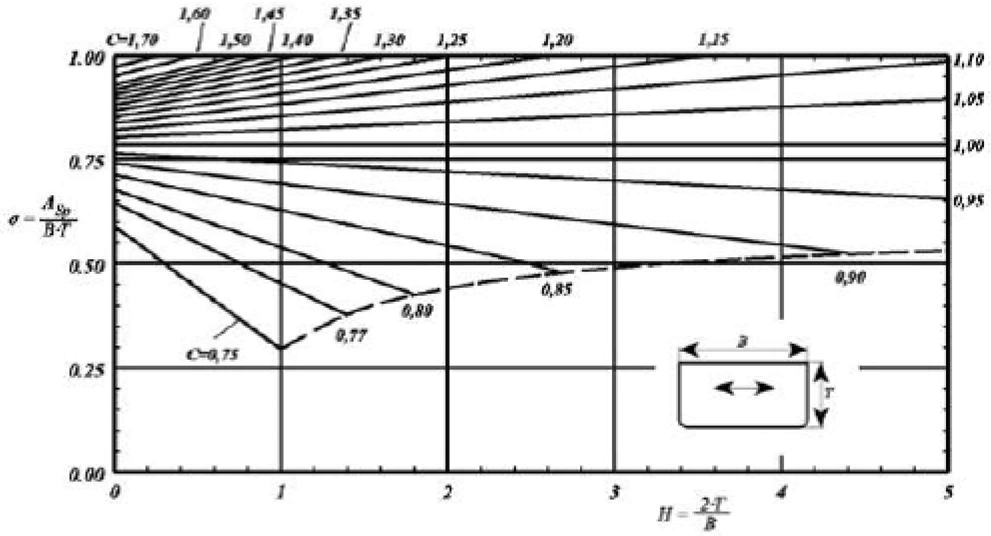

Figure 3.3: Lewis coefficients depending on $H = 2T/B$ and $\sigma = A_{sp}/(BT)$, where A_{sp} is the frame area (taken from [21])

Lewis data are useful especially in the preliminary ship design when the exact ship form is still unknown. Using Lewis coefficient the formulae (3.6), (3.9) and (3.10) are rewritten in the following form:

$$\begin{aligned} m_{22} &= \int_0^L m'_{22} dL = \rho\pi \int_0^L C(x) T^2(x) dL, \\ m_{66} &= \int_0^L x^2 m'_{22} dL = \rho\pi \int_0^L x^2 C(x) T^2(x) dL, \\ m_{26} &= \int_0^L x m'_{22} dL = \rho\pi \int_0^L x C(x) T^2(x) dL \end{aligned} \tag{3.13}$$

The slender body theory of added mass is a strip theory . It means that the resulting mass is obtained by integration of frame mass along the ship length. Every frame flow is considered as a two dimensional one at corresponding cross sections (strips). The slender body theory works well in the middle ship area. In the bow and stern areas the flow is essentially three dimensional. The effect of three dimensional flow on added mass can also be taking into account within the slender body theory using Munk correction factors . The idea of Munk becomes obvious from the following formulae

$$
\begin{aligned}
&m_{22} = R_2(a,b)m_{22\_slender}, m_{66} = R_3(a,b)m_{66\_slender}, \\
&R_2(a,b) = m_{22\_ellipsoid}/m_{22\_slender\_ellipsoid}, \\
&R_3(a,b) = m_{66\_ellipsoid}/m_{66\_slender\_ellipsoid}.
\end{aligned}
\tag{3.14}
$$

Here $R_2(a,b)$ and $R_3(a,b)$ are the Munk's correction factors (see Fig. 3.4). Again, the largest axis 2a is the ship length, 2b is a middle value between the width B and the draught 2 T. The added mass m_{11} can not be determined since the perturbations in x direction are neglected within the slender body theory. To overcome this problem Munk proposed to find m_{11} in a similar way like m_{22} but with the different correction factor:

$$
m_{11} = R_1(a,b)m_{22\_slender}. \tag{3.15}
$$

The added mass $m_{22\_slender\_ellipsoid}$ and $m_{66\_slender\_ellipsoid}$ are obtained from (3.13) taking the fact into account, that the cross section of the rotational ellipsoid is the cylinder which Lewis coefficient is one.

$$
\begin{aligned}
m_{22\_slender\_ellipsoid} &= \frac{4}{3}\pi\rho ab^2, \\
m_{66\_slender\_ellipsoid} &= \frac{4}{15}\pi\rho ab^3
\end{aligned}
\tag{3.16}
$$

As seen from (3.16) the hydrodynamic mass $m_{22\_slender}$ obtained using the slender body theory is exactly equal to the volume of the ellipsoid multiplied with the water density. If the ellipsoid is in the equilibrium state in the water the mass is equal to the volume multiplied with the density (Archimedes law). ***Therefore, the hydrodynamic mass*** m_{22} ***obtained using the slender body theory is equal to the ship mass***.
This result can be used for rough estimation of the mass m_{22}. The added mass m_{11} is about five, eight per cent, whereas the mass m_{66} is about $1.4I_{zz}$ [21].

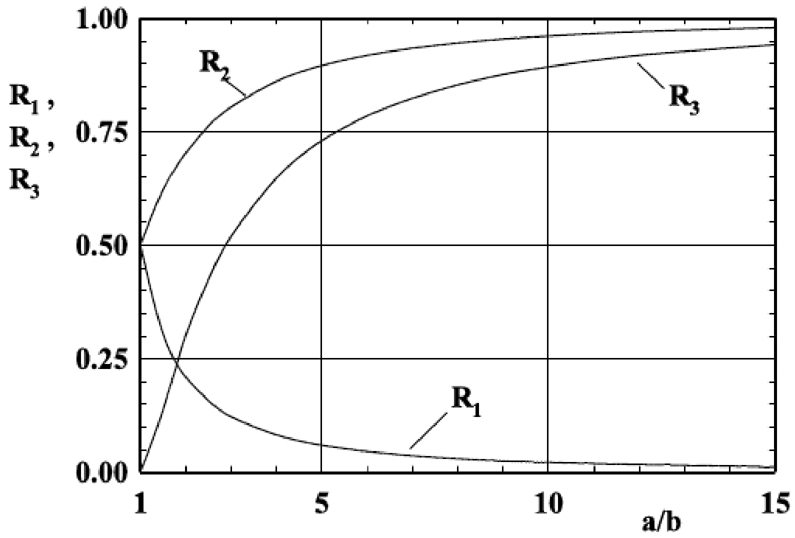

Figure 3.4: Munk's correction factors.

With the Munk corrections the added mass are calculated from formulae

$$m_{11} = \frac{1}{2} R_1 \rho \pi \int_0^L C(x) T^2(x) dx,$$
$$m_{22} = \frac{1}{2} R_2 \rho \pi \int_0^L C(x) T^2(x) dx, \tag{3.17}$$
$$m_{66} = \frac{1}{2} R_3 \rho \pi \int_0^L C(x) T^2(x) dx.$$

The factor 1/2 is introduced into (3.17) because the added mass of the hull is a half of that of the doubled body.

3.4 Exercises

1. The body has the symmetry plane xy. Which added mass are zero?

2. The body has the symmetry plane xz. Which added mass are zero?

3. The body has the symmetry plane yz. Which added mass are zero?

4. The body has two symmetry planes xy and xz. Which added mass are not zero?

5. The body has three symmetry planes xy, yz and xz. Which added mass are not zero?

6. Write the equations for the unsteady motion of the body in X0Y-plane.
$V_1 = V_x$, $V_2 = V_y$, $V_6 = \omega_z$
Write the formulas for the unsteady forces and moments.

7. Write the formulas for the unsteady forces and moments for the unsteady motion of an ellipsoid of revolutions with semi-axis a and b in X0Y plane.
$m_{11} = \rho\pi b^2$, $m_{22} = \rho\pi a^2$, $m_{66} = \rho\pi/8(a^2 - b^2)^2$

8. Write the equation for the emersion of the sphere.

9. Write the equation for the longitudinal motion of the body of revolution with the thrust T.

10. Find the force acting on the flat plate, which fall down on the water at the moment of the contact with the water. Weight of the plate (m) is 10 kg, initial height (h) is 1 m, resistance coefficient (C_w) is 2, $m_{22} = \rho\pi a^2$

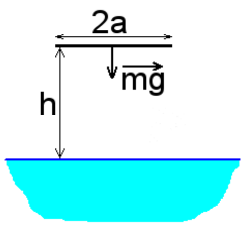

Chapter 4

Steady manoeuvring forces

Summary: The most important part of this chapter is the representation of forces in full and truncated forms which are used in ship theory. Experimental determination of steady manoeuvring forces using PMM, identification and circular motion tests is discussed. A detailed description of force approximation proposed by Krylov Research Shipbuilding Institute is given.

4.1 Introduction

The forces acting on the ship can be subdivided into steady manoeuvring forces steady manoeuvring forces , propulsion forces, forces arising on control elements, wave induced and forces caused by wind and current. In this chapter we consider the steady force component. The steady manoeuvring forces arise on the body moving with steady linear and angular velocities due to viscosity influence. The physical reason of the inception of the steady manoeuvring forces is illustrated in Fig. 2.2. If the ship moves with a steady drift angle in an inviscid flow, the lift force arises in the bow region whereas the down force acts on the stern area (Fig. 2.2a). The resulting force is in accordance with the D' Alambert paradoxon zero. In the viscous fluid the flow in the stern area is changed due to influence of the boundary layer developing along the ship surface beginning from the bow. As a result the down force disappears at the stern part and the resulting force is not zero. This component is referred to as the steady manoeuvring force caused by the drift angle. The forces and moments appear also if the ship moves with any steady linear and angular velocity. In the manoeuvrability theory the steady forces arising due to drift angle and yaw angular velocity are of importance.

4.2 Representation of forces

Using the Reynolds averaged Navier Stokes equations (RANSE) technique, the steady forces can be calculated by direct integration of normal and shear stresses over the wetted ship area. This way requires huge computer resources, is time consuming and the prediction accuracy is often not satisfactory. The experiment is still remaining a main source of the force data used for prediction of manoeuvrability.

The experimental methodology is based on the representation of forces in form of different approximations. For instance, one uses a multivariate Taylor series expansion about the equilibrium condition $V_x = V, V_y = V_z = \omega_x = \omega_y = \omega_z = 0$:

$$F_n(V_x, V_y, V_z, \omega_x, \omega_y, \omega_z) = \sum_{j=0}^{\infty} \left\{ \frac{1}{j!} \left(\tilde{V}_k \frac{\partial}{\partial V_k} \bigg|_{V_x=V, V_y=V_z=\omega_x=\omega_y=\omega_z=0} \right)^j F_n \right\}, \tag{4.1}$$

where $F_n(V_x, V_y, V_z, \omega_x, \omega_y, \omega_z)$ is the force component[1], $n = 1, 2, ..., 6, , ...,$ $F_4(V_x, V_y, V_z, \omega_x, \omega_y, \omega_z) = M_x(V_x, V_y, V_z, \omega_x, \omega_y, \omega_z), .,\ \tilde{V}_1 = V_x - V, \tilde{V}_2 = V_y, ..., \tilde{V}_4 = \omega_x, ..., \tilde{V}_5 = \omega_y, ...$

As a rule the force coefficient are calculated through the coefficients C_x, C_y, C_z, m_x, m_y, m_z

$$F_{x,y,z} = C_{x,y,z} \frac{\rho V^2}{2} A_L, \qquad M_{x,y,z} = m_{x,y,z} \frac{\rho V^2}{2} A_L L,$$

which are represented in the form of Taylor series. The coefficients C_x, C_y, C_z, m_x, m_y, m_z are the function of kinematic parameters and similarity criteria such as the Froude and Reynolds numbers.

The derivatives $\frac{\partial}{\partial V_k}\Big|_{V_x=V, V_y=V_z=\omega_x=\omega_y=\omega_z=0}$ are determined about the equilibrium condition $V_x = V, V_y = V_z = \omega_x = \omega_y = \omega_z = 0$.

4.2.1 Hypothesis of quasi steady motion

Application of the Taylor series implies the hypothesis of quasi steady motion . The latter means that the forces are fully determined by instantaneous values of kinematic parameters neglecting the unsteady effects. The motion

[1] For the sake of brevity both force and moment are meant here and further under the term "force".

history influence is neglected. Strictly speaking the ship hydrodynamics depends on the ship states in previous times, because the wave surface, boundary layer and wake depend on the ship trajectory. However, the unsteady effects can be neglected if the characteristic time scales of the hydrodynamic processes are much smaller than the characteristic times of the ship motion. With the other words the ship motion is much slower than the change of the hydrodynamics characteristics. In this case the hydrodynamics is fully determined by instantaneous ship kinematic characteristics. With the other words, it is assumed that the hydrodynamic coefficients $C_x, C_y, C_z, M_x, M_y, M_z$ are frequency independent. This assumption is not necessary if the motion is modeled using coupled 6DoF simulation (see chapter 10).

4.2.2 Truncated forms

In the shipbuilding the maximum order of the derivatives in the representation (4.1) is three. General forms of (4.1) for different bodies are given in [27]. The representation (4.1) contains high-order derivatives which are hardly to determine. There are no reliable theoretical or empirical means to calculate many of the second - and third-order terms [27]. That is why the expansion (4.1) is used in a very truncated form, which can be derived by further analysis showing that only a part of the derivatives has an essential impact on the ship dynamics. Additionally, the expansions (4.1) are significantly simplified if the ship symmetry is taken into account. In this case

$$\begin{aligned} F_x(0, V_y, 0, 0, 0, 0) &= F_x(0, -V_y, 0, 0, 0, 0), \\ F_y(0, V_y, 0, 0, 0, 0) &= -F_y(0, -V_y, 0, 0, 0, 0), \\ M_z(0, V_y, 0, 0, 0, 0) &= -M_z(0, -V_y, 0, 0, 0, 0). \end{aligned} \tag{4.2}$$

Some of derivatives in (4.1) are zero. For instance, due to symmetry of the drag with respect to the velocity component V_y and ω_z, the derivatives of the drag on V_y and on ω_z at $V_y = V_z = \omega_x = \omega_y = \omega_z = 0$ are zero:

$$\left.\frac{\partial F_x}{\partial V_y}\right|_{V_x, V_y=V_z=\omega_x=\omega_y=\omega_z=0} = 0, \quad \left.\frac{\partial F_x}{\partial \omega_z}\right|_{V_x, V_y=V_z=\omega_x=\omega_y=\omega_z=0} = 0 \tag{4.3}$$

These facts are used to truncate the expansions (4.1).

4.2.3 Cross flow drag principle

The Taylor series expansion was also revisited using the so-called "cross flow drag principle" taken from the wing theory. Let us consider the steady ship motion with velocity components V_x and V_y. The dependence of the transverse force arising on the ship is shown in Fig. 4.1 depending on the drift angle.

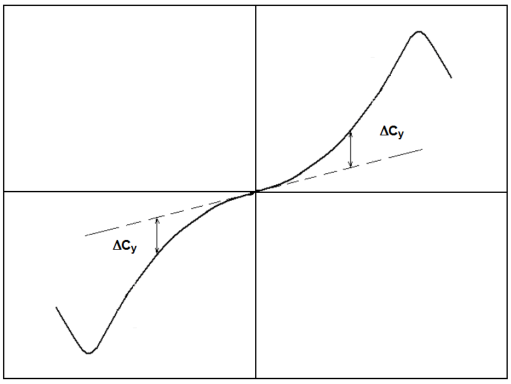

Figure 4.1: Typical dependence of the transverse force on the drift angle, q is the nonlinear part of the force

The dependence of the transverse force coefficient on the drift angle $C_y(\beta)$ consists of two components:

$$C_y(\beta) = C_y^\beta \beta + \Delta C_y \tag{4.4}$$

Here $C_y^\beta \beta$ is the linear component whereas ΔC_y is the nonlinear component. As discussed in the wing theory (see [23], chapter 5.3) the ratio between two components depends on the wing aspect ratio. The ship under the drift angle is a wing with an extremely low aspect ratio $AR \approx 2T/L$. For such a wing the nonlinear part ΔC_y is essential already at small drift angles and overcome the linear component

$$C_y^\beta = \frac{dF_y/d\beta}{\rho V^2 TL} = \frac{\pi}{2}\lambda, \quad m_z^\beta = \frac{dM_z/d\beta}{\rho V^2 TL^2} = \frac{\pi}{4}\lambda. \tag{4.5}$$

where the linear moment component $\beta dM_z/d\beta$ is calculated around the wing middle point.

Formal application of the Taylor series expansion for the case under consideration gives:

$$C_y(\beta) = \frac{dC_y}{d\beta}\beta + \frac{1}{6}\frac{d^3C_y}{d\beta^3}\beta^3 + ... \tag{4.6}$$

The nonlinear component seems to be proportional to $\sim \beta^3$. In order to calculate the nonlinear component ΔC_y, Betz considered the wing under the cross flow $V \sin\beta$. The additional transverse force ΔC_y is interpreted as a drag caused by the cross flow. According to Betz the nonlinear component is proved to be proportional to the drift angle squared but not cubed as in (4.6):

$$\Delta C_y = C_y^{\beta\beta} \beta^2 \tag{4.7}$$

The result (4.7) was confirmed in measurements. The problem now is the positive sign of the nonlinear force both at positive $\beta > 0$ and negative $\beta < 0$ drift angles, although intuitively it is clear that $\Delta C_y(\beta) = -\Delta C_y(-\beta)$. To avoid this contradiction the term β^2 is rewritten in the form $|\beta|\beta$. Therefore,

$$C_y(\beta) = C_y^{\beta} \beta + C_y^{\beta\beta} |\beta|\beta \tag{4.8}$$

The representation with the second order terms $C_y^{\beta\beta}|\beta|\beta$ is used by Norrbin [30], SNAME [27], Sobolev and Fedayevsky [17]. On the contrary Abkowitz [5] uses the terms of the third order to represent the nonlinear components of forces.

4.2.4 Some typical representations used in the ship manoeuvering

With considerations of facts discussed above the force representation proposed by SNAME [27] for manoeuvrability theory reads

$$\begin{aligned} F_x(V_x, V_y, 0, 0, 0, \omega_z) = {} & F_x(V_x, 0, 0, 0, 0, 0) + \\ & + \frac{1}{2}\left\{ \frac{\partial^2 F_x}{\partial V_y^2} V_y^2 + \frac{\partial^2 F_x}{\partial \omega_z^2} \omega_z^2 + \frac{\partial^2 F_x}{\partial V_y \partial \omega_z} V_y \omega_z \right\} \end{aligned} \tag{4.9}$$

$$\begin{aligned} F_y(V_x, V_y, 0, 0, 0, \omega_z) = {} & \frac{\partial F_y}{\partial V_y} V_y + \frac{\partial F_y}{\partial \omega_z} \omega_z + \\ + \frac{1}{2}\left\{ \frac{\partial^2 F_y}{\partial V_y \partial \omega_z} |V_y| \omega_z + \frac{\partial^2 F_y}{\partial V_y^2} |V_y| V_y + \frac{\partial^2 F_y}{\partial \omega_z^2} |\omega_z| \omega_z \right\} & + \frac{1}{6} \frac{\partial^3 F_y}{\partial V_y \partial \omega_z^2} V_y \omega_z^2 \end{aligned} \tag{4.10}$$

$$\begin{aligned} M_z(V_x, V_y, 0, 0, 0, \omega_z) = {} & \frac{\partial M_z}{\partial V_y} V_y + \frac{\partial M_z}{\partial \omega_z} \omega_z + \\ + \frac{1}{2}\left\{ \frac{\partial^2 M_z}{\partial V_y \partial \omega_z} |V_y| \omega_z + \frac{\partial^2 M_z}{\partial V_y^2} |V_y| V_y + \frac{\partial^2 M_z}{\partial \omega_z^2} |\omega_z| \omega_z \right\} & + \frac{1}{6} \frac{\partial^3 M_z}{\partial V_y \partial \omega_z^2} V_y \omega_z^2 \end{aligned} \tag{4.11}$$

Usually, the series expansions (4.9) - (4.11) are applied for force and moment coefficients C_x, C_y and m_z.

In the simplest case the series expansion for the transverse force used in the linear manoeuvrability theory contains a restricted number of terms:

$$\begin{aligned} F_y &= C_y \frac{\rho V^2}{2} A_L \\ C_{y(\beta,\Omega,\delta_R)} &= C_y(\beta_0, 0, \delta_R) + C_y^{\beta}(\beta_0, 0, 0)(\beta - \beta_0) + C_y^{\Omega}(\beta_0, 0, 0)\Omega \end{aligned} \tag{4.12}$$

where $\beta = \arctan V_y/V_x, \Omega = \omega_z L/V, V = \sqrt{V_x^2 + V_y^2}, \delta_R$ is the rudder deflection. The expansion is valid in the vicinity of any operation point $\beta_0, 0, \delta_R$. As seen in (4.12) it is common to represent the forces through the force coefficient which is approximated in the form of the Taylor series expansion on the drift angle $\beta = \arctan V_y/V_x$ and the non-dimensional angular velocity $\Omega = \omega_z L/V$.

Abkowitz [30] proposed force representation using terms up to the third orders:

$$
\begin{aligned}
F_x = {} & F_{x_0} + F_{x\dot{V_x}}\dot{V}_x + F_{xV_x}\Delta V_x + F_{xV_xV_x}{\Delta V_x}^2 + F_{xV_xV_xV_x}{\Delta V_x}^3 + F_{xV_yV_y}V_y^2 \\
& + F_{x\omega_z\omega_z}\omega_z^2 + F_{x\delta_R\delta_R}\delta_R^2 + F_{x\omega_zV_y}\omega_zV_y + F_{x\omega_z\delta_R}\omega_z\delta_R + F_{xV_y\delta_R}V_y\delta_R + \\
& + F_{xV_yV_yV_x}V_y^2\Delta V_x F_{x\omega_z\omega_zV_x}\omega_z^2\Delta V_x + F_{x\delta_R\delta_RV_x}\delta_R^2\Delta V_x + F_{x\omega_zV_yV_x}\omega_zV_y\Delta V_x \\
& + F_{x\omega_z\delta_RV_x}\omega_z\delta_R\Delta V_x F_{xV_y\delta_RV_x}V_y\Delta V_x\delta_R + (1-t)T + F_{x_{ext}}
\end{aligned}
$$

$$
\begin{aligned}
F_y = {} & F_{y0} + F_{yV_x}\Delta V_x + F_{yV_xV_x}{\Delta V_x}^2 + F_{y\omega_z}\omega_z + F_{yV_y}V_y + F_{y\dot{\omega}_z}\dot{\omega}_z + F_{y\dot{V_y}}\dot{V}_y \\
& + F_{y\delta_R}\delta_R + F_{y\omega_z\omega_z\omega_z}\omega_z^3 + F_{yV_yV_yV_y}{V_y}^3 + F_{y\delta_R\delta_R\delta_R}\delta_R^3 + F_{y\omega_z\omega_z\delta_R}\omega_z^2\delta_R + \\
& + F_{y\delta_R\delta_R\omega_z}\delta_R^2\omega_z F_{y\omega_z\omega_zV_y}\omega_z^2V_y + F_{yV_yV_y\omega_z}{V_y}^2\omega_z + F_{y\delta_R\delta_RV_y}\delta_R^2V_y + \\
& + F_{yV_yV_y\delta_R}{V_y}^2\delta_R + F_{y\delta_RV_y\omega_z}\delta_RV_y\omega_z F_{yV_yV_x}V_y\Delta V_x + F_{y\omega_zV_x}\omega_z\Delta V_x + \\
& + F_{y\delta_RV_x}\delta_R\Delta V_x + F_{y\delta_RV_xV_x}\delta_R{\Delta V_x}^2 + F_{y_{ext}}
\end{aligned}
$$

$$
\begin{aligned}
M_z = {} & M_{z0} + M_{zV_x}\Delta V_x + M_{zV_xV_x}{\Delta V_x}^2 + M_{z\omega_z}\omega_z + M_{zV_y}V_y + M_{z\delta_R}\delta_R + \\
& + M_{z\dot{V_y}}\dot{V}_y M_{z\delta_R}\delta_R + M_{z\omega_z\omega_z\omega_z}\omega_z^3 + M_{zV_yV_yV_y}V_y^3 + M_{z\delta_R\delta_R\delta_R}\delta_R^3 + \\
& + M_{z\omega_z\omega_z\delta_R}\omega_z^2\delta_R + M_{z\delta_R\delta_R\omega_z}\delta_R^2\omega_z M_{z\omega_z\omega_zV_y}\omega_z^2V_y + M_{zV_yV_y\omega_z}{V_y}^2\omega_z + \\
& + M_{z\delta_R\delta_RV_y}\delta_R^2V_y + M_{zV_yV_y\delta_R}{V_y}^2\delta_R M_{z\delta_RV_y\omega_z}\delta_RV_y\omega_z + M_{zV_yV_x}V_y\Delta V_x + \\
& + M_{z\omega_zV_x}\omega_z\Delta V_x + M_{zV_yV_xV_x}V_y{\Delta V_x}^2 M_{z\omega_zV_xV_x}\omega_z{\Delta V_x}^2 + M_{z\delta_RV_x}\delta_R\Delta V_x + \\
& + M_{z\delta_RV_xV_x}\delta_R{\Delta V_x}^2 + M_{z_{ext}}
\end{aligned}
\tag{4.13}
$$

The most general form of force representation is the polynomial representation which takes nonlinearity into account. A sample of such a representation is the method proposed by the Krylov Shipbuilding Research Institute (see section 4.3.3 below).

4.3 Experimental determination of steady manoeuvring forces

Despite of a rapid development of numerical methods the experiment is still remaining a main source of manoeuvring force data. Here we discuss three experimental techniques of force determination.

4.3.1 The planar motion mechanism (PMM)

The PMM is used in manoeuvring studies conducted in open water (see Fig. 4.2) and in ice (see Fig. 4.3). This technique has been pioneered in the

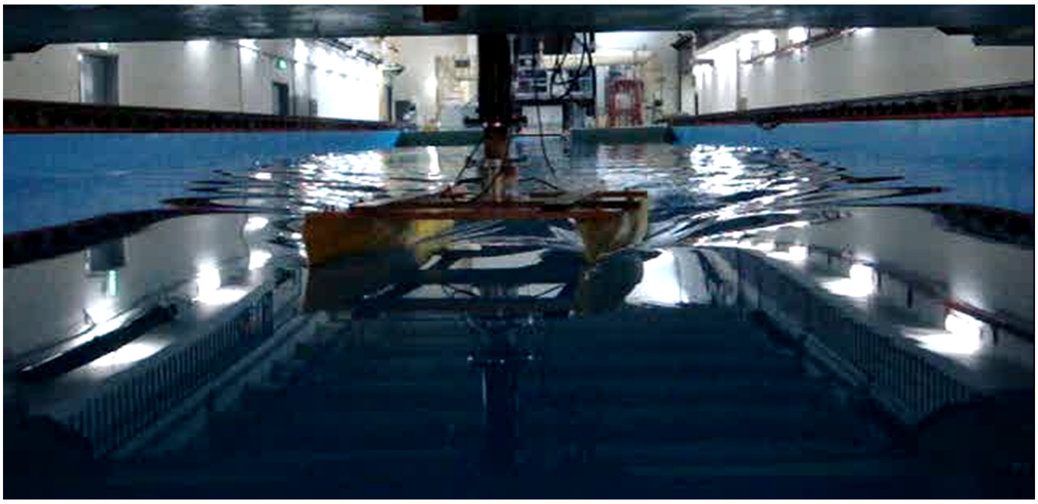

Figure 4.2: PMM tests of the catamaran model NPL at the Seoul National University

USA by Gertler (1959) and Goodman (1960). The PMM allows a model to move in exact, preprogramming patterns while forces, moments and motion around the model are recorded. The model is towed in a testing tank and oscillates harmonically around a steady reference motion. The amplitude of oscillations and the frequency are prescribed by the PMM. For instance the PMM installed at the Oceanic Consulting Corporation, St. Johns, Canada [35] produces the sway oscillations with the amplitude of 4 meters, the sway velocity amplitude of 0.7 m/s and yaw rates up to 60 degree per second in the towing tank with the length of 200 m and the width of 12 m.

The idea of PMM in the simplest version can be easily illustrated using the Taylor series expansion (4.9)-(4.11). Usually the expansions are used to find the forces on the left-hand side of the formulae assuming that all derivatives on the right-hand side are known. In the PMM methodology the forces are measured. The right hand sides of the formulae $F_x(V_x, V_y, 0, 0, 0, \omega_z)$, $F_y(V_x, V_y, 0, 0, 0, \omega_z)$ and $M_z(V_x, V_y, 0, 0, 0, \omega_z)$ are known. The kinematic parameters V_x, V_y, ω_z are prescribed by the PMM at every time instant. Performing tests one obtains, say, M measurement points. The following conditions are valid for each i-th measurement point:

$$F_{xi}(V_{xi}, 0, 0, 0, 0, 0) + \frac{1}{2}\left\{\frac{\partial^2 F_x}{\partial V_y^2} V_{yi}^2 + \frac{\partial^2 F_x}{\partial \omega_z^2}\omega_{zi}^2 + \frac{\partial^2 F_x}{\partial V_y \partial \omega_z} V_{yi}\omega_{zi}\right\} = F_{xi} \quad (4.14)$$

Figure 4.3: Model test with PMM in ice performed by Oceanic Consulting Corporation [1]

$$\frac{\partial F_y}{\partial V_{yi}}V_{yi} + \frac{\partial F_y}{\partial \omega_z}\omega_{zi} + \frac{1}{2}\left\{\frac{\partial^2 F_y}{\partial V_y \partial \omega_z}|V_{yi}|\omega_{zi} + \frac{\partial^2 F_y}{\partial V_y^2}|V_{yi}|V_{yi} + \frac{\partial^2 F_{yi}}{\partial \omega_z^2}|\omega_{zi}|\omega_{zi}\right\}$$
$$+\frac{1}{6}\frac{\partial^3 F_y}{\partial V_y \delta \omega_z^2}V_{yi}\omega_{zi}^2 = F_{yi} \tag{4.15}$$

$$\frac{\partial M_z}{\partial V_y}V_{yi} + \frac{\partial M_z}{\partial \omega_z}\omega_{zi} + \frac{1}{2}\left\{\frac{\partial^2 M_z}{\partial V_y \partial \omega_z}|V_{yi}|\omega_{zi} + \frac{\partial^2 M_z}{\partial V_y^2}|V_{yi}|V_{yi} + \frac{\partial^2 M_z}{\partial \omega_z^2}|\omega_{zi}|\omega_{zi}\right\}$$
$$+\frac{1}{6}\frac{\partial^3 M_z}{\partial V_y \partial \omega_z^2}V_{yi}\omega_{zi}^2 = M_{zi} \tag{4.16}$$

where $i = 1, M$ the measurement point number. Having 16 measurement points, one can calculate 16 unknown derivatives in the system of linear equations (4.14)-(4.16). To increase the reliability of prediction, the number of experimental points is much more than the number of unknown derivatives. The resulting system is over defined (the number of equations is larger than the number of unknowns). In this case the derivatives are found from the condition that the optimal set of derivatives provides the minimum of residuals of the equations (4.14)-(4.16).

The approach using derivatives implies the quasi steady motion. The influence of unsteady effects, influence of frequencies in harmonic motions is not considered. To overcome this disadvantage Bishop and Parkinson [10] proposed to represent forces through the Fourier expansions based on the oscillatory derivatives following to the experience from the airplane aerodynamics. The PMM equipped with the harmonics analysis device is capable of determining the oscillatory derivatives as well (see [10]).

For instance, if only the yaw oscillation motion $\omega = \omega_0 \sin \sigma t, \dot{\omega} = \frac{d\omega}{dt} = \omega_0 \sigma \cos \sigma t$ is studied, the representation of the transverse force looks like

$$F_y(t) = a_1 V \omega + a_2 \dot{\omega} = a_1 V \omega_0 \sin \sigma t + a_2 \omega_0 \sigma \cos \sigma t \qquad (4.17)$$

Three remarkable points should be noted, considering the last formulae

- there is an explicit dependence of forces on time,
- additional term proportional to $\dot{\omega}$ takes unsteady effects (delay of forces change with respect to kinematic parameters change) into account,
- coefficients a_1, a_2 depend not on the time rather than on frequencies σ.

If A and B the coefficients of the Fourier expansion for the force $F_y(t)$ provided from measurements:

$$F_y(t) = A \cos \sigma t + B \sin \sigma t \Rightarrow A = a_2 \omega_0 \sigma, B = a_1 V \omega_0$$

From this we obtain unknown coefficients in (4.17):

$$a_2 = A/\omega_0 \sigma, \quad a_1 = B/V \omega_0$$

4.3.2 Circular motion test. Rotating-arm basin

The rotating-arm basin is the traditional and well-tried facility to determine the manoeuvring forces. The rotating arm is installed in a round form basin with diameters varying from 15 meters to 75 meters. For instance the rotating arm basin of the Krylov Shipbuilding Research Institute is 70 m with depth of 6.7 meters. The sketch of the facility is presented in Fig. 4.4. The model installed on the rotating arm at arbitrary drift angle is free for heave and pitch motions. Changing the distance from the model to the basin center allows one to control the model angular velocity. The frequency of rotation is changed in order to vary the linear speed of the ship motion. The drag, the transverse force and the yaw moment are measured using dynamometers. The forces and moments obtained from measurements are approximated as functions of β and ω_z. Numerical differentiation of these approximations is then used to determine the derivatives. Unsteady effects are fully neglected in the rotating- arm basin tests.

One of the difficulties in the rotating-arm tests is the determination of forces at $\omega_z = 0$ since $\omega_z \neq 0$ due to restriction on the arm length. This problem is easily solved, if the rotating-arm tests are supplied by tests in towing tank at $\omega_z = 0$ and $\beta \neq 0$. Another way which doesn't require additional towing test measurements is the utilization of symmetrical conditions for forces and the moment. Let us consider the Figure 4.5 showing the ship in two turning motions along a circle trajectory at $\omega_z > 0, \beta < 0$ and $\omega_z < 0, \beta > 0$.

The following conditions can be established just from the analysis of the Fig. 4.5:

$$\begin{aligned} F_x(-\beta, \omega_z) &= F_x(\beta, -\omega_z), \\ F_y(-\beta, \omega_z) &= -F_y(\beta, -\omega_z), \\ M_z(-\beta, \omega_z) &= -M_z(\beta, -\omega_z). \end{aligned} \tag{4.18}$$

In the formulae (4.18) β and ω_z are assumed to be positive. The conditions (4.18) are applied to find the hydrodynamic characteristics at $\omega_z < \omega_{zmin}$ using the measurements done at $\omega_z > \omega_{zmin}, \beta < 0$, where ω_{zmin} is the minimum angular velocity which can be attained in the facility. To obtain the force F_y at $(\beta, -\omega_z)$ the measurement is performed at $(-\beta, \omega_z)$. The measured force $F_y(\beta, -\omega_z)$ is then multiplied by (-1). The forces and moment in the range $-\omega_{zmin} < \omega_z < \omega_{zmin}$ can be found from the interpolation of forces between $-\omega_{zmin}$ and ω_{zmin} as illustrated in Fig. 4.6. This procedure requires measurements with positive angular velocity and both positive and negative drift angles.

4.3.3 Identification method

The method uses the data obtained from the tests with self-propelled models or with real ships. During these tests the kinematic parameters of the ship motion, linear and angular velocities as well as the accelerations are measured depending on time. The motion equation systems can be written in the form

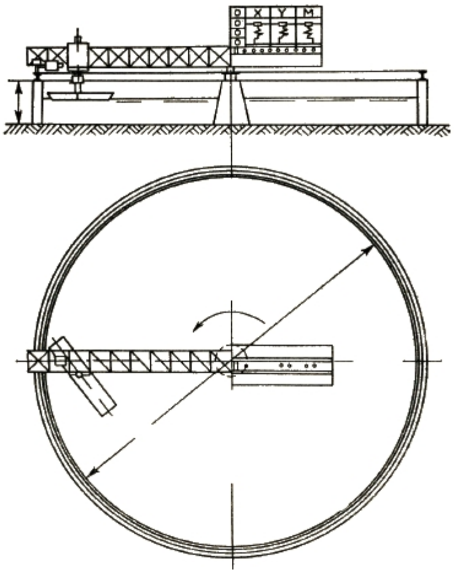

Figure 4.4: Sketch of the rotating-arm facility [35]

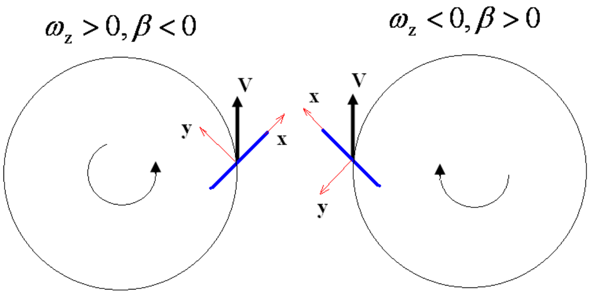

Figure 4.5: Two turning ship motions at $\omega_z > 0, \beta < 0$ and $\omega_z < 0, \beta > 0$

$$
\left\{
\begin{aligned}
& F_{xi}(V_{xi},0,0,0,0,0) + \frac{1}{2}\left\{\frac{\partial^2 F_x}{\partial V_y^2}V_{yi}^2 + \frac{\partial^2 F_x}{\partial \omega_z^2}\omega_{zi}^2 + \frac{\partial^2 F_x}{\partial V_y \partial \omega_z}V_{yi}\omega_{zi}\right\} = \\
& \quad = (m+m_{11})(\dot{V}_i \cos\beta_i - V_i\dot{\beta}_i \sin\beta_i) + (m-m_{22})V_i\omega_{zi}\sin\beta_i, \\
& \frac{\partial F_y}{\partial V_{yi}}V_{yi} + \frac{\partial F_y}{\partial \omega_z}\omega_{zi} + \frac{1}{2}\left\{\frac{\partial^2 F_y}{\partial V_y \partial \omega_z}|V_{yi}|\omega_{zi} + \frac{\partial^2 F_y}{\partial V_y^2}|V_{yi}|V_{yi} + \frac{\partial^2 F_{yi}}{\partial \omega_z^2}|\omega_{zi}|\omega_{zi}\right\} + \\
& \quad + \frac{1}{6}\frac{\partial^3 F_y}{\partial V_y \partial \omega_z^2}V_{yi}\omega_{zi}^2 = (m+m_{22})(\dot{V}_i \sin\beta_i - V_i\dot{\beta}_i\cos\beta_i) + \\
& \quad + (m-m_{11})V_i\omega_{zi}\cos\beta_i, \\
& \frac{\partial M_z}{\partial V_y}V_{yi} + \frac{\partial M_z}{\partial \omega_z}\omega_{zi} + \frac{1}{2}\left\{\frac{\partial^2 M_z}{\partial V_y \partial \omega_z}|V_{yi}|\omega_{zi} + \frac{\partial^2 M_z}{\partial V_y^2}|V_{yi}|V_{yi} + \frac{\partial^2 M_z}{\partial \omega_z^2}|\omega_{zi}|\omega_{zi}\right\} \\
& \quad + \frac{1}{6}\frac{\partial^3 M_z}{\partial V_y \partial \omega_z^2}V_{yi}\omega_{zi}^2 = (I_{zz}+m_{66})\frac{d\omega_{z_i}}{dt}
\end{aligned}
\right.
\tag{4.19}
$$

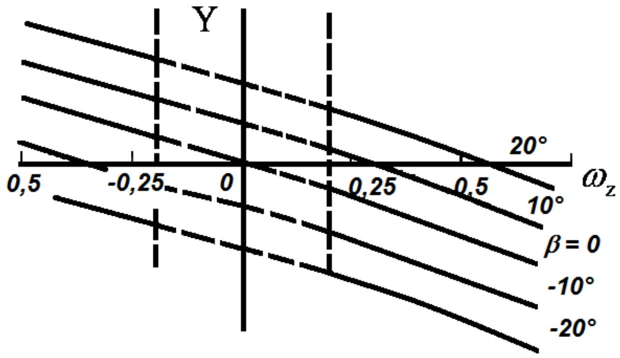

Figure 4.6: Generalization of rotating-arm tests to the range $-\omega_{zmin} < \omega_z < \omega_{zmin}$ [35]

where i is the number of measurement. The system (4.19) can be considered as a system of linear equations for determination of coefficients on the left hand side. The coefficients are assumed to be constant during the motion apart of the drag $F_{xi}(V_{xi}, 0, 0, 0, 0, 0)$ which can be found from any empirical method. Again, like in PMM tests we have more experimental points and the resulting system (4.19) is over defined (the number of equations is larger than the number of unknowns). In this case the derivatives are found from the condition that the optimal set of derivatives provides the minimum of residuals of the equations (4.19). For that different methods of the optimization theory are used.

4.3.4 Approximations of steady manoeuvring forces

Various series of experimental measurements were performed and approximated by different shipbuilding research organizations. Empirical methods of determination of manoeuvring forces are listed in the table 4.1.

Approximation proposed by the Krylov Shipbuilding Research Institute. The approximation proposed by KRSI is advantageous because it takes full nonlinearity of forces into account and it is valid for all drift angles in the wide range from zero to π, i.e. $0 < \beta < \pi$. The forces are subdivided in two components. The first component is caused by the drift angle, whereas the second one arises due to angular velocity ω_z.

The first component is represented in the form:

Method	**Reference**
Abkowitz, M. A. (1964)	Abkowitz, M. A. (1964). "Lectures on Ship Hydrodynamics - Steering and Manoeuvrability." Technical Report Hy-5. Hydro- and Aerodynamic Laboratory. Lyngby, Denmark
NORRBIN (1971)	NORRBIN, N.H. "Theory and Observations on the Use of a Mathematical Model for Ship Manoeuvring in Deep and Confined Waters" SSPA, Gothenburg, Sweden, Publication No. 68, 1971
CLARKE (1983)	CLARKE, D., GEDLING, P., HINE, G., "The Application of Manoeuvring Criteria in Hull Design Using Linear Theory" Transactions of the RINA, London, pp. 45-68, 1983
CLARKE/HORN (1997)	CLARKE, D., HORN, J.R., "Estimation of Hydrodynamic Derivatives" Proceedings of the 11th Ship Control Systems Symposium, Southampton, U. K.,Vol.3, pp. 275-289, 1997
OLTMANN (2005)	OLTMANN, P., "Identification of Hydrodynamic Damping Derivatives - a Pragmatic Approach", International Conference on Marine Simulation and Ship Manoeuvrability, Kanazawa, Japan, August 25th - 28th, 2003
SNAME (1993)	LEWANDOWSKI E., The dynamics of marine craft,World scientific, 2004, 411 p
KSRI	Handbook on ship theory, editor Prof. Voitkunski, Leningrad, Sudostroenie, Vol. III., 1985

Table 4.1: Empirical methods of determination of manoeuvring forces

$$\begin{aligned} F_{x_\beta} &= C_{x\beta}\frac{\rho V^2}{2}A_{L\sigma} \\ F_{y_\beta} &= C_{y\beta}\frac{\rho V^2}{2}A_{L\sigma} \\ M_{z_\beta} &= C_{M\beta}\frac{\rho V^2}{2}A_{L\sigma}L_{\rho\rho} \end{aligned} \tag{4.20}$$

where $A_{L\sigma}$ is the lateral area, $L_{\rho\rho}$ is the ship length between two perpendiculars. The coefficients are approximated as follows:

$$
\begin{aligned}
C_{x\beta} &= -\,0,075\sin\left\{\left[\pi - \arcsin\frac{C_{x0}}{0.075}\right]\left[1-\frac{\beta}{\varphi_x}\right]\right\}, \\
C_{y\beta} &= 0,5C^{\beta}_{y\beta}\sin 2\beta\cos\beta + c_2\sin^2\beta + c_3\sin^4 2\beta \\
C_{M\beta} &= m_1\sin 2\beta + m_2\sin\beta + m_3\sin^3 2\beta + m_4\sin^5 2\beta
\end{aligned}
\tag{4.21}
$$

C_{x0} is the ship drag at zero drift angle. The coefficients in formulae (4.21) are approximated depending on the Froude number $Fn = V/\sqrt{gL_{\rho\rho}}$, ratios $L_{\rho\rho}/B$, $L_{\rho\rho}/T_m$ (T_m is the draught at the midships), position of the center of gravity x_g and block coefficient of the lateral area σ. The angle φ_x is determined from Fig. 4.7.

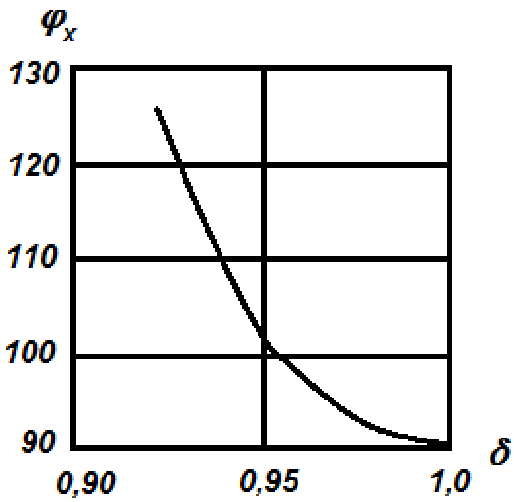

Figure 4.7: Determination of the angle φ_x

The block coefficient of the lateral area is calculated from the formula

$$
\sigma = 1 - \frac{3}{20-i}\cdot\frac{A_c}{L_{\rho\rho}\cdot T_M} + \frac{0,054}{T_M/L_{\rho\rho}}\left(\psi_1+\psi_2\right) \tag{4.22}
$$

for frames depicted in Fig. 4.8. Here i is the frame at which the U-shaped frames become V-shaped. If the ship has U-shaped frames along the whole lengths, i is the frame number where the buttock alleviates in the symmetry plane (see Fig. 4.9). The choice of the area A_c is illustrated in Fig. 4.10.

The formula (4.22) is valid for ships with conventional stern shape shown in Fig. 4.8. For ships with cigar shaped stern (Fig. 4.11 left) and well developed

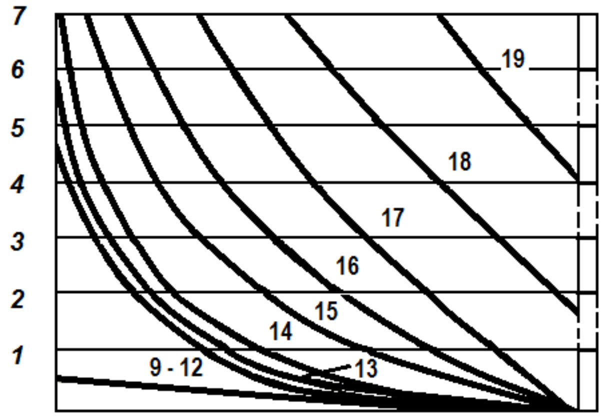

Figure 4.8: Shape of frames in the stern area

deadwood (Fig.4.11 right) the following formulae have to be used:

$\sigma = 0,975 + \frac{0,054}{T_M/L_{\rho\rho}}\left(\psi_1 + \psi_2\right)$ for frames depicted in Fig. 4.11 left

$\sigma = 0,962 + \frac{0,054}{T_M/L_{\rho\rho}}\left(\psi_1 + \psi_2\right)$ for frames depicted in Fig. 4.11 right

Here ψ_1 is the trim angle of the ship at the rest. Calculation of the running ship trim ψ_2 is performed according to the table 4.2.

The lateral area $A_{L\sigma}$, the block coefficient C_B are calculated from:

$$A_{L\sigma} = L_{\rho\rho} \cdot T_M \cdot \sigma$$

$$C_B = \frac{V}{L_{\rho\rho} \cdot B \cdot T_M}$$

The coefficients in (4.21) are calculated from the following approximations:

$$C^{\beta}_{Y\beta} = a_3 \cdot \mathfrak{B} + b_3$$

$$\mathfrak{B} = a_2 \mathfrak{U} + b_2$$

$$a_3 = 0,2392 \cdot C^2_\rho - 0,4009 \cdot C_\rho + 0,1815$$

$$b_3 = 0,4033 \cdot C^2_\rho - 0,6965 \cdot C_\rho + 0,3263$$

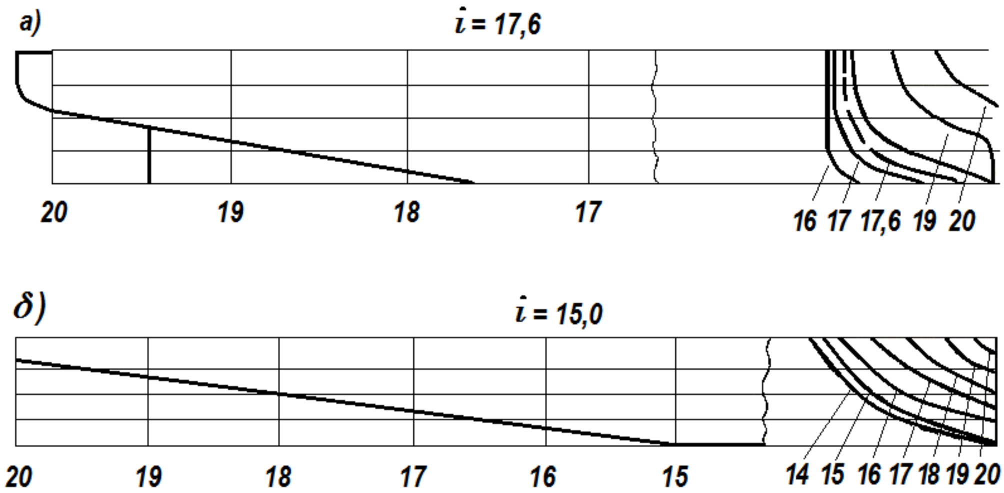

Figure 4.9: Determination of i in the formula (4.22)

$C_M = \frac{A_{s\rho}}{B \cdot T_M}$

$C_P = \frac{C_B}{C_M}$

$\mathfrak{U} = a_1 \left(\frac{L\rho\rho}{B}\right) + b_1$

$a_2 = 16,67 \left(\frac{T_M}{L_{\rho\rho}}\right)^2 - 11,92 \left(\frac{T_M}{L_{\rho\rho}}\right) + 0,06$

$b_2 = -261,1 \left(\frac{T_M}{L_{\rho\rho}}\right)^2 + 213,6 \left(\frac{T_M}{L_{\rho\rho}}\right) - 2,468$

Coefficients are calculated according to the table 4.3.
$c_2 = a_3\mathfrak{B} + b_3,$

Where a_3 and b_3 are calculated from the table 4.4.

$$c_3 = a_2\mathfrak{U} + b_2,$$
$$a_2 = 2,569(T_M/L)^2 - 0,5805(T_M/L) + 0,00183;$$
$$b_2 = -27,7(T_M/L)^2 + 6,428(T_M/L) - 0,01749;$$
$$\mathfrak{U} = a_1(L/B) + b_1,$$

The parameter ϕ is the ratio of the block coefficient to the block coefficient of the middle frame β_m.

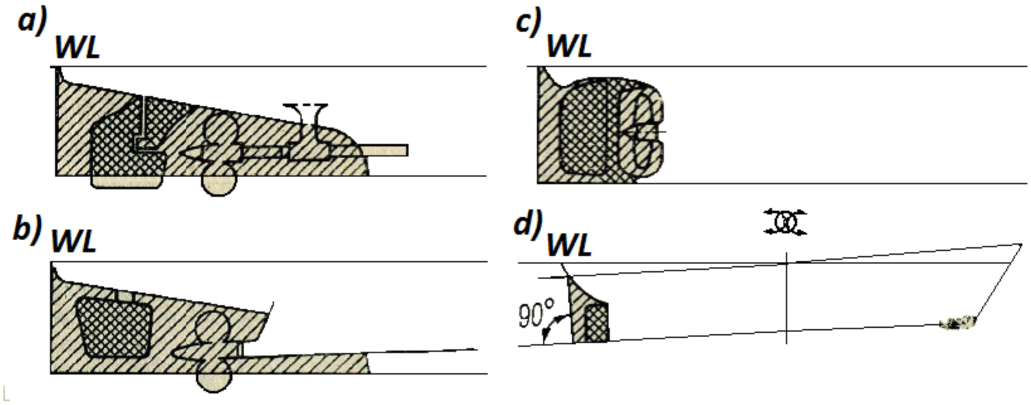

Figure 4.10: Samples of the choice of the area A_c

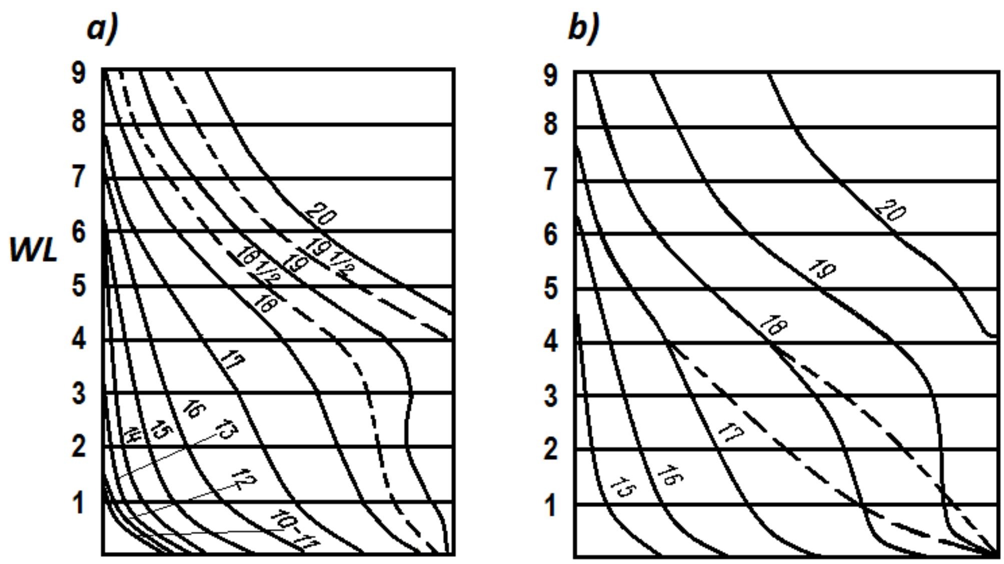

Figure 4.11: Frames in the stern area: left - cigar-shaped stern, right - well developed deadwood

$$
\begin{aligned}
m_1 =& a_1 \cdot \mathfrak{C} + b_1 \\
\mathfrak{C} =& \mathfrak{C}_{\nu 0} + \mathfrak{C}_u \\
a_1 =& -0,1317 \left(\frac{T_M}{L_{\rho\rho}}\right)^2 + 0,05358 \left(\frac{T_M}{L_{\rho\rho}}\right) + 0,000181 \\
b_1 =& -2,361 \left(\frac{T_M}{L_{\rho\rho}}\right)^2 + 0,8653 \left(\frac{T_M}{L_{\rho\rho}}\right) - 0,000161 \\
\mathfrak{U} =& \mathfrak{U} + \mathfrak{C}_\phi
\end{aligned}
$$

Table 4.2: Calculation of ψ_2 and $\overline{x}_g = x_g/L_{\rho\rho}$

Fn	ψ_2	$\overline{x}_g$	**coefficients**
$0.34 <$ Fn < 0.42	$\psi_2 = a_1 \cdot F_n^2 + b_1 \cdot F_n + c_1$	$\overline{x}_g < -0.015$	$a_1 = 525\overline{x}_g^2 + 32,35\overline{x}_g + 1,032$ $b_1 = -345\overline{x}_g^2 + 22,95\overline{x}_g - 0,661$ $c_1 = 50,7\overline{x}_g^2 + 3,725\overline{x}_g + 0,1017$
		$\overline{x}_g > -0.015$	$a_1 = 810\overline{x}_g^2 + 24,6\overline{x}_g + 0,853$ $b_1 = -620\overline{x}_g^2 - 19,9\overline{x}_g - 0,565$ $c_1 = 121\overline{x}_g^2 + 3,84\overline{x}_g + 0,0925$
$0.42 <$ Fn < 0.46	$\psi_2 = a_1 \cdot F_n + b_1$	$\overline{x}_g < -0.02$	$a_1 = -5\overline{x}_g^2 - 0,55\overline{x}_g + 0,151$ $b_1 = 2,5\overline{x}_g^2 - 0,055\overline{x}_g - 0,058$
		$-0.02 < \overline{x}_g \leq 0$	$a_1 = -0,375\overline{x}_g + 0,153$ $b_1 = 2\overline{x}_g^2 + 0,03\overline{x}_g - 0,0583$
		$\overline{x}_g > 0$	$a_1 = -0,375\overline{x}_g + 0,153$ $b_1 = 1,5\overline{x}_g^2 + 0,005\overline{x}_g - 0,0583$
$0.46 < Fn < 0.54$	$\psi_2 = a_1 \cdot F_n + b_1$	$\overline{x}_g < -0.04$	$a_1 = 0,75\overline{x}_g + 0,12$ $b_1 = -0,55\overline{x}_g - 0,043$
		$-0.04 < \overline{x}_g \leq -0$	$a_1 = 0,5\overline{x}_g + 0,112$ $b_1 = -0,42\overline{x}_g + 0,0391$
		$\overline{x}_g > -0.01$	$a_1 = 0,25\overline{x}_g + 0,11$ $b_1 = -0,2967\overline{x}_g - 0,0379$

$0,55 \leqslant \phi \leqslant 0,70$

$$\mathfrak{U}_0 = -235\sigma^2 + 474,2\sigma - 235,8;$$
$$\mathfrak{C}_\phi = -74,67\phi^2 + 110,9\phi - 39,64;$$

$0,70 \lessdot \phi \leqslant 0,85$

$$\mathfrak{U}_0 = -210\sigma^2 + 422,9\sigma - 207,2;$$
$$\mathfrak{C}_\phi = 12\phi^2 - 8,8\phi - 0,64;$$

$\mathfrak{U} > 4$

$$\mathfrak{U} = \mathfrak{U}_0 + \mathfrak{C}_\phi;$$
$$\mathfrak{C}_u = -1,3\mathfrak{U} + 7,8;$$
$$\mathfrak{C}_{\nu 0} = 0,02333(L/B)^2 - 0,045(L/B) + 1,187;$$

Table 4.3: Calculation of a_1 and b_1

L / B	σ	**coefficients**
$4 \leq L/B \leq 6$	$0.93 \leq \sigma \leq 0.95$	$a_1 = 375\sigma^2 - 725,8\sigma + 349,5$ $b_1 = 3000\sigma^2 - 5702\sigma + 2723$
	$0.95 < \sigma \leq 0.97$	$a_1 = 150\sigma^2 - 293,5\sigma + 141,97$ $b_1 = 800\sigma^2 - 1560\sigma + 773,5$
	$\sigma > 0.97$	$a_1 = -1,137\sigma^2 + 0,24\sigma - 0,753$ $b_1 = -4,667\sigma + 17,57$
$6 < L/B \leq 8$	$0.93 \leq \sigma \leq 0.95$	$a_1 = 1000\sigma^2 - 1898\sigma + 900$ $b_1 = 1800\sigma^2 - 3494\sigma + 1705$
	$0.95 < \sigma \leq 0.97$	$a_1 = 175\sigma^2 - 339,8\sigma + 163,9$ $b_1 = -30\sigma + 38,42$
	$\sigma > 0.97$	$a_1 = -0,5\sigma - 0,485$ $b_1 = 516,7\sigma^2 - 1032\sigma + 523,7$
$8 < L/B \leq 10$	$0.93 \leq \sigma \leq 0.95$	$a_1 = 350\sigma^2 - 664,5\sigma + 314,96$ $b_1 = 3600\sigma^2 - 6928\sigma + 3339$
	$0.95 < \sigma \leq 0.97$	$a_1 = -1,5\sigma + 0,985$ $b_1 = 2000\sigma^2 - 3894\sigma + 1901$
	$\sigma > 0.97$	$a_1 = 1,5\sigma + 0,985$ $b_1 = 316,67\sigma^2 - 629,5\sigma + 318$

$\mathfrak{U} \leqslant 4$ $$\mathfrak{C}_u = -1,3\mathfrak{U}_0 + 2,6;$$

$$\mathfrak{E}_{\nu 0} = 0,01792(L/B)^2 + 0,1275(L/B) + 6,113.$$

$$m_2 = -\frac{1n(1,023\sigma)}{11,6\sigma - 9,29}.$$

Table 4.4: Calculation of a_3 and b_3

$T_m/L \leq 0.04$	$a_3 = (T_M/L)^2 + 0,85(T_M/L) + 0,0311;$ $b_3 = -55(T_M/L)^2 + 7,85(T_M/L) + 0,124;$	
$0.04 < T_m/L \leq 0.06$	$a_3 = (T_M/L)^2 + 0,615(T_M/L) + 0,0405;$ $b_3 = 40(T_M/L)^2 - 0,1(T_M/L) + 0,29;$	
$0.06 < T_m/L \leq 0.08$	$a_3 = -5(T_M/L)^2 + 1,05(T_M/L) + 0,036;$ $b_3 = -10(T_M/L)^2 + 2,5(T_M/L) + 0,314;$ $\mathfrak{U} = a_1\sigma + b_1,$ $a_1 = 54,46\phi - 59,43;$ $b_1 = -31,44\phi + 46,8;$ $\mathfrak{B} = a_2(L/B) + b_2,$	
	$\mathfrak{U} \leq 2$	$a_2 = -0,0105\mathfrak{U}^2 - 0,0585\mathfrak{U} + 0,985;$ $b_2 = 0,06\mathfrak{U}^2 - 0,65\mathfrak{U} + 2,91;$
	$2 \lessdot \mathfrak{U} \leq 5$	$a_2 = 0,001\mathfrak{U}^2 - 0,079\mathfrak{U} + 0,98;$ $b_2 = -0,0267\mathfrak{U}^2 - 0,41\mathfrak{U} + 2,78;$
	$\mathfrak{U} > 5$	$a_2 = -0,005\mathfrak{U}^2 - 0,015\mathfrak{U} + 0,81;$ $b_2 = 0,03\mathfrak{U}^2 - 0,89\mathfrak{U} + 3,76.$

$0,55 \leqslant \phi \leqslant 0,72$	$a_1 = 24,65\phi^2 - 29,67\phi + 7,547;$
$0,72 \lessdot \phi \leqslant 0,85$	$a_1 = 5,917\phi - 5,3;$
$0,55 \leqslant \phi \leqslant 0,68$	$b_1 = -60,44\phi^2 + 74,61\phi - 9,255;$
$0,68 \lessdot \phi \leqslant 0,85$	$b_1 = -10,08\phi + 20,34.$

$$m_3 = a_2\mathfrak{U} + b_2,$$

$$a_2 = \left(\epsilon^{8,20939\phi}0,7728 \cdot 10^{-3} - 1,873\right) \cdot 10^{-3};$$
$$b_2 = \left(-e^{7,47893\phi}0,4404 \cdot 10^{-2} + 5,709\right) \cdot 10^{-2};$$
$$\mathfrak{U} = \frac{a_1\sigma + b_1}{\sigma - 1,029},$$

$$a_1 = 31,26 - 9,0146e^{0,066947L/B};$$
$$b_1 = 8,6245e^{0,071419L/B} - 31,26.$$

$$m_4 = \mathfrak{C}_{m_4} + \mathfrak{C}_u,$$

$T_M/L \leqslant 0,028$

$$\mathfrak{C}_{m_4} = -71,88(T_M/L)^2 + 4,238(T_M/L) - 0,066;$$

$0,028 < T_M/L \leqslant 0,040$

$$\mathfrak{C}_{m_4} = -9,375(T_M/L)^2 + 0,8875(T_M/L) - 0,0212;$$

$T_M/L > 0,040$

$$\mathfrak{C}_{m_4} = -3,833(T_M/L)^2 + 0,415(T_M/L) - 0,01117;$$

$$\mathfrak{C}_u = 0,00827\mathfrak{U} - 0,017;$$

$$\mathfrak{U} = \mathfrak{U}_0 + \mathfrak{C}_8,$$

$0,55 \leqslant \phi \leqslant 0,64$

$$\mathfrak{U}_0 = -140,62\phi^2 + 180,62\phi - 53,35;$$

$0,64 < \phi \leqslant 0,74$

$$\mathfrak{U}_0 = -56,67\phi^2 + 75,10\phi - 20,2;$$

$0,74 < \phi \leqslant 0,85$

$$\mathfrak{U}_0 = -216,7\phi^2 + 312,8\phi - 108,51;$$

$0,93 \leqslant \phi \leqslant 0,96$

$$\mathfrak{C}_S = 1900\sigma^2 - 3696\sigma + 1796;$$

$0,96 \lessdot \sigma \leqslant 1,0$

$$\mathfrak{C}_S = 3917\sigma^2 - 810,4\sigma + 416,4.$$

It is assumed that the rotation with the angular velocity ω_z does not contribute to the ship resistance C_x and to the side force C_y. The contribution to the yaw moment is calculated from the following approximations:

$$M = \frac{\rho A_{L\sigma} L}{2}\left[-C_{M0}L^2|\omega|\omega - C_{M\omega}\frac{1}{\pi}\left(\nu^2 + L^2\omega^2\right)\sin\pi\Omega\right]$$

$$\Omega = \frac{\Omega'}{\sqrt{1+\Omega'^2}}, \qquad \Omega' = \frac{\omega_z L}{V}$$

$$C_{M0} = 0,059c_2;$$

$$C_{M\omega} = C_{M\omega}^{\omega} + a_1|\sin\beta| + a_2\left\{1 - \cos\left[(2\pi - 4|\beta|)\cos\beta + 0,1|\sin 2\beta|\right]\right\},$$

$$C_{M\omega}^{\omega} = (0,739 + 8,7T_M/L)\left(1,611\sigma^2 - 2,873\sigma + 1,33\right).$$

$$a_1 = 0,09 - C^{\omega}_{M\omega} - 0,0033\left(\frac{L}{B} - 7\right) - 20\left(\frac{T_M}{L} - 0,005\right)^2 +$$
$$+0,4(\sigma - 0,9) + 0,05(\beta_M - 0,9);$$
$$a_2 = 0,008\frac{L}{B} + 0,9\left(\frac{T_M}{L} - 0,05\right) + 0,45(\sigma - 0,955).$$

4.4 Exercises

Study of Manoeuvrability
To study the manoeuvrability of a ship standard manoeuvres are performed. Usually turning circle and zig-zag manoeuvres are used to judge the steering capabilities. Use the manoeuvring software MANIS (Manoeuvring in sea)[2] to conduct the following computations.

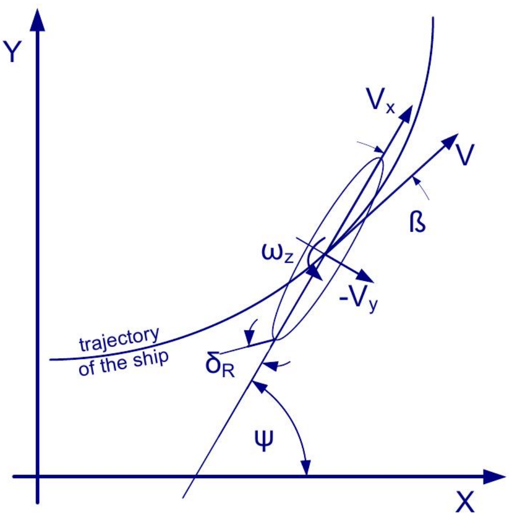

Figure 4.12: Coordinates system for manoeuvring ships

Turning Circle Manoeuvre
Perform a turning circle manoeuvre for $\delta_R = 20°$. To see the influence of the ship′s velocity, set propeller revolution to 1, 2 and 4 rps respectively. Set initial longitudinal velocity first! Also vary the draught about ± 3 m. Study the influence on the static velocity reduction, static drift angle and static turning radius.

[2] http://www.lemos.uni-rostock.de/lehre/schiffstheorie-i/

Spiral Manoeuvre

Do a spiral manoeuvre for the ship, plot the dimensionless yaw rate (Ω) over the rudder angle (δ_R) for different turning circle manoeuvres using $-10° < \delta_R < 10°$. Show the influence of trim ($\pm 3m$) on the behavior of the ship. Plot the dimensionless yaw rate over the rudder angle and discuss the effect on the dynamic stability according to the curves.

Zig-Zag Manoeuvre

Accomplish 10/10 zig-zag manoeuvres. Vary the velocity (propeller revolution), trim and draught, respectively. Plot the value of the first overshoot angle, time period and the initial turning ability (ITA, see figure 4.13) over the velocity, trim and draught. Figure out which variation has the biggest impact on each criterion.

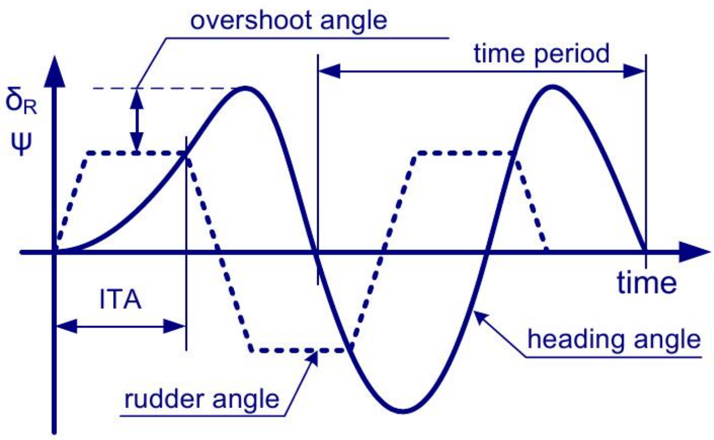

Figure 4.13: Development of rudder and heading angle during zig-zag manoeuvre

Ship Extension

The shipowner asked to extend the ship to increase the loading capacity. Therefore a parallel midships section with length of10 % of the ships length will be added amidships. As a side condition, the static turning diameter must not exceed a rise of 10 % compared to the old ship configuration at a rudder angle of $\delta_R = 20°$. Compute the parameters ($L, B, T, C_B, C_M, ...$) for the new ship if necessary and implement them in MANIS. If the new turning circle diameter exceeds a rise of 10 %, apply changes in the ship configuration like rudder area or effective aspect ratio of the rudder to match the criteria.

Note: Before starting a case, check the correlation between propeller revolution and initial velocity. Therefore, carry out a turning circle with $\delta_R = 0°$, and make sure that the static velocity is sufficiently close (first decimal place) to the initial velocity. Vary one parameter at a time, only! No cross-coupling!

Formulae:

$$C_B = \frac{\nabla}{LBT} \quad C_M = \frac{A_{midship}}{BT} \quad \Omega = \frac{L}{V}\omega_z \quad \Omega = \frac{L}{R}$$

Table 4.5: Variations of different ship parameters

Propeller revolution	n_{prop}	$1.0, 2.0, 4.0$	rpm
Draught (change)	ΔT	$-3.0, 0.0, +3.0$	m
Trim	tr	$-3.0, 0.0, +3.0$	m

To evaluate the studies on manoeuvrability use graphs and plot them -if appropriate- in the same diagram. Describe the graphs and the influence of the different varied parameters on the manoeuvring parameters. Make sure everyone uses a different ship! Use alphabetic order of your first names!

Chapter 5

Calculation of steady manoeuvring forces using slender body theory

Summary: The simplest theory of steady manoeuvring forces determination is presented in this chapter. The application of this theory is only possible in conjunction with Kutta condition.

5.1 Force distribution on the slender body in the potential flow

The formalism of the slender body theory is based on the potential inviscid theory and asymptotic estimations (2.3). The governing equations are derived using the concept of the active cross section with the thickness Δx at the abscissa x (see Fig. 5.1). First, we consider the steady ship motion under a positive drift angle. Due to ship motion the ship frame in the cross section is moved with the velocity $V_y = -V \sin\beta$ in y direction. The momentum of the flow in the cross section reads:

$$\Delta P = m'_{22} V_y \Delta x = -\rho\pi C(x) T^2(x) V \sin\beta \Delta x \tag{5.1}$$

According to the momentum theorem, the transverse force acting on the frame of the doubled body at x is calculated through the time derivative of the momentum in the earth fixed reference system

$$\Delta F_y = -\frac{d(\Delta P)_a}{dt} \tag{5.2}$$

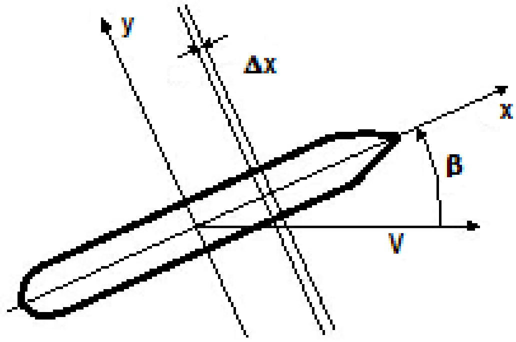

Figure 5.1: Active cross section along the ship length

The change of the flow momentum is caused by the change of the frame in the cross section due to motion with the velocity $V_x = V\cos\beta$. The time derivative can be replaced by the derivative on x coordinate

$$dx = -V\cos\beta dt \Rightarrow \frac{dx}{dt} = -V\cos\beta$$

$$\Delta F_y = -\frac{d(\Delta P)_a}{dt} = -\frac{d(\Delta P)}{dx}\frac{dx}{dt} \tag{5.3}$$

Substitution of the equation (5.1) into (5.3) gives

$$\Delta F_y = -\frac{d(\Delta P)}{dx}\frac{dx}{dt} = -\rho\pi\frac{d(C(x)T^2(x))}{dx}V^2\sin\beta\cos\beta\Delta x \tag{5.4}$$

Herewith the derivative of the transverse force on x coordinate is:

$$\frac{dF_y}{dx} = \frac{\Delta F_y}{\Delta x} = -\rho\pi\frac{d(C(x)T^2(x))}{dx}V^2\sin\beta\cos\beta \tag{5.5}$$

Since the drift angle is assumed to be small $\sin\beta \sim \beta, \cos\beta \sim 1$, the last expression takes the form

$$\frac{dF_y}{dx} = -\rho\pi V^2\frac{d(C(x)T^2(x))}{dx}\beta \tag{5.6}$$

The distribution of $C(x)T^2(x)$ and $\frac{dF_y}{dx}$ along the ship is presented in Fig. 5.2. The $C(x)T^2(x)$ has maximum in the central part of the ship where the frame shapes are full, i.e. $C(x)$ is maximum. In the bow and stern regions either $C(x) = 0$ or $T^2(x) = 0$. The derivative $\frac{d(C(x)T^2(x))}{dx}$ and the force distribution $\frac{dF_y}{dx}$ are maximal in bow and stern regions. In the central part along the ship length the $C(x)T^2(x)$=const and no force $\frac{dF_y}{cx}$=0 arises within this region. This force distribution is in accordance with the force scheme given

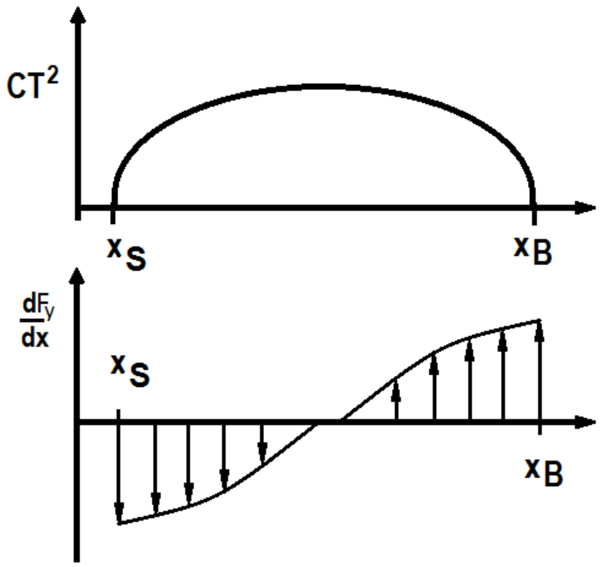

Figure 5.2: Distribution of $C(x)T^2(x)$ and of the transverse force (5.6) along the ship length

in Fig. 2.2.

The force arising within the ship length from x to the bow $x = x_B$ is

$$F_y(x) = \int\limits_x^{x_B} \frac{dF_y}{dx} dx = -\rho\pi V^2 \int\limits_x^{x_B} \frac{d(C(x)T^2(x))}{dx} dx\beta = \rho\pi V^2 C(x)T^2(x)\beta \tag{5.7}$$

At $x = x_S$, $F_y(x_S) = \rho\pi V^2 C(x_S)T^2(x_S)\beta$ is zero because $C(x_S)T^2(x_S) = 0$ what is in accordance with the paradox of d'Alambert. On the contrary, the moment is not zero

$$\begin{aligned} \int\limits_{x_S}^{x_B} \frac{dF_y}{dx} x dx = -\rho\pi \int\limits_{x_S}^{x_B} \frac{d(C(x)T^2(x))}{dx} x dx V^2\beta = \\ = \rho\pi \int\limits_{x_S}^{x_B} C(x)T^2(x) dx V^2\beta = m_{22}V^2\beta \end{aligned} \tag{5.8}$$

This moment is exactly equal to the Munk moment

$$M_{Munk} = V_x V_y (m_{22} - m_{11}) \approx V^2 m_{22} \beta \tag{5.9}$$

what is quite expectable, because no other moment can arise during the steady motion.
Let us consider a more complicated ship motion with the drift angle and the angular velocity. The ship velocity V is kept constant. The presence of the angular velocity causes additional velocity in the each cross section along the ship

$$\omega_z x = \frac{V}{R} x = V \Omega \frac{x}{L} \tag{5.10}$$

which should be added to the incoming velocity due to the drift angle

$$V_y(x) = -V \sin \beta + V \Omega \frac{x}{L} \approx -V(\beta - \Omega \frac{x}{L}) = -V \beta(x) \tag{5.11}$$

where $\beta(x)$ is the effective drift angle which is variable along the ship length. The formulae (5.6) - (5.7) have to be rewritten taking variability of the drift angle along the ship

$$\begin{aligned} \frac{dF_y}{dx} &= -\rho \pi V^2 \frac{d(C(x)T^2(x)\beta(x))}{dx} = -\rho \pi V^2 \frac{d(C(x)T^2(x)(\beta - \Omega \frac{x}{L}))}{dx} = \\ &= -\rho \pi V^2 \left[\frac{d(C(x)T^2(x))}{dx} \beta - \frac{d(C(x)T^2(x))}{dx} \frac{x}{L} \Omega - C(x)T^2(x) \frac{\Omega}{L} \right] \end{aligned} \tag{5.12}$$

$$\begin{aligned} F_y(x) = \int_x^{x_B} \frac{dF_y}{dx} dx = -\rho \pi V^2 \left[\int_x^{x_B} \frac{d(C(x)T^2(x))}{dx} dx \beta - \int_x^{x_B} \frac{d(C(x)T^2(x))}{dx} \frac{x}{L} dx \Omega \right. \\ \left. - \int_x^{x_B} C(x)T^2(x) dx \frac{\Omega}{L} \right] = \rho \pi V^2 \left[C(x)T^2(x)\beta - \frac{x}{L} C(x)T^2(x)\Omega \right] \end{aligned} \tag{5.13}$$

Distributions of the transverse force components proportional to terms $\frac{d(C(x)T^2(x))}{dx}\frac{x}{L}$ and $C(x)T^2(x)$ along the ship length are presented in Fig. 5.3. Analyzing the upper picture, please note that the origin is in the ship center, i.e. $x_B > 0$ and $x_S < 0$. Therefore $-\frac{d(C(x)T^2(x))}{dx}\frac{x}{L}$ is negative both in bow and stern regions. As in the case $\Omega = 0$ the full transverse force is zero when $\Omega \neq 0$, i.e. $F_y(x_H) = 0$. Again, like in the previous case $\beta \neq 0$, $\Omega = 0$ the moment is not zero.

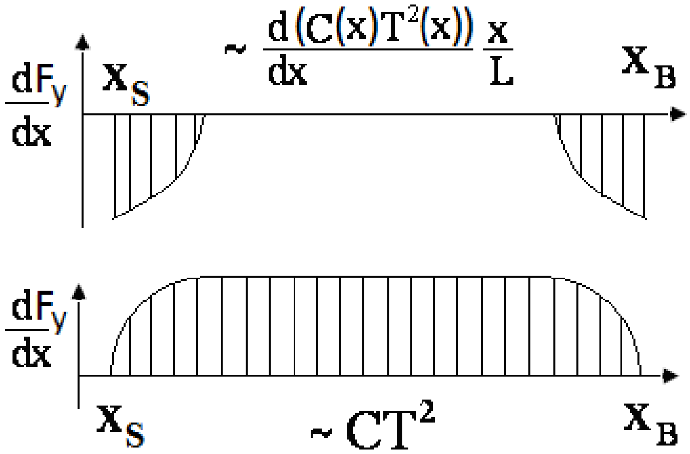

Figure 5.3: Distribution of the transverse force components proportional to terms $\sim \frac{d(C(x)T^2(x))}{dx}\frac{x}{L}$ and $\sim C(x)T^2(x)$ along the ship length

5.2 Improvement of the slender body theory. Kutta condition

At a glance the slender body theory is not practical because it is not capable predicting the transverse force. This problem can be overcome in a way similar to the famous Kutta condition introduced in the airfoil theory (see chapter 5.4 in [23]). As explained above the force arises due to a drastic change of the flow in the stern area (see Fig. 2.2b). This change is caused due to viscosity influence. The boundary layer is developed starting from the bow. The vortices of the boundary layer shed from the stern alter the flow. As a result the force acts only on the front part of the ship. According to the slender body theory it is assumed that the force arises within the ship section starting from the bow to the widest frame. This choice can be established using the similarity between the ship and the wing of small aspect ratio.

Let us consider the wing under a small angle of attack β (Fig. 5.4) and $\Omega = 0$. Because the aspect ratio is small the flow around of any transversal wing section is nearly two dimensional like it is shown for section AB (see Fig. 5.4 a and b). The incident velocity is $V \sin\beta$ in each wing section. According to the vortex wing theory (see chapter 5 in [23]) each section contains transversal bound vortices generating the lift and free streamwise vortices which are necessary to make the transversal vortices closed at infinity. The traces of longitudinal free vortices in different cross sections along the wing are shown in Fig. 5.4c. To understand the vortex scheme better the reader is referred to the section 5.9.2.2 in [23]. Both free and bound vortices induce the downwash to counterbalance the incident velocity $V \sin\beta$. If the aspect ratio is small the contribution from the bound vortices can be neglected. Indeed, as said above, locally in each transversal section the wing acts on the fluid like a plate with infinite chord. The problem is quasi two dimensional at each x. The bound vortices in front of the section induce negative downwash velocities whereas the bound vortices behind the section induce the positive up wash velocity. Since the cross section is changed slowly the downwash and up wash contributions are nearly equal. The resulting velocity is zero. On the contrary the contribution of free vortices is significant. Each free vortex shed from the section at x propagates along the wing downstream and influences the sections downstream. The total intensity of free vortices is growing along the wing chord. The no penetration condition is satisfied in each section:

$$\underbrace{\int_{-B(x)/2}^{B(x)/2} \frac{\gamma(y)}{y-\eta}\, dy}_{\text{normal velocity component induced by free vortices}} = 2\pi V \sin\beta \tag{5.14}$$

The local span $B(x)$ is changed along the x axis. Let us assume that the no penetration condition was satisfied at $x = x$ and we proceed to the next section at $x = x + \Delta x$. The next section has the span from $-B(x+\Delta x)/2$ to $B(x+\Delta x)/2$ consisting the old part from $-B(x)/2$ to $B(x)/2$ and new winglets $[-B(x+\Delta x)/2, -B(x)/2]$ and $[B(x)/2, B(x+\Delta x)/2]$. The free vortices shed from the section at x would be able to satisfy the no penetration condition within $-B(x)/2$ to $B(x)/2$. But they are not sufficient to satisfy the no penetration condition on the whole width from $-B(x+\Delta x)/2$ to $B(x+\Delta x)/2$. New free vortices have to arise at $x = x + \Delta x$. According to the fluid mechanics theorem the vortex lines should be the closed lines. It means that the appearance of the longitudinal vortices leads automatically to the appearance of the transversal bound vortices. They generate the lift in the section $x = x + \Delta x$.

Let us consider now two sequential sections HG with the largest span and IJ. The span of IJ is either the same or smaller than that of HG. No new winglets arise. It is assumed that the flow does not follow the wing contour rather than separates at the section with the maximum width. The free vortices coming from the section HG are able to satisfy the no penetration condition on the whole span in the section IJ because they were able to do it on a larger span at x. No new free vortices are necessary. It means no bound vortices appear in the sections behind HG. Therefore, no lift is generated behind the section HG.

Generalizing this analysis to a slender body theory, it is assumed that the transverse force appears only on the ship part in front of the maximum width frame section at x_{max}. This section can be identified as the section where the product $C(x)T^2(x)$ is maximal. Therefore, the first term in (5.12) $-\rho\pi V^2 \frac{d(C(x)T^2(x))}{dx}\beta$ has to be integrated from x_{max} to x_B.

Let us consider now the case $\beta = 0, \Omega \neq 0$. In this case the no penetration condition reads:

$$\underbrace{\int_{-B(x)/2}^{B(x)/2} \frac{\gamma(y)}{y-\eta}\, dy}_{\text{normal velocity component induced by free vortices}} = 2\pi\omega_z x \tag{5.15}$$

The force arises due to two reasons. First, like in the case $\beta \neq 0, \Omega = 0$ new free vortices arise in each section downstream due to change of the wing span. Second, the new free vortices appear because the right side of the equation (5.15) is changed along the wing chord. The first effect is described by the second term in (5.12) $\rho\pi V^2 \frac{d(C(x)T^2(x))}{dx}\frac{x}{L}\Omega$, whereas the second effect by the third term $C(x)T^2(x)\frac{\Omega}{L}$. The contribution of the term $\rho\pi V^2\Omega/L\frac{d(C(x)T^2(x)x)}{dx}$ to the transverse force caused by the rotation is calculated as follows:

- between x_{max} and x_B this term is realized in the full form $\rho\pi V^2\Omega/L\frac{d(C(x)T^2(x)x)}{dx}$,
- behind the x_{max} the second term in $\rho\pi V^2\Omega/L\frac{d(C(x)T^2(x)x)}{dx} = \rho\pi V^2\Omega/L\left\{C(x)T^2(x) + x\frac{d(C(x)T^2(x))}{dx}\right\}$

is zero because the frames of the modified body are not changed behind x_{max} due to flow separation at x_{max} (compare sections HG, IJ and KL in Fig. 5.4c). It is assumed, that the oscillations of the ship wake are neglected at small ω_z.

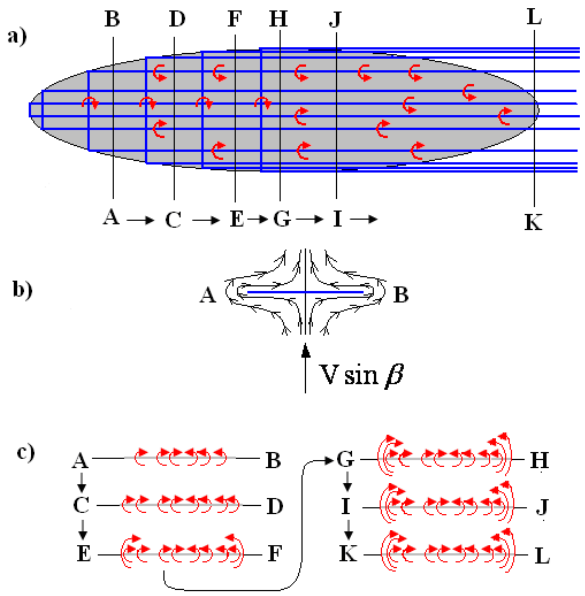

Figure 5.4: Explanation of force appearance on the slender body using similarity with the flow around the wing with small aspect ratio

With these considerations the transverse force distribution along a slender body takes the form:

$$\frac{dF_y}{dx} = -\rho\pi V^2 \left[\frac{d(C(x)T^2(x))}{dx} \beta - \frac{d(C(x)T^2(x))}{dx} \frac{x}{L}\Omega - C(x)T^2(x)\frac{\Omega}{L} \right]$$
$$\text{at} \quad x_{\max} \leq x \leq x_B \tag{5.16}$$

$$\frac{dF_y}{dx} = \rho\pi V^2 C(x)T^2(x)\frac{\Omega}{L} \quad \text{at} \quad x_S \leq x \leq x_{\max} \tag{5.17}$$

The total force and moment are obtained by integration:

$$F_y = \frac{\rho\pi V^2}{2} \left[CT^2_{\max}\, \beta - CT^2_{\max} \frac{x_{\max}}{L}\Omega + \frac{\Omega}{L} \int\limits_{x_S}^{x_{\max}} C(x)T^2(x)dx \, \right] \tag{5.18}$$

$$
\begin{aligned}
M_z &= \int\limits_{x_H}^{x_B} x\frac{dF_y}{dx}dx = \\
&= -\frac{\rho\pi}{2}V^2\left[\beta\int\limits_{x_{\max}}^{x_B} x\frac{d(C(x)T^2(x))}{dx}dx - \frac{\Omega}{L}\times\right. \\
&\left.\left\{\int\limits_{x_{\max}}^{x_B} x^2\frac{d(C(x)T^2(x))}{dx}dx + \int\limits_{X_H}^{x_B} C(x)T^2(x)xdx\right\}\right]
\end{aligned}
\tag{5.19}
$$

Here, additionally the factor 1/2 is introduced because the force acting on the ship is a half of the force acting on doubled body. CT^2_{max} is the value of CT^2 at x_{max}.

Introducing the force coefficients, we obtain from (5.18)

$$
C_y = C_y^\beta\beta + C_y^\Omega\Omega = \frac{\pi}{A_L}CT^2_{\max}\beta + \frac{\pi}{A_L}\left[-\frac{x_{\max}}{L}CT^2_{\max} + \int\limits_{x_H/L}^{x_{\max}/L} CT^2 d(\frac{x}{L})\right]\Omega
$$

These formulae take a very simple form for the case $C = const, T = const$:

$$
\begin{aligned}
&F_y = C_y\frac{\rho V^2}{2}LT, C_y = C_y^\beta\beta + C_y^\Omega\Omega, \\
&M_z = m_z\frac{\rho V^2}{2}L^2T, m_z = m_z^\beta\beta + m_z^\Omega\Omega, \\
&C_y^\beta = \frac{\pi C\lambda}{2}, m_z^\beta = \frac{\pi C\lambda}{4}, \\
&C_y^\Omega = \frac{\pi C\lambda}{4}, m_z^\Omega = -\frac{\pi C\lambda}{8}.
\end{aligned}
\tag{5.20}
$$

where $\lambda = \frac{2T}{L}$ the coefficients in (5.20) are nondimensionalized by use of the ship length L and the lateral area $A_L = L \cdot T$. The moment is calculated around the ship center. Since $m_z^\Omega < 0$ the moment component $m_z^\Omega\Omega$ is the stabilizing one, whereas $m_z^\beta\beta$ causes the instability.

The forces, obtained using the slender body theory, contain only the linear components. The nonlinear components should be added additionally.

5.3 Exercises

1. Calculate the added mass for m_{55} and m_{35} for the slender body.

2. Calculate the Lewis coefficient for the frame ($x = a/2$) of the ellipsoid of revolution with semi-axis $a = 5$ m and $b = 1$ m.

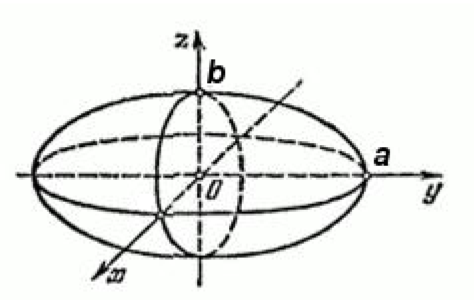

Chapter 6

Forces on ship rudders

Summary: Different rudder constructions used in shipbuilding are discussed in this chapter. General representation of forces arising on rudder at different conditions of ship motion is consdered. A special attention is paid to analysis of rudder- hull iand rudder-propeller interactions.

6.1 Introduction

The ship rudders are wings with the small and moderate aspect ratio which is varied in the range between 0.5 and 3.0. The relative thickness of rudders is between 10 and 30 per cent. The rudder area A_R is chosen from the following two conditions:

- stability of the motion (see chapter 7),
- required ship manoeuvrability.

The rudder design is performed in two steps. In the first design step the rudder area is chosen from the conditions of the motion stability and required manoeuvrability. In the second stage the structure of the rudder and the torque moment on the rudder stock are calculated. Typical ratios of the lateral ship area LT to the rudder area A_R are presented in table 6.1.
Det Norske Veritas (see [9]) recommends the following estimation for the ratio $\frac{A_R}{LT}$:

$$\frac{A_R}{LT} \geq 0.01 \left(1 + 25 \left(\frac{B}{L} \right)^2 \right)$$

The largest rudder deflection angle is customary 35 degrees.

Table 6.1: The ratio of the lateral ship area to the rudder area

Ship type	LT/A_R
Cruise liner	85
Merchant ships	40 - 60
Sea tugs	30 - 40
River ships	12 - 22
Small boats	18 - 25

The following aspects should be taken into account when hydrodynamics of the rudder is considered:

- To increase the rudder efficiency a part of the rudder is located in the propeller slipstream . In this case the rudder is also efficient at small and zero ship speeds.
- The slipstream induces not only the additional axial velocity but also additional transverse velocities on the rudder. As a result the local angle of attack of the rudder is varied between zero and 15 degrees even for a non- deflected rudder in the propeller slipstream.
- The rudder is located in the ship wake. Its hydrodynamics is strongly influenced by the wake.
- The upper side of the rudder is located close to the ship hull.

The ship hull has a positive effect on the transverse force arising on the rudder. If the gap between the hull and the rudder is zero, the effective aspect ratio of the rudder is twice the nominal value. The transverse force and the lift to drag ratio is getting larger. The explanation of this fact is illustrated in Fig. 5.17 of the manuscript [23]. Is the gap getting larger the positive effect quickly disappears. For customary gaps, the increase of the transverse force due to hull influence is only from five to ten percent.

The aim to improve the rudder efficiency motivated the engineers of the firm Becker Marine Systems [2] to invent the twisted rudders (see Fig. 6.1):
"Conventional rudders are placed behind the propeller with the rudder cross section arranged symmetrically about the vertical rudder center plane. However, this arrangement does not consider the fact that the propeller induces a strong rotational flow that impinges on the rudder blade. This results in areas of low pressure on the blade that induce cavitation and associated

erosion problems. To avoid cavitation and to improve the manoeuvrability performance of a full spade rudder, Becker has enhanced the development of twisted leading edge rudder types",

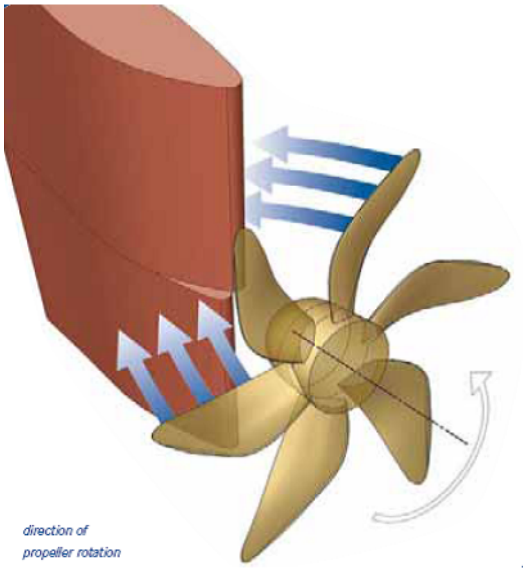

Figure 6.1: Twisted leading edge rudder invented by Becker Marine System [2]

Various rudder types have been developed over the years. A comprehensive overview of rudder types is given in [32]. Figure 6.2a shows the simplex balance rudder which is mounted on the closed frame (marked by the grey color). The rudder is rotated around the stock being the part of the frame. The rudder with heel bearing (simplex) (Fig. 6.2b) belongs to the cheapest and the most common rudder type formerly built. Since the heel increases the non-homogeneity of the ship wake what in its turn increases the propeller induced vibration, this type of rudders is used rarely, mostly it is applied for small boats and some fishery vessels. Spade rudder (Fig. 6.2c) is popular for ferries, ro- ro ships and special craft. Semi-balanced rudders (Fig. 6.2d) are used to reduce the bending moment acting on the rudder. To the most modern rudder types is the flapped rudder designed by Becker Marine Systems. The side force on the moving rudder can be sufficiently increased using the flap deflection (see Fig. 6.3).

Size and costs of the rudder engine are determined by the necessary maximum torque at the rudder stock. The stock moment is zero if the center of effort for the transverse rudder force lies on the rudder stock axis. That is why the rudder stock is usually displaced from the leading edge. The ratio of the rudder area in front of the stock to the total area varies in the range between 0.05 and 0.35.

Typical profile shapes of ship rudders are presented in Fig. 6.4 [2]. The rudder profile is usually chosen from the following conditions

- the flow is non cavitating,
- The critical angle α_{crit} corresponding to the stall effect is as large as possible,
- the drag to transverse force ratio is minimal.

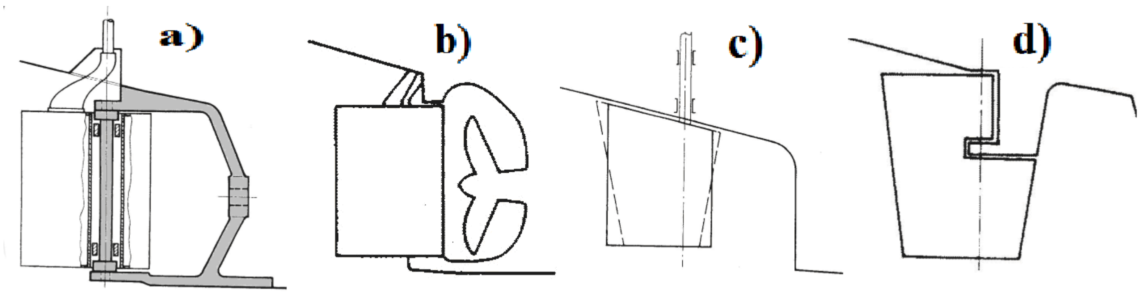

Figure 6.2: Various rudder types [32]

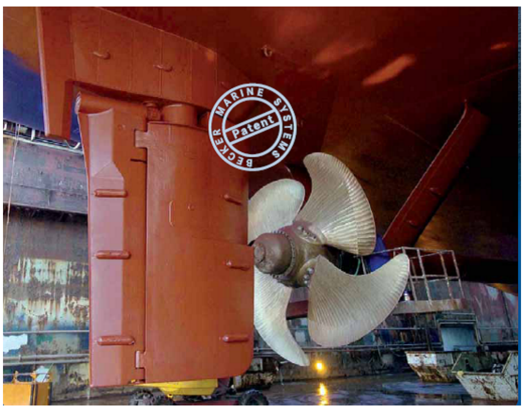

Figure 6.3: Flapped rudder invented by Becker Marine System [2]

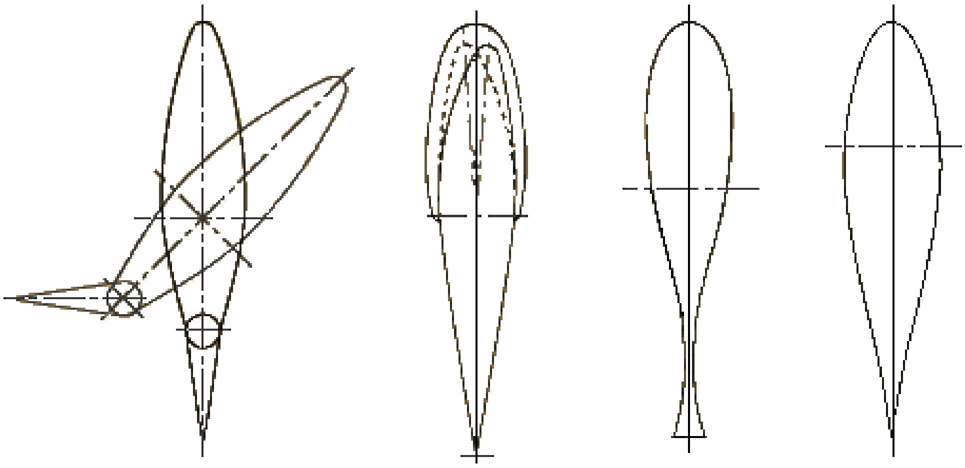

Figure 6.4: Typical profile shapes of ship rudders [2]

6.2 General representation of forces on the rudder

The forces on the rudder are calculated using the common representation through the coefficients $\tilde{C}_{xR}, \tilde{C}_{yR}, \tilde{m}_{zR}$:

$$\begin{aligned} X_R &= \tilde{C}_{xR} \frac{\rho V_{eff}^2}{2} A_R, \\ Y_R &= \tilde{C}_{yR} \frac{\rho V_{eff}^2}{2} A_R, \\ M_{ZR} &= \tilde{m}_{zR} \frac{\rho V_{eff}^2}{2} A_R C. \end{aligned} \tag{6.1}$$

where V_{eff} is the effective velocity at the rudder location, A_R is the rudder area, and C is the characteristic rudder chord. To be substituted into equations (2.17) the transverse rudder force has to be made non-dimensional with respect to the ship velocity V and the lateral ship area A_L:

$$C_{yR} = \frac{Y_R}{\frac{\rho V^2}{2} A_L} = \frac{\tilde{C}_{yR} \frac{\rho V_{eff}^2}{2} A_R}{\frac{\rho V^2}{2} A_L} = \tilde{C}_{yR} \left(\frac{V_{eff}}{V} \right)^2 \frac{A_R}{A_L} \tag{6.2}$$

$$C_{xR} = \frac{X_R}{\frac{\rho V^2}{2} A_L} = \frac{\tilde{C}_{xR} \frac{\rho V_{eff}^2}{2} A_R}{\frac{\rho V^2}{2} A_L} = \tilde{C}_{xR} \left(\frac{V_{eff}}{V} \right)^2 \frac{A_R}{A_L} \tag{6.3a}$$

and the moment:

$$m_{zR} = \frac{M_{zR}}{\frac{\rho V^2}{2} A_L L} = \frac{\tilde{m}_{zR} \frac{\rho V_{eff}^2}{2} A_R C}{\frac{\rho V^2}{2} A_L L} = \tilde{m}_{zR} \left(\frac{V_{eff}}{V} \right)^2 \frac{A_R}{A_L} \frac{C}{L} \tag{6.3b}$$

One of the important problems of the rudder design is the minimisation of the ratio C_{xR}/C_{yR}. The transverse force coefficient is taken from measurements or calculations performed for the wing under the angle of the attack α which is equal to the efficient rudder deflection angle $\alpha = \delta_{R,eff}$. Since the lift coefficient is always positive at the positive α whereas the transverse force is negative at the positive rudder deflection angle δ the negative sign is additionally introduced in (6.2) to use $\tilde{C}_{yR}$ directly from the wing measurements:

$$C_{yR}(\delta_R) = -\tilde{C}_{yR} \left(\frac{V_{eff}}{V} \right)^2 \frac{A_R}{A_L} \tag{6.4}$$

The rudder is used to create the control moment M_{zR}. If there is no other information the arm of the rudder transverse force can be approximately estimated as the half of the ship length:

$$M_{zR}(\delta_R) = \frac{L}{2} Y_R(\delta_R). \tag{6.5}$$

The moment coefficient reads then:

$$m_{zR}(\delta_R) = -\frac{1}{2} C_{yR}(\delta_R). \tag{6.6}$$

The moment (6.5) is calculated about the ship center. It is supposed that C_{yR} is positive in the formula (6.6). In reality, C_{yR} is negative for positive rudder deflections $\delta_R > 0$.

The rudder is located in the region which is strongly influenced by the ship hull. The ship hull influence is expressed through the following effects:

- the incoming velocity is not equal to the ship velocity V rather than it equals to an effective velocity $V_{eff} \neq V$. The difference between V and V_{eff} is due two effects:
  - the velocity is decelerated because of the wake effect $(1 - w)V$, where w is the wake number .
  - the velocity on the rudder is accelerated by the propeller.
- the angle of attack is less than the angle of attack determined from pure geometric point of view (flow straightening effect).

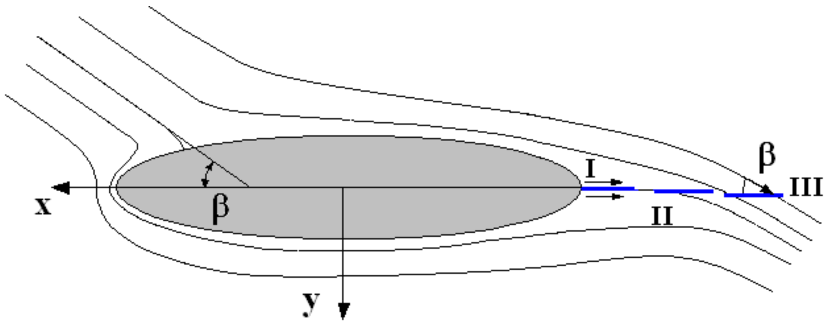

Figure 6.5: Angle of attack of the rudder at different distances from the ship hull moving with the drift angle β: I - the rudder is very close to the hull, angle of attack is zero, II - intermediate position of the rudder, the angle of attack is between zero and β, III - the rudder is far from the hull, angle of attack is equal to ship drift angle β

The first effect is discussed in the subsection 6.3. The second effect is illustrated in Fig. 6.5. If the rudder is very close to the hull, it is located in the area of the hydrodynamic shadow. The effective angle of attack is zero. If the rudder is far from the hull the influence of the hull can be neglected. The rudder is moving in the free stream. The angle of attack is equal to the ship drift angle β. In the intermediate case the angle of attack is between zero and β. The hull influence on the angle of attack is taken into account by the coefficient κ . The rudder angle without the hull influence is:

$$\delta_{R,eff} = \delta_R - (\beta - \Omega \frac{x_r}{L}) \tag{6.7}$$

The effective rudder angle with account for the hull influence reads:

$$\delta_{R,eff} = \delta_R - \kappa(\beta - \Omega \frac{x_r}{L}) \tag{6.8}$$

where x_r is the arm of the transversal force acting on the rudder.
The ship hull influence coefficient κ can be found from the following empirical estimations:

- $\kappa = 0.3$ if the rudder is located at the distance less than the half of the chord from the deadwood,
- $\kappa = 0.3$ if the rudders are located on ship boards and its projection on the side view is crossed with the deadwood,
- $\kappa = 0.5$ if the rudders are located at the distance larger than the half of the chord from the deadwood,
- $\kappa = 1.0$ for ships without deadwood.

6.3 Determination of the force coefficients

The force coefficients can be determined in wind tunnel tests, from RANS computations or from empirical formulae. The rudder is considered as a wing under the angle of attack α which is equal to the effective rudder angle $\delta_{R,eff}$ (6.8). The effective velocity of flow to the rudder V_{eff} is determined in the next subsection. The angle of attack and the velocity V_{eff} are assumed to be constant on the whole rudder. For the angle of attacks less than the critical angle of attack α_{crit} corresponding to the stall effect, the force and moment coefficients can be calculated from the approximation of the series of measurements performed by different authors (see [9]):

$$\begin{aligned}
&\tilde{C}_{yR} = 2\pi\frac{\lambda(\lambda+0.7)}{(\lambda+1.7)^2}\sin\alpha + C_Q\sin\alpha|\sin\alpha|\cos\alpha,\\
&\tilde{C}_{xR} = \frac{\tilde{C}_{yR}^2}{\pi\lambda} + C_Q|\sin\alpha|^3 + C_{D0},\\
&\tilde{m}_{zR} = -\left(2\pi\frac{\lambda(\lambda+0.7)}{(\lambda+1.7)^2}\sin\alpha\cos\alpha + \frac{\tilde{C}_{yR}^2}{\pi\lambda}\sin\alpha\right)\cdot\left(0.47 - \frac{\lambda+2}{4(\lambda+1)}\right) -\\
&0.75(C_Q\sin\alpha|\sin\alpha|\cos^2\alpha + C_Q|\sin\alpha|^3\sin\alpha).
\end{aligned} \tag{6.9}$$

The first term in the approximation for C_{yR} takes the linear part of the force into account, whereas the second a the nonlinear one. The coefficient C_Q is around 1.0 ($C_Q \approx 1$) for the rudders with sharp upper and lower edges. The first term in the approximation of C_{xR} is derived using the lifting line theory and the concept of the optimal wing with elliptical load distribution along the span. The second term takes the contribution of nonlinear effects arising due to the cross flow with the velocity $V\sin\alpha$ (see the subsection 4.1.3). The coefficient C_{D0} is the surface friction calculated from the approximation $C_{D0} = 2.5\frac{0.075}{(logRe-2)^2}$. The moment coefficient is calculated with respect to the leading edge of the rudder. If the leading edge is not vertical the position at the mean height of the rudder is used as a reference point. The aspect ratio is calculated as the chord c at the rudder mean height b/2 multiplied with span and divided by the rudder area A_R, i.e. $\lambda = bc(b/2)/A_R$. The Reynolds number uses the velocity, the mean chord C and the kinematic viscosity as the characteristic quantities: $Re = V_{eff}C/\nu$. The formulae are valid only up to the critical angle of attack α_{crit}.

6.4 Interaction between the rudder and propeller

6.4.1 Increase of the rudder force due to propeller slipstream

Since the rudder is located in the propeller slipstream, the flow around the rudder is accelerated (see Fig. 6.6a). The axial velocity is increased from the point A in front of the propeller to point D in the rudder region being continuous. Because of the flow acceleration the propeller slipstream experiences the contraction (see Fig. 6.6b). The pressure sinks in the front of the propeller due to the suction effect caused by the propeller (see Fig. 6.6c). The pressure in the propeller disc jumps from the value p_B to the value $p_c, p_c \sim p_B$. The propeller acts on the fluid as the energy source raising the pressure from p_B to p_c. The thrust on the propeller is $T = A_0(p_c - p_B)$, where A_0 is the propeller disc area.
To find a simple estimation of the flow speed, it is assumed that the velocity is constant over the whole rudder area. Let us consider the Bernoulli equation along the streamline connecting four points A, B, C and D (see Fig. 6.7). A direct application of the equation is not allowed because the equation is valid if no energy is additionally put along the line. Since the propeller is the energy source, the Bernoulli equation can be applied separately between points A and B

$$\underbrace{p + \frac{\rho V_A^2}{2}}_{\text{point A}} = \underbrace{p_B + \frac{\rho V_B^2}{2}}_{\text{point B}} \tag{6.10}$$

and between C and D

$$\underbrace{p + \frac{\rho V_D^2}{2}}_{\text{point D}} = \underbrace{p_C + \frac{\rho V_C^2}{2}}_{\text{point C}} \tag{6.11}$$

Velocities V_B and V_C are equal $V_B = V_C$ since the velocity is continuous on the propeller disk. The velocity at the point D is larger than the velocity at the point A: $V_D = V_A + u$, where u is the additional velocity induced by the propeller (see Fig. 6.6a). Subtracting (6.10) from (6.11) one obtains:

$$p_C - p_B = \frac{\rho V_D^2}{2} - \frac{\rho V_A^2}{2} = \frac{\rho}{2} V_A^2 \left(\frac{(V_A + u)^2}{V_A^2} - 1 \right) \tag{6.12}$$

The propeller loading coefficient is:

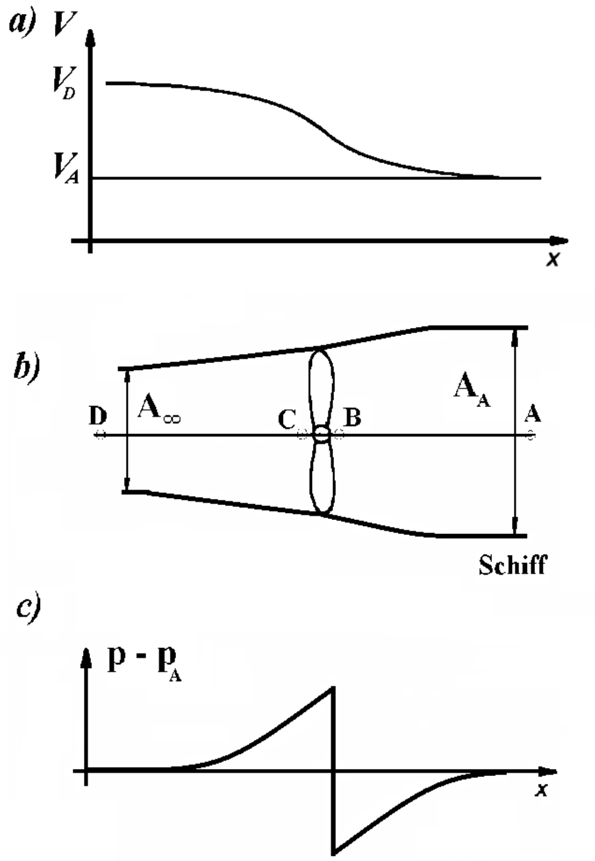

Figure 6.6: Distribution of the axial velocity (a), slipstream contraction (b), and the pressure distribution (c) in the slipstream

$$c_S = \frac{T}{\frac{\varrho}{2} V_A^2 A_0} \tag{6.13}$$

Remembering that $T = A_0(p_C - p_B)$ and use of (6.12) results in

$$c_S = \frac{T}{\frac{\varrho}{2} V_A^2 A_0} = \frac{p_C - p_B}{\frac{\varrho}{2} V_A^2} = \frac{(V_A + u)^2}{V_A^2} - 1 \tag{6.14}$$

The effective velocity $V_{eff} = V_A + u$ around the rudder is obtained from (6.14)

$$V_{eff} = V_A + u = V_A \sqrt{1 + c_S} \tag{6.15}$$

The velocity in the front of the propeller is calculated with account for the wake influence:

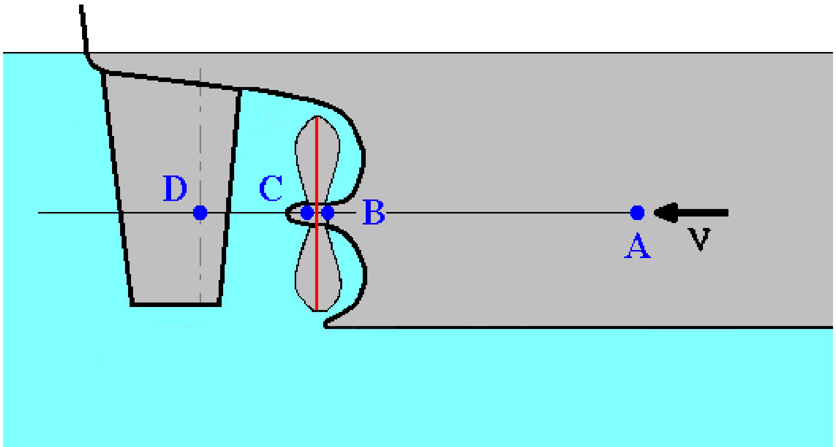

Figure 6.7: The streamline ABCD

$$V_A = (1 - w)V \tag{6.16}$$

where w is the wake number. Herewith the final formula for the effective velocity is

$$\boxed{V_{eff} = (1 - w)\sqrt{1 + c_S}V} \tag{6.17}$$

Formulae (6.1), (6.8), (6.9) and (6.17) are sufficient to calculate the forces and the moment arising on the rudder.

6.4.2 Unbalanced lateral force due to propeller jet swirl

The propeller has a twofold effect on the rudder. First, the propeller accelerates the flow in the axial direction making the longitudinal velocity in the jet much larger than the advanced speed (6.17). The second effect of the propeller on the rudder is due to swirl of the propeller jet . The propeller produces not only additional longitudinal velocities but also additional circumferential velocities. The distribution of the circumferential velocity across the jet is asymmetric. The velocity in the upper part of the jet is slightly smaller due to the hull influence (reduction of the flow velocity due to viscous effect of solid walls, i.e. boundary layer effect). The circumferential velocity in the lower part of the propeller jet, where the influence of the hull is weaker, is larger.

The flow swirl is the reason for the inception of the additional unbalanced lateral force on the rudder placed into the propeller jet. This force arises even on non- deflected rudder. The direction of this force corresponds to the swirling direction, i.e. the additional lateral force is negative for right handed propeller.
This effect can easily be explained taking the fact into account that the rudder is both hydrodynamically and geometrically asymmetric. For a non-deflected rudder behind the right handed propeller, the swirling flow results in the negative lateral force in the upper part, whereas the positive force arises in the lower part of the rudder (see Fig. 6.8). Due to the hull and the free surface effects the force in the upper part of the rudder is larger than that in the lower one. The difference between two forces results in the unbalanced lateral force pushing the stern to starboard and turning the ship counter-clockwise.

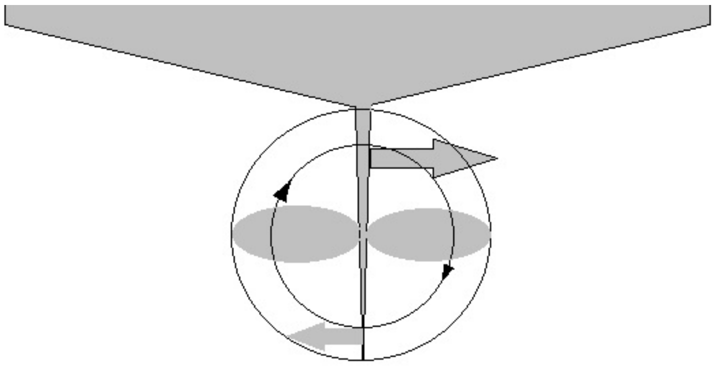

Figure 6.8: Origin of the unbalanced lateral force on the rudder in swirled propeller slipstream

6.5 Exercises

1. The ship velocity is $V_S = 18$ kn. The drift angle is $\beta = 10°$, the angular velocity is $\Omega = 0$. The wake number is $w = 0.3$.

   Calculate the side force on the rudder if rudder angle is $\delta_R = 30°$, height of the rudder is $T_R = 5m$, the area of the rudder is $A_R = 10m^2$. Use propeller loading coefficient $c_S = 1.0$, ship hull influence coefficient $k = 0.5$.

   Calculate the side force for two different rudder types (I and II).

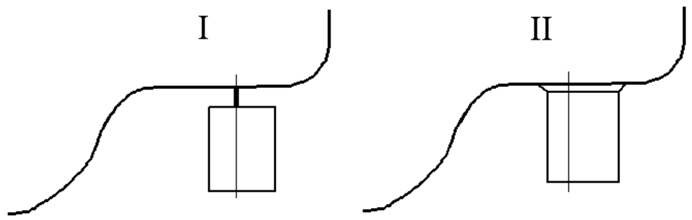

2. A ship performs a steady turning circle, estimate the ship′s rudder-induced side force, yaw moment and bending moment at the rudder shaft.

   The ship is characterized by:
   $L = 100m$; $B = 20m$; $T = 9m$; $Thrust = 1.000kN$; $w = 0.25$;
   $V_D = 10kn$; $D_{prop} = 6.5m$; $x_R/L = 0.7$, $k = 0.3$

   The manoeuvre has the following parameters:
   $R = 5L$; $\beta = 6°$; $\delta_R = 24°$; $V_{turning} = 0.6V_D$

Chapter 7

Transversal forces and yaw moment on propeller

Summary: The study object of this chapter are lateral forces arising on propeller and hull due to hull - propeller interaction and horizontal and upward oblique flow.
Due to asymmetry of the incoming flow the propeller produces not only the thrust but also the transversal forces making the ship maneuvering more complicated. In this chapter we analyze a few hydrodynamic effects resulting in the transversal forces on propeller.

7.1 Additional transversal forces on propeller due to non-uniformity of the ship wake

The propeller is located in the ship wake. In the case of odd number of propellers installed on ship additional transverse force arises on the propeller due to non-uniformity of the ship wake . Schematic vertical distribution of the axial velocity in front of the propeller is shown in Fig.7.1.
Non uniform distribution of the stream velocity results in the appearance of the transverse force and yaw moment. To illustrate the creation of the transverse force let us consider two profiles 1 and 2 on a four blades right-handed propeller (Fig.7.2). The profiles are moving in circumferential direction with the local velocity ωr. The incoming stream has then velocity $V = -\omega r$. Axial velocity in the ship wake u_x reduces the angle of attack φ.
The typical dependence of the propeller profile drag on the angle of attack is shown in 7.2.
The induced angle of attack α_I is calculated as

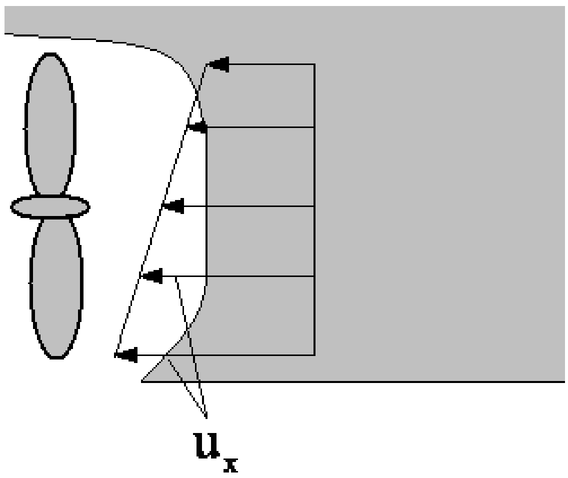

Figure 7.1: Schematic vertical distribution of the axial velocity in front of the propeller

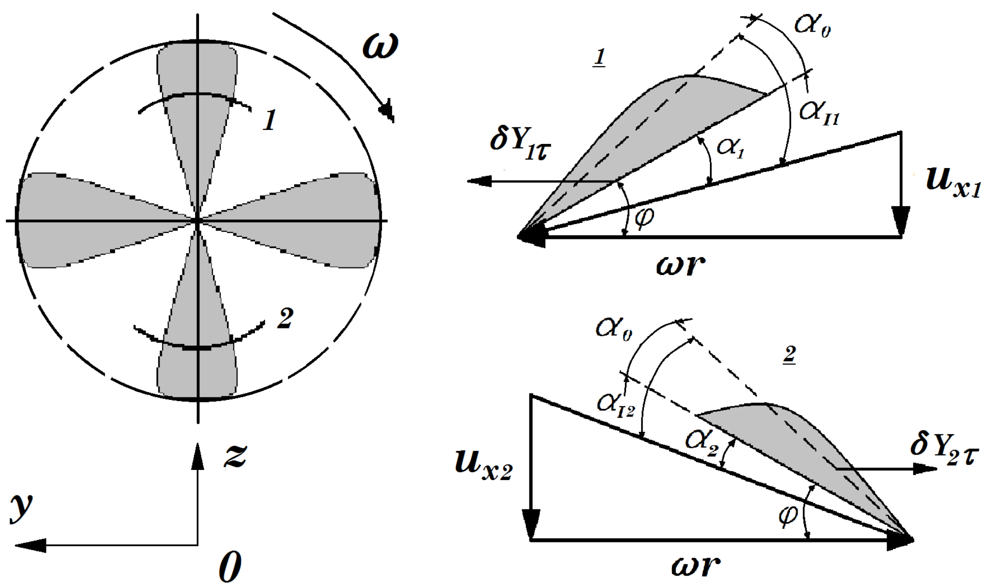

Figure 7.2: Explanation of transverse force creation on a propeller in ship wake

$$\alpha_I = \alpha + \alpha_0 = \varphi + \alpha_0 - \frac{u_x}{V}$$

where α_0 is the zero lift angle of attack. In the present analysis we neglect the induced velocities. More detailed analysis of speed triangle relations can

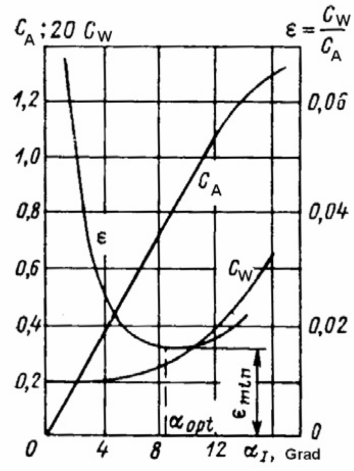

Figure 7.3: Hydrodynamic coefficients of the propeller profiles [7]

be found in [22], Chapter 1 and Figure 1.25. The drag coefficient can be represented via Taylor expansion:

$$c_w = c_w(\alpha_I = 0) + \frac{1}{2}\frac{\partial^2 c_w}{\partial \alpha_I^2}(\alpha_I = 0)\alpha_I^2 + ... \tag{7.1}$$

Here it was used that $\partial c_w/\partial\alpha_I(\alpha_I = 0) = 0$ according to Fig. 7.3. The total drag on the profiles 1 and 2 according to (7.1) is:

$$\delta Y_{1\tau} = (c_w + \frac{1}{2}\frac{\partial^2 c_w}{\partial \alpha_I^2}\alpha_{I1}^2)\varrho\frac{V^2 + u_{x1}^2}{2}cdr$$
$$\delta Y_{2\tau} = -(c_w + \frac{1}{2}\frac{\partial^2 c_w}{\partial \alpha_I^2}\alpha_{I2}^2)\varrho\frac{V^2 + u_{x2}^2}{2}cdr$$

Here c is the local chord and dr is the radius increment.
Let assume that $\frac{u_x}{V} \ll \varphi + \alpha_0$. Then the following asymptotic estimations are valid

$$\begin{aligned} &V^2 + {u_x}^2 \sim V^2 \\ &{\alpha_I}^2 \sim (\varphi + \alpha_0)^2 - 2\frac{u_x}{V}(\varphi + \alpha_0). \end{aligned} \tag{7.2}$$

The sum of $\delta Y_{1\tau}$ and $\delta Y_{2\tau}$:

$$\delta Y_{1\tau} + \delta Y_{2\tau} = \frac{u_{x2} - u_{x1}}{V}(\varphi + \alpha_0)\frac{\partial^2 c_w}{\partial {\alpha_I}^2} > 0$$

is positive since $u_{x2} > u_{x1}$.

Considering consequently profiles in the upper blade and lower blade positions in the same manner as it has just been done above one can explain the creation of the transverse force caused by the non uniformity of the ship wake. The direction of the force depends on the propeller turning direction. The positive transverse force appears on the right handed propeller (Fig.7.4 left), whereas the negative transverse force appears on the left handed propeller (Fig.7.4 right).

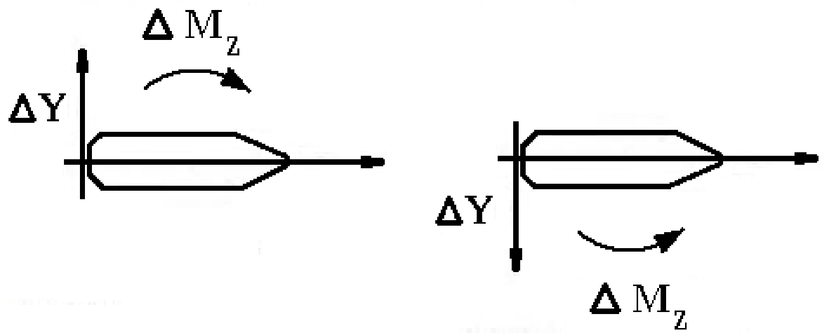

Figure 7.4: Transverse force on the right handed (left) and left handed (right) propellers

7.2 Additional transversal forces on propeller due to oblique flow

The transverse force arises on propeller in oblique flow , i.e. on propeller under the local drift angle caused by the ship drift motion and rotation with the angular velocity Ω. Let us β is the local drift angle in place of right handed propeller. To explain the creation of this force we consider the scheme similar to that shown in Fig.7.2. The inflow on the propeller has a transverse component $V \sin\beta$ (see Fig.7.5).
The drag forces acting on the upper and lower profiles are

$$\delta Y_{1\tau} = \frac{C_{D1}\rho A}{2}(\omega r + V\sin\beta)^2 \tag{7.3}$$

$$\delta Y_{2\tau} = -\frac{C_{D2}\rho A}{2}(\omega r - V\sin\beta)^2 \tag{7.4}$$

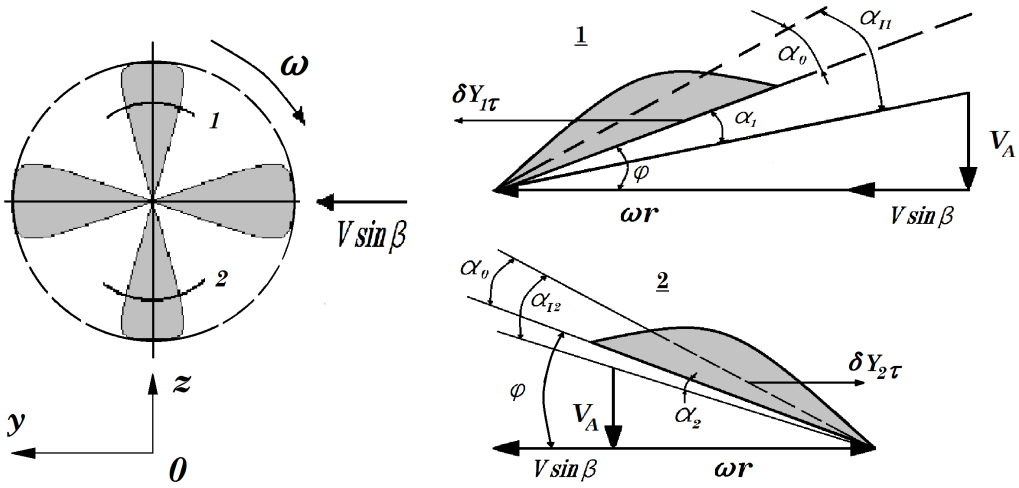

Figure 7.5: Explanation of transverse force creation in oblique flow

where C_D is the profile drag coefficient. Using the Taylor expansion (7.1) it is easy to show that $C_{D1} > C_{D2}$ since $\alpha_{I1} > \alpha_{I2}$. The magnitude of tangential force $\delta Y_{1\tau}$ is larger than that of $\delta Y_{2\tau}$ since $C_{D1} > C_{D2}$ and $(\omega r + V \sin\beta) > (\omega r - V \sin\beta)$. Considering consequently profiles in the upper blade and lower blade positions on the same manner as it has just been done above one can explain the creation of the positive transverse force caused by the oblique flow. The sum of these two components yields the transverse force which is not zero.

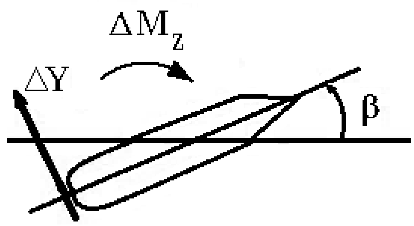

Figure 7.6: Transverse force on the propeller in oblique flow

As seen in Fig.7.6 the additional forces arising due to oblique flow are stabilizing ones. This force produces the negative moment and reduces the reason of the oblique flow appearance, i.e. the drift angle and the angular velocity. We considered above the right handed propellers. The same conclusions can also be drawn for left handed propellers.

Additional forces due to oblique flow can be estimated from the formula:

$$\Delta Y = \rho n^2 D^4 \left\{ 2K_Q\left(J=0\right) - J\frac{dK_Q}{dJ} \right\} J \tan\beta,$$

where n is the rotation number per second, D is the diameter of propeller, J is the advance ratio, K_Q is the torque coefficient.

7.3 Moment on the propeller due to upward oblique flow at the propeller location

In the stern area of the ship the flow has upward direction as shown schematically in Fig. 7.7 and 7.8.

Figure 7.7: Upward oblique flow in the ship stern area (side view)

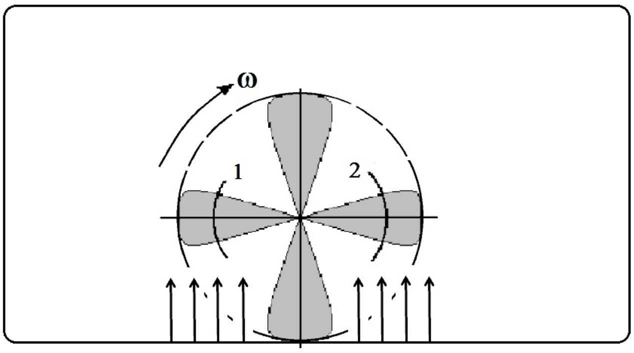

Figure 7.8: Upward oblique flow in the ship stern area (as viewed from the stern)

As seen in Fig. 7.8 the incoming velocity of the blade profile 1 is less than that of the profile 2 for the right handed propeller. Therefore, the thrust produced by the profile in the position 2 is larger than that in the position

1. Fig. 7.9 illustrates this fact and explains the appearance of the moment resulting in the turning the boat counter-clockwise. The clockwise moment arises on the left handed propeller. The center of effort of the resulting thrust force is shifted towards the starboard. For the left handed propeller the center of effort is shifted towards the port side.

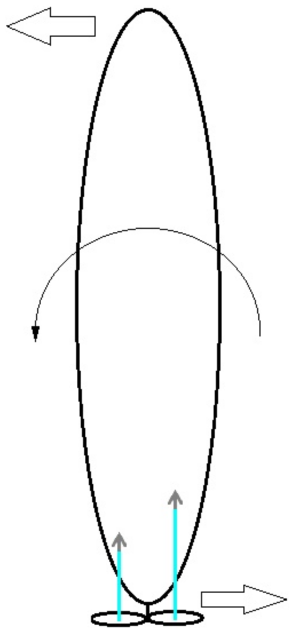

Figure 7.9: Counter-clockwise moment on the right handed propeller arising due to upward oblique flow in the ship stern area

Let us consider the two screw ship. For two propellers rotating outwards the centers of effort of thrust forces are displaced from the propeller axes towards boards (see Fig. 7.10 a)). On the contrary, the centers of thrust forces are closer to the middle line plane for propellers rotating inwards (see Fig. 7.10 b)). The reason of these displacements is again the upward oblique flow resulting in different thrusts as explained above for the one screw ship (Fig. 7.7-7.9). If ship performs often maneuvering in small spaces using two propellers with different thrusts, the outward rotation (Fig. 7.10 a)) is more advantageous than the inward one since the arm of thrust forces is larger. Inward rotation is advantageous for ships maneuvering mostly by rudder action. The positive effect of propellers on the rudder installed amidships is larger when propellers rotate inwards.

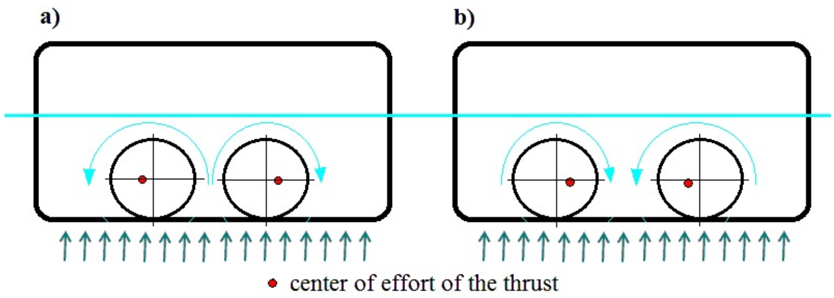

Figure 7.10: Displacement of the center of effort of the thrust depending for propeller rotation outwards (a) and inwards (b)

7.4 Additional moments on the propeller during manoeuvring

Different thrusts arise on two propellers in the turning circle. One propeller gets into the wake (dashed area) whereas the other moves in a free stream (see Fig. 7.11). The thrust of the propeller P can be substantially larger than that of the propeller S. This effect is reflected in the dependence of the moment coefficient m_z on the turning circle diameter referred to the ship length D/L for two ships (Fig. 7.12). The results were obtained experimentally for the bare hull (dashed line) and hull with propeller (solid line). One ship is a full bottomed ship with propellers located close to the hull. The second ship is a slender ship with two big propellers located relatively far from the hull. The reader is invited to recognize which ship is the ship A and which one is the ship B.

7.5 Additional lateral force on the hull caused by propeller

A rotating propeller induces the transversal velocities both in the propeller jet and outside it. During the forward gear (motion) the effect of the propeller jet swirl on the hull is usually negligible. However, it can be very large for the reverse gear. Due to stagnation effects caused by the hull which is typical for all bodies and mostly of potential character the axial velocity is smaller in the upper part of the hull (see Fig. 7.13b) than in the lower one (Fig. 7.13a). Therefore, the angle of attack and the lateral force in the upper submerged part of the hull are larger than in the lower. The resulting unbalanced lateral force corresponds to the rotation direction.

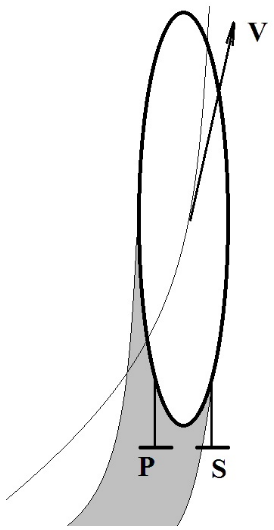

Figure 7.11: Differences in propeller flow during the ship maneuvering

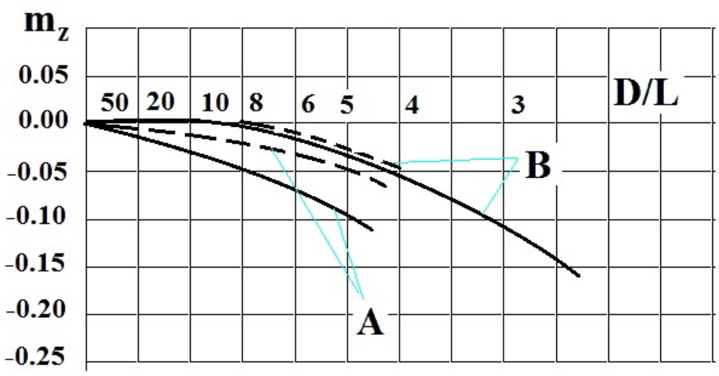

Figure 7.12: Moment coefficient of the ship hull with and without propeller in the turning circle manoeuver [5]

7.6 Exercise

Investigate the course angle oscillation of the tanker KVLCC2 and container ship KCS at different sea conditions. The ship geometry parameters can be taken from the table 7.1. Consider both regular and irregular sea states. The irregular sea state should be specified for the North Atlantic region according to STANAG 4194 (ANEP11). Use the code KUWIK which can be downloaded from http://www.lemos.uni-rostock.de/cfd-software/. The drift angle is 0°, the Lewis coefficients can be taken from Fig. 3.3.

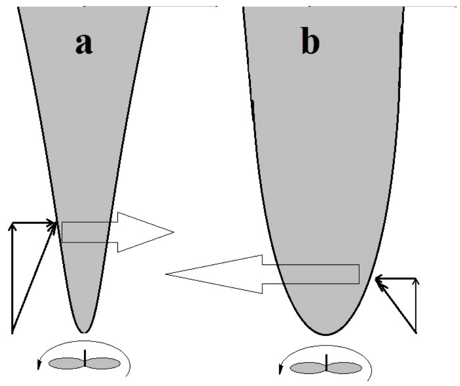

Figure 7.13: Moment coefficient of the ship hull with and without propeller in the turning circle manoeuver

Table 7.1: Ship geometrical parameters for exercise

Parameter			KVLCC2	KCS
Length	L	$[m]$	325,5	232,5
Beam	B	$[m]$	58,0	23,5
Draught	T	$[m]$	20,8	10,8
Speed	V	$[kn]$	22,0	18,5
Block coefficient	C_B	$[-]$	0,81	0,65
main frame fullness coefficient	C_M	$[-]$	0,99	0,98
Vertical position of the center of gravity	$VCOG$	$[m]$	$0,4 \cdot T$	$0,4 \cdot T$
Rudder area	A_R	$[m^2]$	136,7	54,4
Skeg area	A_{skeg}	$[m^2]$	$0,02 \cdot L \cdot T$	$0,02 \cdot L \cdot T$

Calculate the course angle oscillations $\Delta\Psi$ for both ships and wave course (encountering) angle $0° \leq \phi \leq 180°$ with $\Delta\phi = 15°$ for seastate 5.

a) Change the length in range of $\pm 10\%$.

b) Change the draught in range of $\pm 10\%$.

c) Change the block coefficient in range of $\pm 10\%$.

Find the wave course angle with the maximum course angle oscillations. Investigate impact of the ratios L/B, B/T und CB on the course angle oscillations. Study the course angle oscillations at sea states 4, 5 and 6. The results should be presented in form of report with graphical illustrations.

Chapter 8

Yaw stability

Summary: Linear Hurwitz analysis is utilized in this chapter to derive the condition of the ship stability with three degree of freedom. Influence of ship geometry on stability and regulations of the stability are analysed using simple estimations for forces taken from the slender body theory. Trajectories of a stable ship at straight course and in turning circle are presented.

8.1 Introduction

The aim of this chapter is the study of the ship ability to perform the stable motion. The ship moves with constant speed at zero drift angle and zero angular velocity. At the time instant t=0 the ship experience perturbations

$$\begin{aligned} \beta =&\beta_*, \\ \Omega =&\Omega_*. \end{aligned} \tag{8.1}$$

If the drift angle and angular velocity after perturbations increase the ship motion becomes unstable. If β and Ω decay the ship motion is stable. The analysis of the perturbation evolution is performed under assumption that the drift angle β, angular velocity Ω and change of the speed are small, i.e.:

$$\beta \sim O(\varepsilon), \Omega \sim O(\varepsilon), V'/V \sim O(\varepsilon) \tag{8.2}$$

Please note that speaking about the stability we assume that the rudder and other control devices are not active.

8.2 Linearization of the motion equations

The analysis is based on the linearized form of the equations (2.17)

$$\begin{cases} \kappa_x \frac{V'}{V} \cos\beta - \kappa_x \beta' \sin\beta + \kappa_y \Omega \sin\beta = C_x, \\ -\kappa_y \frac{V'}{V} \sin\beta - \kappa_y \beta' \cos\beta + \kappa_x \Omega \cos\beta = C_y, \\ \mu\Omega \frac{V'}{V} + \mu\Omega' = m_z. \end{cases} \tag{8.3}$$

Asymptotic analysis of the left hand and right hand sides of (8.3) yields

$$\underbrace{\kappa_x \frac{V'}{V} \cos\beta}_{O(\varepsilon)} - \underbrace{\kappa_x \beta' \sin\beta}_{O(\varepsilon^2)} + \underbrace{\kappa_y \Omega \sin\beta}_{O(\varepsilon^2)} = \underbrace{C_x^{\beta\beta}\beta^2 + C_x^{\Omega\Omega}\Omega^2 + ...}_{O(\varepsilon^2)}$$

$$- \underbrace{\kappa_y \frac{V'}{V} \sin\beta}_{O(\varepsilon^2)} - \underbrace{\kappa_y \beta' \cos\beta}_{O(\varepsilon)} + \underbrace{\kappa_x \Omega \cos\beta}_{O(\varepsilon)} = \underbrace{C_y^{\beta}\beta + C_y^{\Omega}\Omega}_{O(\varepsilon)} +$$
$$+ \underbrace{C_y^{\beta\beta}\beta\,|\beta| + C_y^{\Omega\Omega}\Omega\,|\Omega| + ...}_{O(\varepsilon^2)}$$

$$\underbrace{\mu\Omega \frac{V'}{V}}_{O(\varepsilon^2)} + \underbrace{\mu\Omega'}_{O(\varepsilon)} = \underbrace{m_z^{\beta}\beta + m_z^{\Omega}\Omega}_{O(\varepsilon)} + \underbrace{m_z^{\beta\beta}\beta\,|\beta| + m_z^{\Omega\Omega}\Omega\,|\Omega| + ...}_{O(\varepsilon^2)}$$

Neglecting terms proportional to ϵ^2 the system (8.3) is reduced to

$$\begin{cases} \kappa_x \frac{V'}{V} \cos\beta = 0, \\ \kappa_x\Omega - \kappa_y\beta' = C_y^{\beta}\beta + C_y^{\Omega}\Omega, \\ \mu\Omega' = m_z^{\beta}\beta + m_z^{\Omega}\Omega. \end{cases} \tag{8.4}$$

From the first equation follows that the ship speed remains constant if $\beta \sim O(\epsilon), \Omega \sim O(\epsilon)$.

$$V = const \tag{8.5}$$

The system (8.4) is then reduced to two equations:

$$\begin{cases} \kappa_y\beta' + C_y^{\beta}\beta - C_y^{*\Omega}\Omega = 0, \\ \mu\Omega' - m_z^{\Omega}\Omega - m_z^{\beta}\beta = 0. \end{cases} \tag{8.6}$$

where $C_y^{*\Omega} = \kappa_x - C_y^{\Omega}$. The equations can be decoupled. The angular velocity and its time derivative are found from the first equation

$$\Omega = \frac{1}{C_y^{*\Omega}} \left(\kappa_y\beta' + C_y^{\beta}\beta\right) \Rightarrow \Omega' = \frac{1}{C_y^{*\Omega}} \left(\kappa_y\beta'' + C_y^{\beta}\beta'\right) \tag{8.7}$$

The result (8.7) is then substituted into the second equation (8.6)

$$\frac{\mu}{C_y^{*\Omega}}\left(\kappa_y\beta'' + C_y^{\beta}\beta'\right) + \frac{m_z^{\Omega}}{C_y^{*\Omega}}\left(-\kappa_y\beta' - C_y^{\beta}\beta\right) - m_z^{\beta}\beta = 0$$
$$\Downarrow$$
$$\beta'' + \beta'\left(\frac{C_y^{\beta}\mu - \kappa_y m_z^{\Omega}}{\mu\kappa_y}\right) + \beta\left(-\frac{C_y^{\beta}m_z^{\Omega} + m_z^{\beta}C_y^{*\Omega}}{\mu\kappa_y}\right) = 0 \tag{8.8}$$
$$\Downarrow$$
$$\beta'' + 2a\beta' + b\beta = 0$$

where $2a = \frac{C_y^{\beta}\mu - \kappa_y m_z^{\Omega}}{\mu\kappa_y}$, $b = -\frac{C_y^{\beta}m_z^{\Omega} + m_z^{\beta}C_y^{*\Omega}}{\mu\kappa_y}$. Similar operations are performed to get the differential equation for Ω:

$$\Omega'' + 2a\Omega' + b\Omega = 0 \tag{8.9}$$

8.3 Evolution of perturbations

The solutions of differential equations (8.8) and (8.9) are seeking in the form

$$\begin{aligned} \beta(\tau) &= \beta_1 e^{p_1\tau} + \beta_2 e^{p_2\tau}, \\ \Omega(\tau) &= \Omega_1 e^{p_1\tau} + \Omega_2 e^{p_2\tau}. \end{aligned} \tag{8.10}$$

The time derivatives are calculated by differentiation of (8.10)

$$\begin{aligned} \beta'(\tau) = \beta_1 p_1 e^{p_1\tau} + \beta_2 p_2 e^{p_2\tau} &\Rightarrow \beta''(\tau) = \beta_1 p_1^2 e^{p_1\tau} + \beta_2 p_2^2 e^{p_2\tau} \\ \Omega'(\tau) = \Omega_1 p_1 e^{p_1\tau} + \Omega_2 p_2 e^{p_2\tau} &\Rightarrow \Omega''(\tau) = \Omega_1 p_1^2 e^{p_1\tau} + \Omega_2 p_2^2 e^{p_2\tau} \end{aligned} \tag{8.11}$$

The solution (8.10) should satisfy the initial conditions (8.1) at $\tau \to 0$

$$\begin{cases} \beta(0) = \beta_1 + \beta_2 = \beta_*, \\ \Omega(0) = \Omega_1 + \Omega_2 = \Omega_*, \\ \beta'(0) = \beta_1 p_1 + \beta_2 p_2 = 0, \\ \Omega'(0) = \Omega_1 p_1 + \Omega_2 p_2 = 0. \end{cases} \tag{8.12}$$

Substituting (8.10) and (8.11) into (8.8) results in

$$\begin{aligned} &\beta_1 e^{p_1\tau}(p_1^2 + 2ap_1 + b) + \beta_2 e^{p_2\tau}(p_2^2 + 2ap_2 + b) = 0 \\ &p_1^2 + 2ap_1 + b = 0, p_2^2 + 2ap_2 + b = 0. \end{aligned} \tag{8.13}$$

and in (8.9)

$$\begin{aligned} &\Omega_1 e^{p_1\tau}(p_1^2 + 2ap_1 + b) + \Omega_2 e^{p_2\tau}(p_2^2 + 2ap_2 + b) = 0, \\ &p_1^2 + 2ap_1 + b = 0, p_2^2 + 2ap_2 + b = 0 \end{aligned} \tag{8.14}$$

p_1 and p_2 are found from the algebraic equation

$$\begin{aligned} p^2 + 2ap + b &= 0 \\ p_{1,2} &= -a \pm \sqrt{a^2 - b} \end{aligned} \tag{8.15}$$

The system (8.12) along with the solutions (8.14) is now closed and can be used to find the coefficients $\beta_1, \beta_2, \Omega_1$ and Ω_2. The coefficients p_1 and p_2 are real since the product $m_z^\beta C_y^{*\Omega}$ and the expression $a^2 - b$ are always positive:

$$a^2 - b = \frac{\left(C_y^\beta \mu\right)^2 + \left(\kappa_y m_z^\Omega\right)^2 - 2C_y^\beta \mu\kappa_y m_z^\Omega + 4\mu\kappa_y C_y^\beta m_z^\Omega + 4\mu\kappa_y m_z^\beta C_y^{*\Omega}}{4(\mu\kappa_y)^2} =$$

$$= \frac{\left(C_y^\beta \mu\right)^2 + \left(\kappa_y m_z^\Omega\right)^2 + 2C_y^\beta \mu\kappa_y m_z^\Omega + 4\mu\kappa_y m_z^\beta C_y^{*\Omega}}{4(\mu\kappa_y)^2} = \frac{\left(C_y^\beta \mu + \kappa_y m_z^\Omega\right)^2 + 4\mu\kappa_y m_z^\beta C_y^{*\Omega}}{4(\mu\kappa_y)^2} > 0 \tag{8.16}$$

The coefficient a is for conventional ships positive $2a = \frac{C_y^\beta \mu - \kappa_y m_z^\Omega}{\mu\kappa_y} > 0$ since $m_z^\Omega < 0$ and other coefficients in the formula for a are positive. Two following cases are to be considered

- Case 1: b is positive, $p_1 = -a - \sqrt{a^2 - b} < 0, p_2 = -a + \sqrt{a^2 - b} < 0$
- Case 2: b is negative, $p_1 = -a - \sqrt{a^2 - b} < 0, p_2 = -a + \sqrt{a^2 - b} > 0$

In the first case

$$\begin{aligned} \beta(\tau \to \infty) &= 0, \\ \Omega(\tau \to \infty) &= 0. \end{aligned} \tag{8.17}$$

the perturbation go to zero and the ship motion is stable. In the second case

$$\begin{aligned} \beta(\tau \to \infty) &\sim \beta_2 e^{p_2\tau} \to \infty, \\ \Omega(\tau \to \infty) &\sim \Omega_2 e^{p_2\tau} \to \infty, \end{aligned} \tag{8.18}$$

the solution diverges and the ship motion is unstable.

8.4 Criterion of the stability

Therefore, the stability condition reads: the coefficient b should be positive

$$-\frac{C_y^\beta m_z^\Omega + m_z^\beta C_y^{*\Omega}}{\mu\kappa_y} > 0 \Rightarrow \frac{C_y^\beta m_z^\Omega + m_z^\beta C_y^{*\Omega}}{\mu\kappa_y} < 0 \Rightarrow C_y^\beta m_z^\Omega + m_z^\beta C_y^{*\Omega} < 0 \tag{8.19}$$

Therefore, the condition of the yaw stability can be written in one of the following forms:

$$\boxed{m_z^\beta C_y^{*\Omega} + C_y^\beta m_z^\Omega < 0} \tag{8.20}$$

$$\boxed{m_z^\beta C_y^{*\Omega} < -C_y^\beta m_z^\Omega} \tag{8.21}$$

$$\boxed{-\frac{m_z^\Omega}{C_y^{*\Omega}} > \frac{m_z^\beta}{C_y^\beta}} \tag{8.22}$$

Since m_z^Ω is negative for common ships the last inequality takes the form:

$$\frac{\left|m_z^\Omega\right|}{C_y^{*\Omega}} > \frac{m_z^\beta}{C_y^\beta} \tag{8.23}$$

or

$$X^\Omega > X^\beta \tag{8.24}$$

The center of effort of the force arising due to the angular velocity should lie in front of the center of effort of the force arising due to the drift angle.

8.5 Influence of ship geometric parameters on the stability

Using estimations (5.20) $C_y^\beta = \frac{\pi C\lambda}{2}, m_z^\beta = \frac{\pi C\lambda}{4}, C_y^\Omega = \frac{\pi C\lambda}{4}, m_z^\Omega = -\frac{\pi C\lambda}{8}$ the criterion (7.20) can be written in the form with explicit dependence on geometric parameters

$$\frac{\pi C\lambda}{4}\left(C_B\frac{B}{T}\lambda - \frac{\pi C\lambda}{4}\right) - \frac{\pi C\lambda}{8}\frac{\pi C\lambda}{2} < 0 \tag{8.25}$$

The following estimation for κ_x was taken into account

$$\kappa_x = \frac{m + m_{11}}{\frac{\varrho}{2}A_L L} \approx \frac{m}{\frac{\varrho}{2}A_L L} = C_B\frac{B}{T}\lambda$$

The final form of (8.25) reads:

$$\frac{1}{2} > \frac{C_B B}{\pi C T} \tag{8.26}$$

The influence of the ship geometry on the stability is summarized in the table below

Increase of	Influence on the stability
$\frac{B}{T}$	negative
C_B	negative
C	positive

8.6 Trajectory of a stable ship after perturbation

A stable ship after perturbation is moving along a new straight path with new heading angle $\psi(\tau \to \infty)$. The trajectory of the ship in the earth-fixed system is calculated using (8.10)

$$\psi(\tau) = \int_0^\tau \Omega d\tau = \int_0^\tau (\Omega_1 e^{p_1\tau} + \Omega_2 e^{p_2\tau}) d\tau = \frac{\Omega_1}{p_1}(e^{p_1\tau} - 1) + \frac{\Omega_2}{p_2}(e^{p_2\tau} - 1) \tag{8.27}$$

The coordinates of the ship are determined from (2.9) and (8.27)

$$\begin{aligned}
&\tfrac{x_0}{L} = \textstyle\int_0^\tau \cos(\psi - \beta) d\tau \approx \tau, \\
&\tfrac{y_0}{L} = \textstyle\int_0^\tau \sin(\psi - \beta) d\tau \approx \int_0^\tau (\psi - \beta) d\tau = \\
&= -\left(\tfrac{\Omega_1}{p_1} + \tfrac{\Omega_2}{p_2}\right)\tau + \tfrac{\Omega_1}{p_1^2}(e^{p_1\tau} - 1) + \tfrac{\Omega_2}{p_2^2}(e^{p_2\tau} - 1) - \tfrac{\beta_1}{p_1}(e^{p_1\tau} - 1) - \tfrac{\beta_2}{p_2}(e^{p_2\tau} - 1)
\end{aligned} \tag{8.28}$$

At large time $\tau \to \infty$ the formulae (8.27) and (8.28) are reduced to

$$\begin{aligned}
\tfrac{x_0}{L} &= \tau, \\
\tfrac{y_0}{L} &= -\left(\tfrac{\Omega_1}{p_1} + \tfrac{\Omega_2}{p_2}\right)\tau - \left(\tfrac{\Omega_1}{p_1^2} + \tfrac{\Omega_2}{p_2^2} - \tfrac{\beta_1}{p_1} - \tfrac{\beta_2}{p_2}\right).
\end{aligned} \tag{8.29}$$

$$\psi(\tau \to \infty) = -\left(\frac{\Omega_1}{p_1} + \frac{\Omega_2}{p_2}\right) \tag{8.30}$$

The ship trajectory is presented in Fig. 8.1

8.7 Steady ship motion in turning circle

In this subsection we give simple estimations of the radius and the drift angle when ship performs a steady turning circle. The estimations are derived using the assumptions (7.2). Stable ship motion along the turning circle trajectory is described by two last equations in the system (7.4) taking two following facts into account:

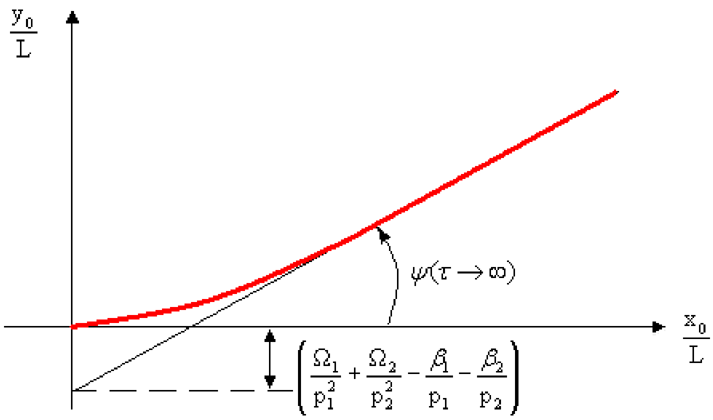

Figure 8.1: The trajectory of the stable ship after perturbation

- since the motion is steady, the time derivatives are zero $\beta' = 0, \Omega' = 0$,
- the turning circle manoeuvre implies application of the rudder. Therefore, the additional force - C_{YR} should be added to the r.h.s. of the y-equation and the additional moment m_{zR} to the r.h.s. of the Ω equation. The sign of the additional force is negative, since the positive rudder angle results in the negative transverse force.

The system (7.4) is then reduced to:

$$\begin{cases} \kappa_x \Omega = C_y^\beta \beta + C_y^\Omega \Omega - C_{yR}, \\ 0 = m_z^\beta \beta + m_z^\Omega \Omega + m_{zR}. \end{cases} \tag{8.31}$$

The drift angle and the angular velocity are found from the solution of the system of linear equations (8.31)

$$\Omega_c = -\frac{C_y^\beta m_{zR} + m_z^\beta C_{yR}}{m_z^\Omega C_y^\beta + m_z^\beta C_y^{*\Omega}}, \qquad \beta_c = \frac{-C_y^{*\Omega} m_{zR} + m_z^\Omega C_{yR}}{m_z^\beta C_y^{*\Omega} + m_z^\Omega C_y^\beta}. \tag{8.32}$$

The turning circle radius is calculated from the definition of Ω

$$\Omega_c = \frac{\omega_z L}{V} = \frac{V}{R_c}\frac{L}{V} = \frac{L}{R_c} \Rightarrow R_c = \frac{L}{\Omega_c} \tag{8.33}$$

8.8 Regulation of the stability

The expression $m_z^\beta C_y^{*\Omega} + C_y^\beta m_z^\Omega$ is not a quantity to measure the stability. Rather the roots p_1 and p_2 characterizing the rate of the perturbation decay can be considered as the stability measure. From one side, the ship has to be stable. From the other side, the ship may not be too stable, since in this case the ship is hardly to steer.

At present there is no widely accepted measure of the stability. Kleinau [21] proposes to regulate the position of the apparent center of rotation along the ship. The apparent center of rotation x_D is the point where the local incoming flow velocity is zero:

$$V(\beta_c - \Omega_c \frac{x_D}{L}) = 0 \Rightarrow \frac{x_D}{L} = \frac{\beta_c}{\Omega_c} \tag{8.34}$$

It is assumed that the arm of the transverse force is L/2, i.e. $m_{zR} = -\frac{1}{2}C_{yR}$. Substitution (8.32) into (8.34) yields

$$\frac{x_D}{L} = \frac{\beta_c}{\Omega_c} = \frac{C_y^{*\Omega} - 2m_z^{\Omega}}{C_y^{\beta} + 2m_z^{\beta}} = \frac{\left(C_B\frac{B}{T}\lambda - \frac{\pi C\lambda}{4}\right) + \frac{\pi C\lambda}{4}}{\frac{\pi C\lambda}{2} + \frac{\pi C\lambda}{2}} = \frac{C_B B}{\pi CT}{}^{1} \tag{8.35}$$

Comparing with (8.26) we obtain a new formulation of the stability condition

$$\boxed{\frac{x_D}{L} < \frac{1}{2}} \tag{8.36}$$

The center of rotation should lie within the ship length behind the bow. Practical experience (see [21]) shows that the well steered stable ship has the center of rotation at $x_D = (0.3 \div 0.4)L$

$$\boxed{\frac{x_D}{L} = 0.3 \div 0.4} \tag{8.37}$$

8.9 Exercises

1. Calculate the stability criterion for the ship with following parameters: $L = 60$ m, $T_1 = 5$ m, $C_B = 0.8$, $C = 1.5$.

   Make the calculation for three different ship width: $B_1 = 8$ m, $B_2 = 12$ m and $B_3 = 15$ m and plot the dependence of criterion on the ship width. Use formel (7.20) for criterion.

$$C_y^{\beta} = \frac{\pi \cdot c \cdot \lambda}{2}, \quad C_y^{\Omega} = \frac{\pi \cdot c \cdot \lambda}{4}, \quad m_z^{\beta} = \frac{\pi \cdot c \cdot \lambda}{4}, \quad m_z^{\Omega} = -\frac{\pi \cdot c \cdot \lambda}{8}$$

[1] $\kappa_x = C_B\frac{B}{T}\lambda$. Please prove!

$$C_y^{\Omega *} = \kappa_x - C_y^{\Omega}, \quad \kappa_x = \frac{m + m_{11}}{\rho/2 \cdot A_L \cdot L}, \quad m_{11} = k_{11} \cdot m$$

2. Make the calculation of the stability criterion for another ship draught $T_2 = 4$ m and plot the dependence of criterion on the ship width as well.

Chapter 9

Manoeuvrability Diagram. Experimental study of the manoeuvrability

Summary: This, one of the most important chapters of the book, is devoted to the experimental methods of ship manoeuvrability including turning circle, zig-zag, spiral, pull-out an stop tests. Experimental results are basis for the manoeuvrability diagram which illustrates the ship stability, controlability and manoeuvrability.

9.1 Stability at large drift angle and large angular velocity

Stability analysis at large drift angle β_* and angular velocity Ω_* is performed in a similar way as the stability analysis described in the previous chapter for the case $(\beta_* = 0, \Omega_* = 0)$. The criterion of the stability is obtained in the same form as (8.22)

$$-\frac{m_z^{\Omega}(\beta_*, \Omega_*)}{C_y^{*\Omega}(\beta_*, \Omega_*)} > \frac{m_z^{\beta}(\beta_*, \Omega_*)}{C_y^{\beta}(\beta_*, \Omega_*)} \tag{9.1}$$

with the difference that the derivatives $m_z^{\Omega}(\beta_*, \Omega_*)$, $m_z^{\beta}(\beta_*, \Omega_*)$, $C_y^{*\Omega}(\beta_*, \Omega_*)$ and $C_y^{\beta}(\beta_*, \Omega_*)$ are calculated at (β_*, Ω_*) and not at $(\beta_* = 0, \Omega_* = 0)$ as done previously. In this case the nonlinear effects are taken into account. For instance, the derivative of the transverse force on the drift angle looks differently at $(\beta_* = 0, \Omega_* = 0)$ and (β_*, Ω_*):

$$
\begin{aligned}
C_y(\beta) &= C_y^{\beta}\beta + C_y^{\beta\beta}\beta^2, \\
\frac{\partial C_y}{\partial \beta} &= C_y^{\beta} + 2C_y^{\beta\beta}\beta, \\
\left.\frac{\partial C_y}{\partial \beta}\right|_{\beta=0} &= C_y^{\beta}, \\
\left.\frac{\partial C_y}{\partial \beta}\right|_{\beta=\beta_*} &= C_y^{\beta} + 2C_y^{\beta\beta}\beta_*
\end{aligned}
\tag{9.2}
$$

The term $2C_y^{\beta\beta}\beta_*$ is responsible for nonlinear effects. Effect of the nonlinear terms changes the ship dynamics qualitatively.
The ship which is unstable at $(\beta_* = 0, \Omega_* = 0)$ experiences an unstable motion, moves into the turning trajectory and arrives a stable motion state along a circle at certain (β_*, Ω_*), at which the ship becoming stable.

Without account for nonlinear terms the ship remains unstable at every drift angle and angular velocity.

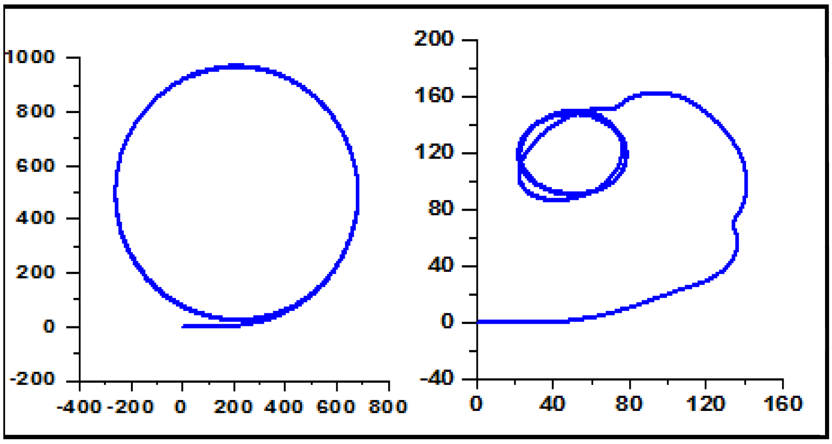

Figure 9.1: Turning circle of a container ship with the length 232 m (left) and of the same ship with the length reduced up to 62 m (right). In the second case the ship is unstable at $\Omega = \beta = 0$

9.2 Diagram $\Omega - \beta$

The ship stability can be estimated from the slope of the dependencies of the dimensionless angular velocity on the drift angle derived from the system (8.31)

$$\begin{cases} \kappa_x \Omega = C_y^\beta \beta + C_y^\Omega \Omega - C_{yR}, \\ 0 = m_z^\beta \beta + m_z^\Omega \Omega + m_{zR}. \end{cases}$$

The angular velocity can be found from this system:

$$\Omega_f = \frac{C_y^\beta}{C_y^{*\Omega}}\beta - \frac{C_{yR}}{C_y^{*\Omega}} \qquad \text{from the first equation for the y- force} \tag{9.3}$$

$$\Omega_m = -\left(\frac{m_z^\beta}{m_z^\Omega}\beta + \frac{m_{zR}}{m_z^\Omega}\right) \text{from the second equation for the z- moment} \tag{9.4}$$

The slope of the dependence $\Omega_f(\beta)$ is $\frac{C_y^\beta}{C_y^{*\Omega}}$ whereas $-\frac{m_z^\beta}{m_z^\Omega}$ is the slope of the dependence $\Omega_m(\beta)$. According to the criterion (8.22) the slope $\frac{C_y^\beta}{C_y^{*\Omega}}$ should be larger $\frac{C_y^\beta}{C_y^{*\Omega}} > -\frac{m_z^\beta}{m_z^\Omega} \Rightarrow -\frac{m_z^\Omega}{C_y^{*\Omega}} > \frac{m_z^\beta}{C_y^\beta}$. It was considered that the coefficient m_z^Ω is negative. Typical dependencies $\Omega_f(\beta)$ and $\Omega_m(\beta)$ are presented in Fig. 9.2 for stable ship (left) and unstable ship (right). Since we used linear representation of forces both dependencies are linear. The crossing points of the lines $\Omega_f(\beta)$ and $\Omega_m(\beta)$ with the vertical axis are

$$\begin{aligned} \Omega_f|_{\beta=0} &= -\frac{C_{yR}}{C_y^{*\Omega}} < 0 \quad \text{for positive rudder angles} \quad \delta_R > 0 \\ \Omega_f|_{\beta=0} &= -\frac{C_{yR}}{C_y^{*\Omega}} > 0 \quad \text{for negative rudder angles} \quad \delta_R < 0 \end{aligned} \tag{9.5}$$

$$\Omega_m|_{\beta=0} = -\frac{m_{zR}}{m_z^\Omega} > 0 \quad \text{for positive rudder angles} \quad \delta_R > 0 \tag{9.6}$$

$$\Omega_m|_{\beta=0} = -\frac{m_{zR}}{m_z^\Omega} < 0 \quad \text{for negative rudder angles} \quad \delta_R < 0 \tag{9.7}$$

The crossing points of two lines $\Omega_f(\beta) = \Omega_m(\beta)$ are equilibrium points at which both equations of the system (8.31) are satisfied, i.e. the total transverse force and the total yaw moment are zero.

If the nonlinear force and moment components are taken into account the dependencies $\Omega_f(\beta)$ and $\Omega_m(\beta)$ are nonlinear. Typical picture for the stable ship is presented in Fig. 9.3a. Again, the crossing points are equilibrium

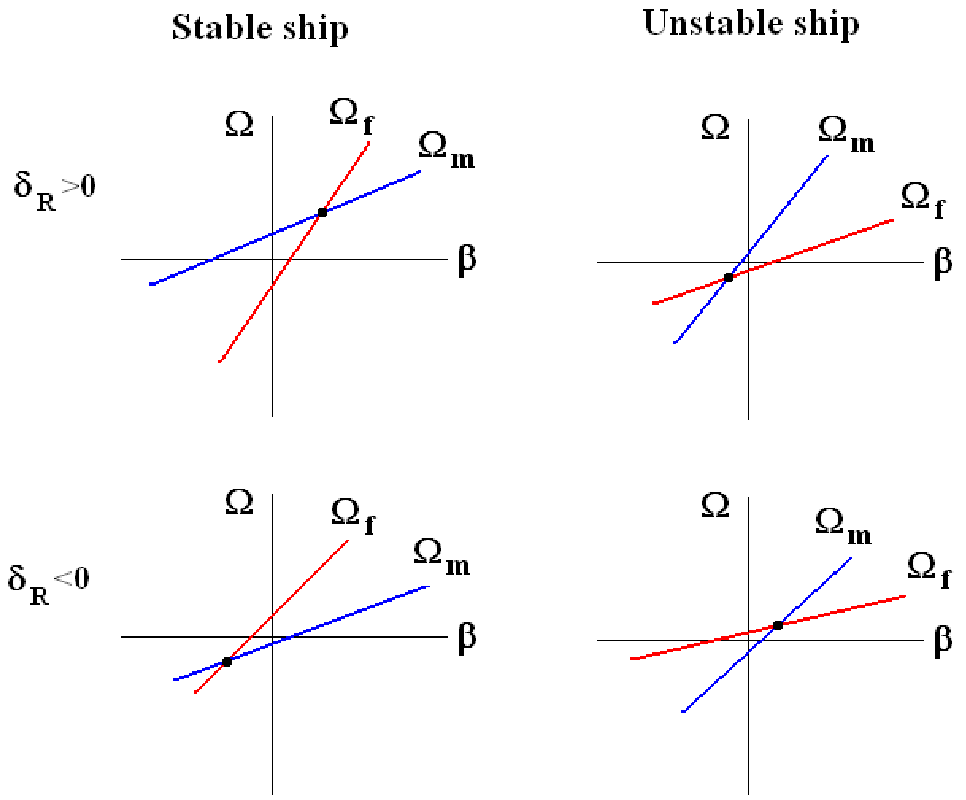

Figure 9.2: Typical dependencies $\Omega_f(\beta)$ and $\Omega_m(\beta)$ for stable ship (left) and unstable ship (right)

points. The diagram 9.3 can be redrawn into the diagram of manoeuvrability showing the dependence of the angular velocity Ω (or the turning circle radius) on the rudder angle δ_R (Fig. 9.3b). Each point along the curve $\Omega(\delta_R)$ is the equilibrium point. At each equilibrium point the slope of the curve $\Omega_f(\beta)$ is larger than that of the curve $\Omega_m(\beta)$. Therefore, the ship is stable.

Typical picture for the unstable ship is presented in Fig. 9.4a. Again, the crossing points are equilibrium points which are subdivided into stable points (filled circles) and unstable points (bars). At stable points the slope of the curve $\Omega_f(\beta)$ is larger than that of the curve $\Omega_m(\beta)$. The diagram 9.4a can be redrawn into the diagram of manoeuvrability (Fig. 9.4b). This procedure is illustrated in Fig. 9.4b. To map the plane $\Omega - \beta$ into the plane $\Omega - \delta_R$, each point corresponding to a certain rudder angle δ_R in $\Omega - \beta$ plane is projected onto line $\delta_R = const$ in $\Omega - \delta_R$ plane. The line corresponding to the equilibrium states has a typical S-shaped form for unstable ship.

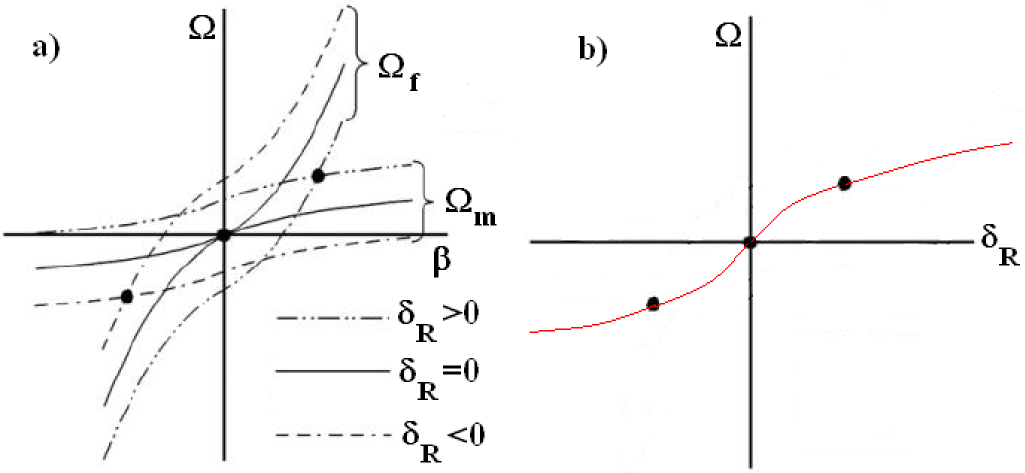

Figure 9.3: Typical dependencies $\Omega_f(\beta)$, $\Omega_m(\beta)$ and $\Omega(\delta_R)$ for a stable ship

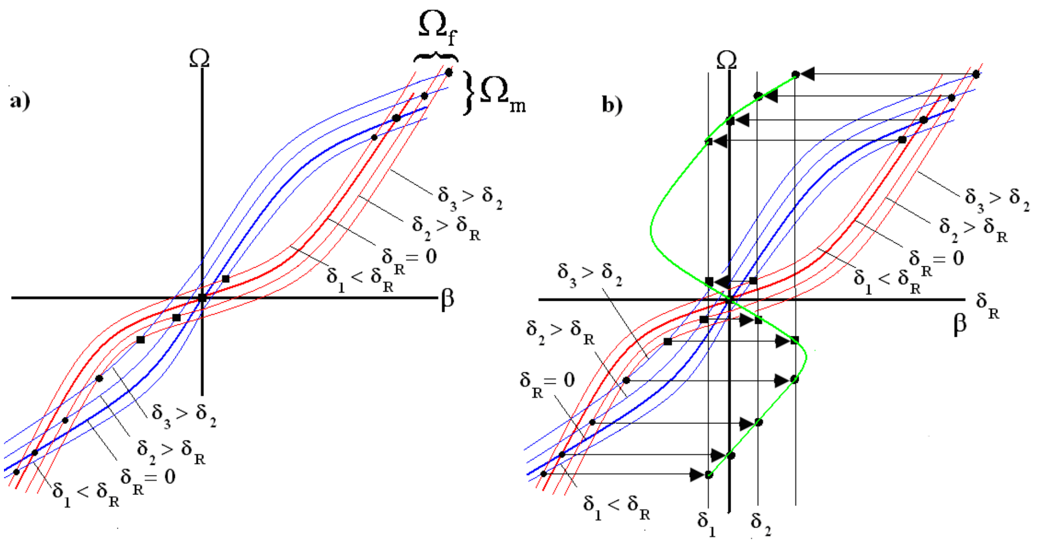

Figure 9.4: Typical dependencies $\Omega_f(\beta)$, $\Omega_m(\beta)$ and $\Omega(\delta_R)$ for an unstable ship

9.3 Manoeuvrability diagram

The dynamic yaw stability can also be analyzed using dependencies of the dimensionless angular velocity Ω on the rudder angle which can be either calculated or obtained from the trial tests. Typical dependencies $\Omega(\delta_R)$ are shown in Fig. 9.5 for the stable ship a) and unstable ship b). The ship is stable if the slope of the curve $\Omega(\delta_R)$ is positive and vice versa the ship is unstable if $\frac{\partial\Omega}{\partial\delta_R} < 0$. The negative slope is observed at small rudder angles corresponding to small drift angles. At large rudder and drift angles the nonlinear components of force and moment secure the yaw stability as was already mentioned above. The derivative $\frac{\partial\Omega}{\partial\delta_R}$ characterizes the ship controllability. If the derivative $\frac{\partial\Omega}{\partial\delta_R}$ is zero, the ship is not steerable. The value of $\frac{\partial\Omega}{\partial\delta_R}$ should be large but restricted. The infinite derivative $\frac{\partial\Omega}{\partial\delta_R} = \infty$ is the sign of the yaw instability.

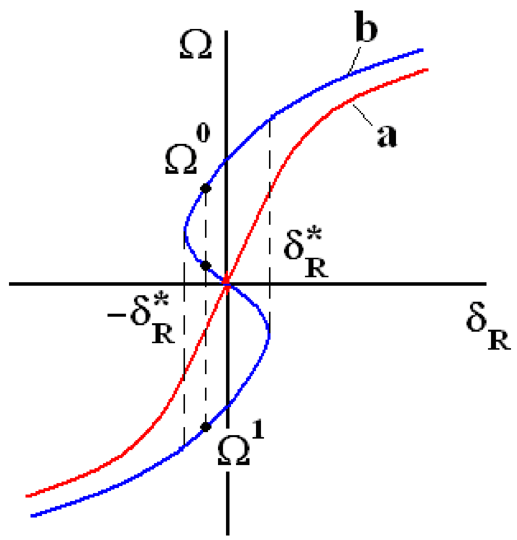

Figure 9.5: Manoeuvrability diagram

In the rudder angle range between $-\delta_R^* < \delta < \delta_R^*$ there exists three possible turning circles for the unstable ship. The ship is not steerable in this range. The ship oscillates between two angular velocities corresponding to stable states Ω^0 and Ω^1.

The manoeuvrability diagram can be used for solution of the following practical problems:

- estimation of the ship stability from the condition $\frac{\partial\Omega}{\partial\delta_R} > 0$.
- estimation of the critical rudder angles $-\delta_R^*$ and δ_R^* from the condition $\frac{\partial\Omega}{\partial\delta_R} = \infty$,
- estimation of the angular velocity and turning circle radius for the given rudder angle. This task has unique solution only for stable ships.
- design of the control system.

9.4 Experimental manoeuvring tests

The manoeuvring properties of ships are validated in sea trials with full-scale ships. The tests are performed in deep, unrestricted water under calm environment conditions. The ship has the full load (summer load line draught) and even keel condition. The ship motion parameters are measured usually by GPS. The main manoeuvring tests are:

- turning circle test
- zigzag manoeuvre
- spiral manoeuvre
- pull-out manoeuvre
- stop manoeuvre

9.4.1 Turning circle

The test is started from straight motion with the design speed. After that the rudder is deflected to an angle δ_R and the speed is a little reduced due to increase of the resistance. The test is performed as long as the ship course angle is changed from zero to at least 540 degrees. The following parameters are measured in turning circle test:

- tactical diameter (see Fig. 9.6)
- maximum advance (see Fig. 9.6)
- transfer at 90° change of heading (see Fig. 9.6)
- times to change heading from 90° to 180°
- transfer loss of steady speed.

Typical tactical diameters lie in the range between 4.5 - 7 ship lengths for slender ships, 2.4 - 4 for short and full ships. Conventional ships have heel outwards in the turning circle. According to IMO regulations [15][1] the advance should not exceed 4.5 ship lengths and tactical diameter should not exceed five ship lengths.

9.4.2 Zigzag manoeuvre

The zigzag test is started from the straight motion with the design speed. The rudder is turned at δ^* degrees to the port side and is kept constant until the heading angle attains δ^* degrees to the port side. After that the

[1] Standards should be applied to ships of all rudder and propulsion types, of 100 m in length and over, and chemical tankers and gas carriers regardless of the length. The standards should not be applied to high-speed craft.

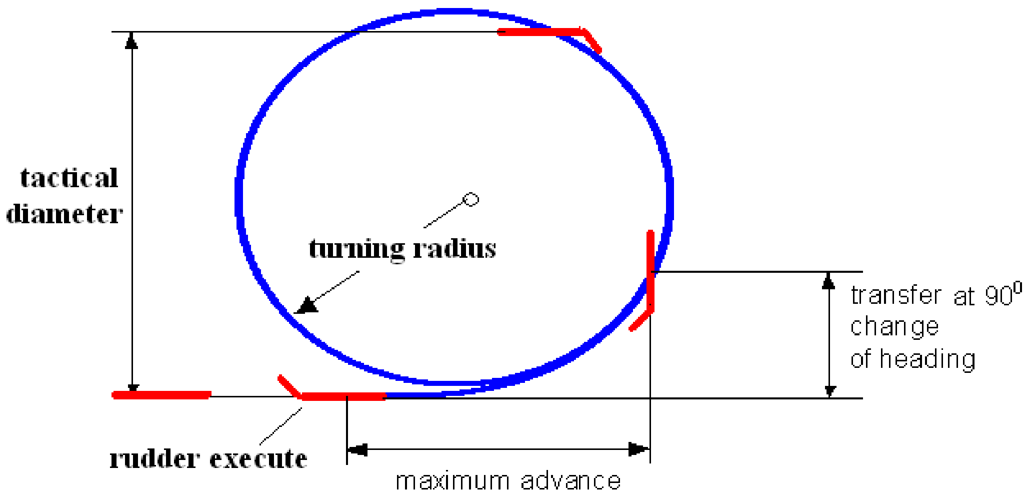

Figure 9.6: Geometric parameters of the turning circle

rudder is deflected to δ^* degrees to the starboard and is kept constant until the heading angle attains the value δ^* to the starboard. After that the whole procedure is repeated. Typical values of δ^* are 10 and 20 degrees.

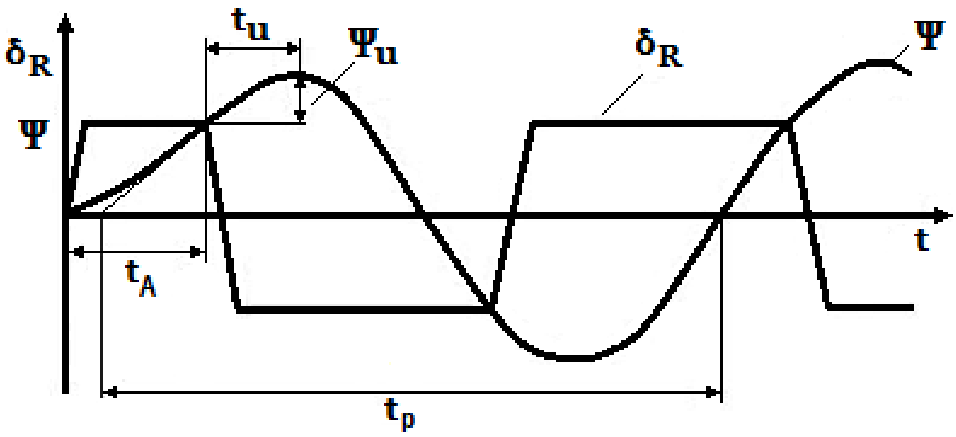

Figure 9.7: Parameters of the zigzag manoeuvre

Fig. 9.7 shows the parameters of the zigzag manoeuvre as given by Kleinau [21]:

- initial turning time t_A ,
- time t_U from the rudder reversion time instant to the time corresponding to the maximum heading angle,
- overshoot angle Ψ_U,
- period of the first heading oscillation.

According to Brix [11] the initial turning time t_A is about one to one and half of ship length travel time. The time t_U lies in the range between 0.5 and 2 ship travel length time. The overshoot angle is between 5 and 15 degrees. Small values of t_A and Ψ_U pointed out the big ship stability. According to IMO regulations [15] „with the application of 10° rudder angle to port/starboard, the ship should not have traveled more than 2.5 ship lengths by the time the heading has changed by 10° from the original heading".
According to IMO regulations [15][2] the parameters of zig-zag test should fulfill the following conditions (taken from [15]):

- The value of the first overshoot angle in the 10°/10° zig-zag test should not exceed:
  10° if L/V is less than 10 s;
  20° if L/V is 30 s or more; and
  $(5 + 1/2(L/V))$ degrees if L/V is 10 s or more, but less than 30 s, where L and V are expressed in m and m/s, respectively.
- The value of the second overshoot angle in the 10°/10° zig-zag test should not exceed:
  25°, if L/V is less than 10 s;
  40°, if L/V is 30 s or more; and
  $(17.5 + 0.75(L/V))$ degrees, if L/V is 10 s or more, but less than 30 s.
- The value of the first overshoot angle in the 20°/20° zig-zag test should not exceed 25°.

9.4.3 Spiral manoeuvre

The aim of the spiral test is the determination of data to draw the manoeuvring diagram $\Omega(\delta_R)$ (see Fig. 9.5). At the beginning of the test the rudder is turned at the maximum deflection angle δ_{Rmax}. As soon as the steady turning circle motion is attained the minimum turning radius, R_{min} corresponding to δ_{Rmax} is measured. The maximum angular velocity Ω_{max} is calculated. The rudder angle is gradually decreased and R and Ω are determined for each rudder angle in steady circle motions. The procedure is repeated for the rudder angle range from δ_{Rmax} to -3 -5 degrees. Herewith, the right branch of the curve $\Omega(\delta_R)$ is obtained. Then the tests are performed for the rudder angle range from $-\delta_{Rmax}$ to +3 +5 degrees. The left branch of the curve $\Omega(\delta_R)$ is obtained. For the stable ship both branches match each other.

[2] Standards should be applied to ships of all rudder and propulsion types, of 100 m in length and over, and chemical tankers and gas carriers regardless of the length. The standards should not be applied to high-speed craft.

The diagram $\Omega(\delta_R)$ is used to estimate the turning ability and yaw stability of the ship.

9.4.4 Pull-out manoeuvre

The full spiral test is time consuming and requires much place. The pull-out manoeuvre allows one to get the manoeuvrability diagram at reduced costs. At the beginning of the test the rudder is turned at the maximum deflection angle δ_{Rmax}. The minimum turning radius R_{min} corresponding to δ_{Rmax} is measured. The maximum angular velocity Ω_{max} is calculated. After that the rudder angle is set at zero and kept constant until a steady motion is attained. Then the rudder angle stepwise is decreased towards small negative values until the rotation direction is changed (Ω is getting negative). The right branch of the curve $\Omega(\delta_R)$ is obtained. To get the left branch, the whole procedure is repeated beginning from $-\delta_{Rmax}$ through zero towards positive rudder angle values. The manoeuvrability diagram gained from the pull-out test is used only for the yaw stability analysis.

9.4.5 Stop manoeuvre

At the beginning of this manoeuvre the engine is stopped and then reversed at full astern. The manoeuvre ends when the ship motion speed becomes zero. The stopping time and the stopping distance are measured. According to IMO regulations [15][3] the stopping distance should not exceed 15 ship lengths.

9.5 Exercises

1. The ship has the following parameters: L=232 m, T=10 m, B=32 m, The Lewis coefficient of the main frame C=0.75, the wake number w=0.2, V=10 m/sec. Thrust loading coefficient is 1.0. Find the rudder area A_R from the condition that the ship turning circle diameter is five ship lengths at $\delta_R = 35°$. The aspect ratio of the rudder is three.
   Tips:

   - Use the formulae $C_y^\beta = \frac{\pi C\lambda}{2}, m_z^\beta = \frac{\pi C\lambda}{4}, C_y^\Omega = \frac{\pi C\lambda}{4}, m_z^\Omega = -\frac{\pi C\lambda}{8}$, $\kappa_x = C_B \frac{B}{T}\lambda$.

[3] Standards should be applied to ships of all rudder and propulsion types, of 100 m in length and over, and chemical tankers and gas carriers regardless of the length. The standards should not be applied to high-speed craft.

- Find the block coefficient C_B from the condition of the proper stability $\frac{x_D}{L} = 0.35$ and formula (8.35).

2. The ship has the following parameters: L=232 m, T=10 m, B=64 m, the Lewis coefficient of the main frame C=0.75. The block coefficient is 0.7. Prove the yaw ship stability. How to make this ship stable? Tips:

   - Use the formulae $C_y^\beta = \frac{\pi C\lambda}{2}, m_z^\beta = \frac{\pi C\lambda}{4}, C_y^\Omega = \frac{\pi C\lambda}{4}, m_z^\Omega = -\frac{\pi C\lambda}{8}$, $\kappa_x = C_B \frac{B}{T}\lambda$.

3. Determine the ratio of longitudinal and cross flow velocity for a ship with $\frac{x_D}{L} = 0.5$ at a steady turning circle with a diameter of D=10*L! Use linearized formulae from chapter 7.

4. Compute the relative increase of a ship's steady turning radius after a ship extension of 10m if L=100 m, B=20 m, T=10 m, C_B=0.6 with rectangular cross section.
   Tips:
   Consider rudder forces and moment unchanged! Determine Lewis coefficient from chart, compute new value for C_B. Use formulae from Chapter 7.6.

Chapter 10

Influence of different factors on the manoeuvrability

Summary: Influence of different factors on the ship stability, controlability and manoeuvrability is shown. A special attention is paid to shallow water effects and wall influence.

10.1 Influence of the seaway

The influence of the seaway on the ship stability can be detrimental if the ship speed is getting equal to the wave speed in following waves. The ship losses the stability, turns quickly perpendicular to the wave propagation direction. This effect disappears when the difference between the ship and wave speeds increases. In head waves the ship stability and manoeuvrability are sufficiently better than in the following waves.

10.2 Shallow water effect

The shallow water effect takes place when the water depth is smaller than four ship draughts $H < 4T$. The shallow water influenced both the ship added mass and force acting on the ship. The added mass coefficients

$$\bar{k}_{11} = m_{11\_shallow\_water}/m_{11\_deep\_water},$$
$$\bar{k}_{22} = m_{22\_shallow\_water}/m_{22\_deep\_water}$$
$$\bar{k}_{66} = m_{66\_shallow\_water}/m_{66\_deep\_water}$$

are presented in Fig.10.1. As seen the added mass are increased drastically due to shallow water effect. The transverse force is also increased. This effect can be easily explained by the blocking effect caused by the ship in shallow water. In this case each frame is streamed not in unrestricted flow but in a narrow channel as it is shown in Fig.10.3. The frame blocks the flow in the channel. Obviously the force is much larger when the depth is small. The force and moment increase due to shallow water effects is illustrated in Fig.10.2 and 10.3. The only non increasing derivative is the derivative of the force on the angular velocity C_y^Ω. Very interesting is the dependence of the transverse force and the moment on the Fn number in shallow water (Fig.10.4). The measurement is performed for a merchant ship at H/T=3.5 and angular velocity $\Omega = 0.67$ deg/sec. Like in the deep water case the coefficients are independent on the Fn number at $Fn < 0.2$. Critical effects take place when the Froude number based on the depth H attains the value around one $Fn_H = \frac{V}{\sqrt{gH}} \approx 1$. Similarly to the drag the transverse force and the yaw moment experiences jump-like behaviour around $Fn_H = \frac{V}{\sqrt{gH}} \approx 1$.

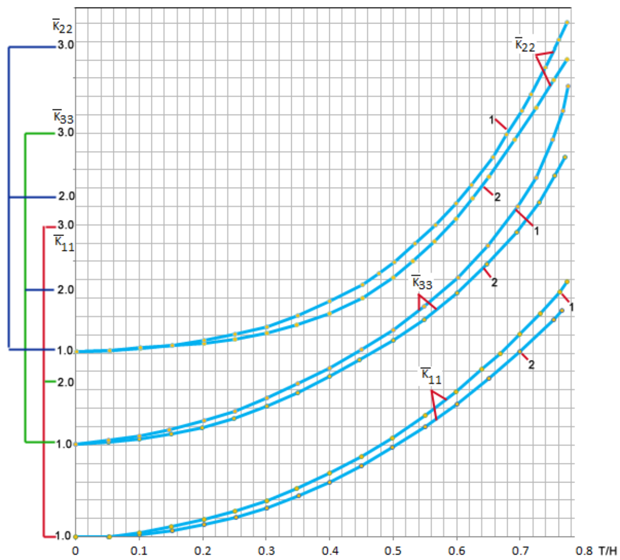

Figure 10.1: Shallow water effect on the added mass. $1 - C_B = 0.52, 2 - C_B = 0.8$ [35]

Consider the stable ship motion in the turning circle with the angular velocity Ω and the constant rudder angle. When the water depth is getting small, the term in the Y- force equation $C_y^\beta \beta + \left(C_y^\Omega - \kappa_x\right)\Omega - C_{yR} = 0$ proportional to the angular velocity $C_y^\Omega - \kappa_x$ remains nearly constant (see Fig.10.2) whereas the term proportional to the drift angle C_y^β is substantially increased. The equilibrium is then possible when the drift angle β decreases. Indeed, the drift angle during the turning circle motion is much smaller than

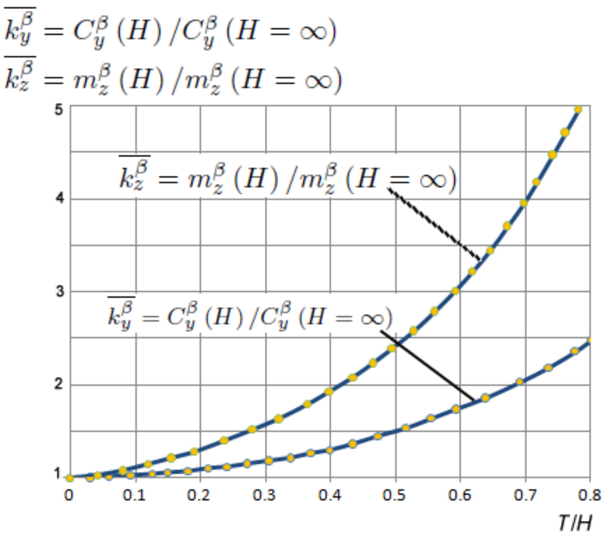

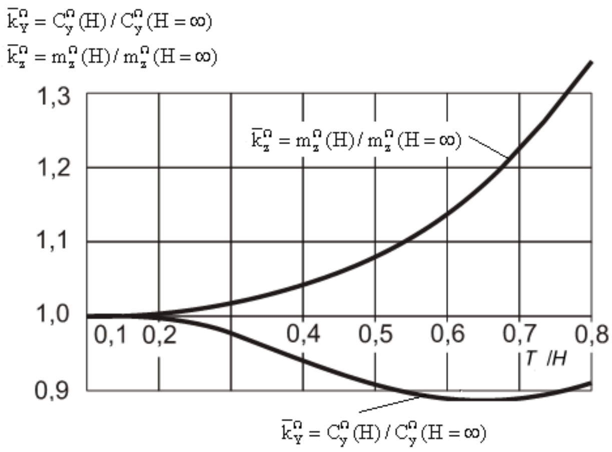

Figure 10.2: Shallow water effects on transverse force and moment derivatives on drift angle and angular velocity for a merchant ship. $\bar{k}_Y^\beta = C_y^\beta(H)/C_y^\beta(H = \infty)$, $\bar{k}_z^\beta = m_z^\beta(H)/m_z^\beta(H = \infty)$, $\bar{k}_Y^\Omega = C_y^\Omega(H)/C_y^\Omega(H = \infty)$ and $\bar{k}_z^\Omega = m_z^\Omega(H)/m_z^\Omega(H = \infty)$ [35]

on the deep water (see Fig.10.5). Reduction of the drift angle results in the decrease of the ship speed drop. Figure 10.6 displaying the dependence $\kappa_v = \frac{\text{speed in shallow water}}{\text{speed in deep water}}$ on the angular velocity gained from full-scale measurements supports this fact. As to the moment equation $m_z^\beta \beta + m_z^\Omega \Omega + m_{zR} = 0$, both terms proportional to Ω and β increase sufficiently. According to considerations above the drift angle is getting smaller when the ship comes to the shallow water. The term $m_z^\beta \beta$ is changed weakly because the decrease of β is counterbalanced by the increase of the moment derivative m_z^β. To

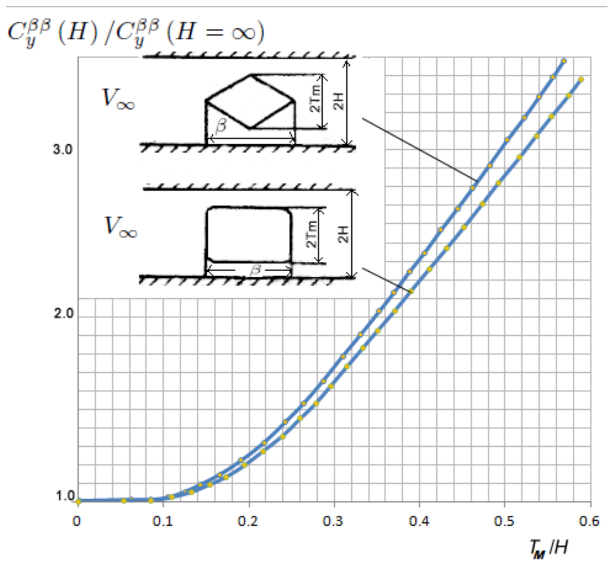

Figure 10.3: Shallow water effect on the derivative $C_y^{\beta\beta}$ [35]

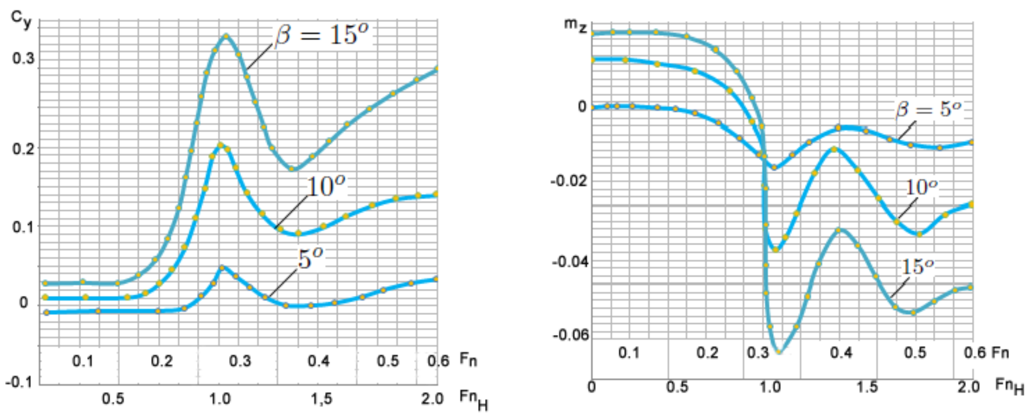

Figure 10.4: Shallow water effect on the transverse force and yaw moment at different Fn numbers [35]

counterbalance the increase of the derivative m_z^Ω and to hold the balance in moments, the angular velocity should also become small. Therefore, the angular velocity decreases when the water depth is getting smaller at $H \to 0$. The turning circle radius increases when $H \to 0$. The turning ability of ship is getting worse in shallow water. It is illustrated in Fig. 10.7 showing the dependence $\kappa_\Omega = \frac{\Omega \text{ in shallow water}}{\Omega \text{ in deep water}}$ on T/H ratio.

The shallow water has negative effect on the yaw stability. Fig. 10.8 shows the manoeuvrability diagram of a tanker at different ratios H/T. As seen

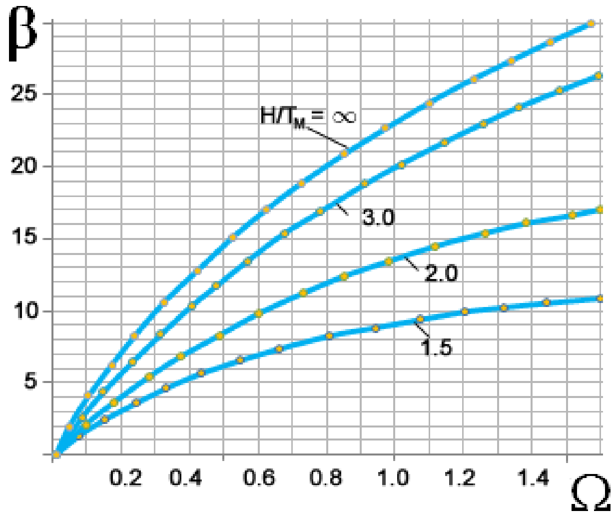

Figure 10.5: Shallow water effect on the drift angle [35]

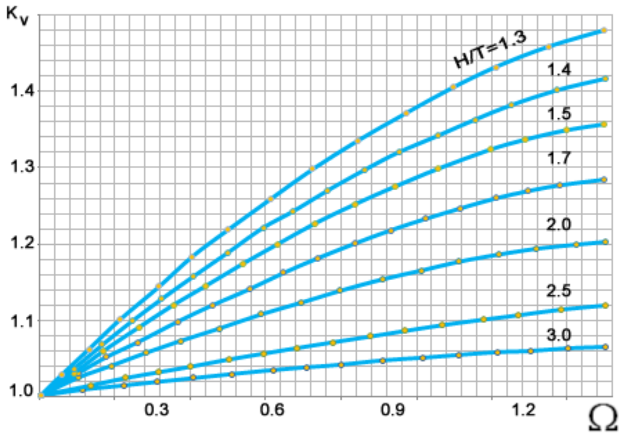

Figure 10.6: Shallow water effect on the ship speed reduction [35]

the tanker becomes unstable at $H/T \sim 1.5$. The zigzag manoeuvre is also influenced by the shallow water effects. Particularly, the overshoot angle is decreased when $H \to 0$.

10.3 Influence of the wall on a mooring ship

This effect takes place when the distance between the wall and the ship is smaller than four ship widths $H < 4B$. When the ship is moving close to the wall (Fig. 10.9) additional force and moment arise due to interaction between

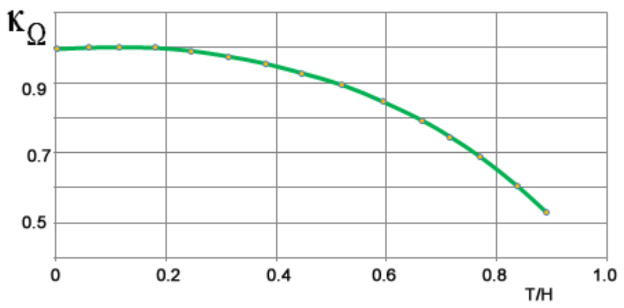

Figure 10.7: Shallow water effect on the reduction of the angular velocity in turning circle [35]

the wall and the ship. When the angle between the wall and the ship ϕ is small the flow channel between the ship and the wall is getting narrow. According to the continuity equation the flow is accelerated between the ship and the wall. From Bernoulli equation follows, that an under pressure region occurs between the ship and the wall. In the bow region the transverse force Y_1 is positive whereas a strong negative suction force Y_2 appears in the region of the minimum distance between the ship and the wall. Usually at small ϕ $Y_2 > Y_1$ and the ship experiences the attraction effect. The resulting moment is positive and leads to the ship motion away from the wall. At large angles ϕ both the resulting force and the moment are positive and displace the ship away from the wall. At each ϕ the operator has to put much effort to hold the ship parallel to the wall.

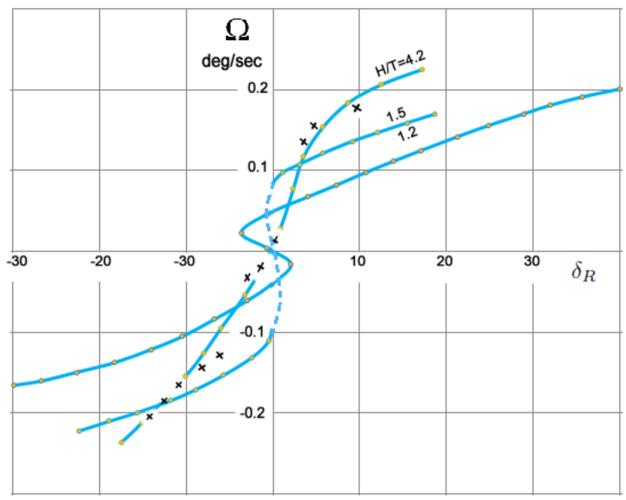

Figure 10.8: Manoeuvrability diagram of a tanker in shallow water [35]

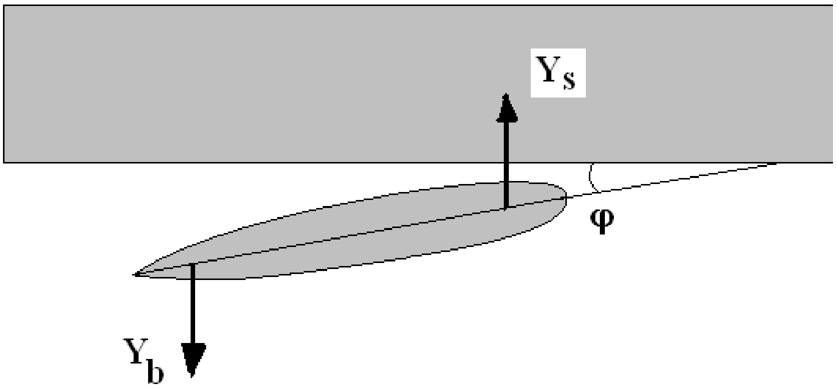

Figure 10.9: Interaction of the ship with wall during the mooring

10.4 Influence of the inclined wall or of inclined bottom

The same effects as in the case of the wall are observed in cases of the inclined wall or of inclined bottom. The difficulties of ship control are illustrated in Fig. 10.10 showing the rudder angle necessary to hold the ship on a given course in shallow water at different speeds. The Froude number Fn_H is based on the speed and water depth, i.e. $Fn_H = V/\sqrt{gH}$. At small H and velocities the ship can become fully non steerable and moves in direction of the water depth enlargement.

10.5 Control questions

1. How do main ship parameters influence the ship's stability?

2. Why is it disadvantageous, if a ship is too stable?

3. Draw a manoeuvrability diagram for a stable and an unstable ship. Why $\frac{\partial \Omega}{\partial \delta_R}$ is becoming smaller at large δ_R? What values do rudder angles usually have?

4. Does the ship's bow point inside or outside of a turning circle? Explain this effect. What is the relation between Ω and R?

5. How is the absolute ship velocity changed during a turning circle manoeuvre? Explain this.

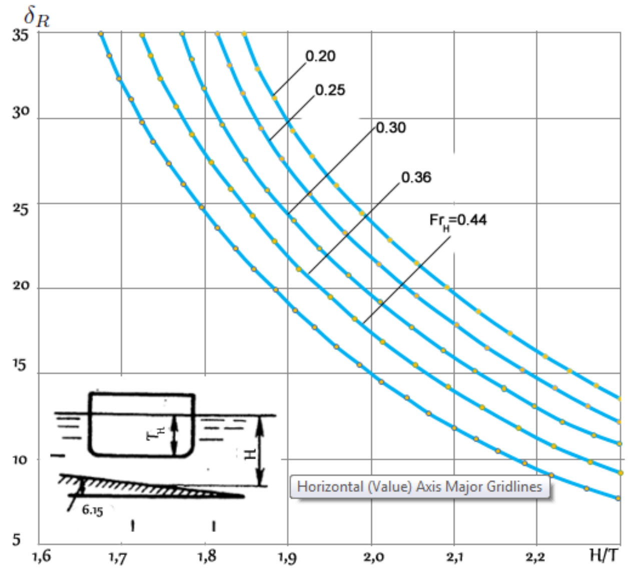

Figure 10.10: The rudder angle required to hold the ship course during the motion above the inclined bottom [35]

6. What is the influence of the ship's velocity on the turning circle diameter?

7. How does the velocity influence the Zig-Zag manoeuvre? Draw a representative diagram.

8. How does the stability influence the Zig-Zag manoeuvre? Draw a representative diagram.

9. Which manoeuvres are undertaken to prove the ship manoeuvrability?

10. Does the propeller influence the dynamic yaw stability? How?

11. Draw the trajectories for a stable and an unstable ship after a short transversal perturbation.

12. Which hydrodynamic derivatives can be determined using Circular Motion Test (CMT)?

13. What is the physical meaning of the ratio $X^\beta = C_m^\beta / C_y^\beta$? Where X^β should lay from the stability point of view?

14. Consider the equations of motion for a ship. Using identification method, which values do we measure, which values do we compute?

15. What are the principal differences between the PMM-test and the identification method?

16. Derive the Criterion of the static stability of airplanes.

Chapter 11

Application of computational fluid dynamics for manoeuvrability problems

Summary: The chapter is devoted to the description of modern numerical techniques to calculate the forces acting on manoeuvring ships. The ship fixed forms of the Navier-Stokes and URANS equations are derived. Problems of grid generation and moving grid technologies are discussed.

11.1 Introduction

As discussed above the viscous effects play a deciding role on the forces arising during the ship manoeuvering. At present the conventional methods based on experimental force determination and their approximations (see Chapter 4) are still the main instrument in manoeuvrability study. Since the accuracy of the mathematical model is still not satisfactory, the experimental methods will remain as the main tool of force determination for the next relatively long term. However, last decades much effort is put in the development and validation of computational fluid dynamics methods (CFD) for manoeuvering purposes. These methods are very attractive because they are general and don't need any kind of linearizations with respect to the drift angle, yaw velocity, etc. They allow to perform six degree of freedom coupled calculations and investigate the interaction between the different ship motions on manoeuvrability characteristics. Also the seaway influence on manoeuvrability can be taken into account.
The CFD methods are used at present in two ways. First they can be used for the force determination for particular ship motions. For instance, the forces

are determined when the ship has only the drift angle or only the yaw velocity. The coupled motions within the framework of the PMM or circular motion test methodology can also be studied. Such numerical tests are referred to the CFD based or numerical PMM tests. The forces are then determined like in PMM tests, approximated in form of, say, Abkowitz representation (4.13). The approximations are used then in motion simulations like it done in the code Manis (http://www.lemos.uni-rostock.de/lehre/schiffstheorie-i/).
Otherwise, the CFD methods are used to calculate both the dynamics (solution of ordinary differential equations (1.13)) and fluid dynamics equations (usually Unsteady Reynolds Averaged Navier Stokes Equations) in a coupled manner. At each time instant the forces are calculated from the Navier Stokes Equation and then used to alter the kinematic parameters. Such CFD applications are refereed to as the 6DOF (six degree of freedom) procedure. Application of the 6DOF procedure does not imply the use of classical hydrodynamic mass which become not necessary.

11.2 Basic Equations

11.2.1 6DOF Motion equations

The basic equations used for 6DOF systems are the equations (1.13) derived in the first chapter for the ship fixed coordinate system. Expressing the static moments S_x, S_y and S_z through the coordinates of the gravity center x_g, y_g and z_g we obtain:

$$
\left\{
\begin{array}{l}
m[(\frac{dV_x}{dt} + \omega_y V_z - \omega_z V_y) - x_g({\omega_y}^2 + {\omega_z}^2) - \\
- y_g(\frac{d\omega_z}{dt} - \omega_x\omega_y) + z_g(\frac{d\omega_y}{dt} + \omega_x\omega_z)] = F_x \\
m[(\frac{dV_y}{dt} - \omega_x V_z + \omega_z V_x) + x_g(\frac{d\omega_z}{dt} + \omega_x\omega_y) - y_g({\omega_x}^2 + {\omega_z}^2) \\
- z_g(\frac{d\omega_x}{dt} - \omega_y\omega_z)] = F_y \\
m[(\frac{dV_z}{dt} + \omega_x V_y - \omega_y V_x) - x_g(\frac{d\omega_y}{dt} - \omega_x\omega_z) + y_g(\frac{d\omega_x}{dt} + \\
+ \omega_y\omega_z) - z_g({\omega_x}^2 + {\omega_y}^2)] = F_z \\
I_{xx}\frac{d\omega_x}{dt} - (I_{yy} - I_{zz})\omega_y\omega_z - I_{xy}(\frac{d\omega_y}{dt} - \omega_x\omega_z) - I_{yz}({\omega_y}^2 - {\omega_z}^2) - \\
- I_{xz}(\frac{d\omega_z}{dt} + \omega_x\omega_y) + m[y_g(\frac{dV_z}{dt} + \omega_x V_y - \omega_y V_x) - \\
- z_g(\frac{dV_y}{dt} - \omega_x V_z + \omega_z V_x)] = M_x \\
I_{yy}\frac{d\omega_y}{dt} - (I_{xx} - I_{zz})\omega_x\omega_z - I_{xy}(\frac{d\omega_x}{dt} + \omega_y\omega_z) - I_{yz}(\frac{d\omega_z}{dt} - \omega_x\omega_y) - \\
- I_{xz}({\omega_z}^2 - {\omega_x}^2) + m[z_g(\frac{dV_x}{dt} + \omega_y V_z - \omega_z V_y) - \\
- x_g(\frac{dV_z}{dt} + \omega_x V_y - \omega_y V_x)] = M_y \\
I_{zz}\frac{d\omega_z}{dt} - (I_{xx} - I_{yy})\omega_x\omega_y - I_{xy}({\omega_x}^2 - {\omega_y}^2) - I_{yz}(\frac{d\omega_y}{dt} + \omega_x\omega_z) - \\
- I_{xz}(\frac{d\omega_x}{dt} - \omega_y\omega_z) + m[x_g(\frac{dV_y}{dt} - \omega_x V_z + \omega_z V_x) - y_g(\frac{dV_x}{dt} + \\
+ \omega_y V_z - \omega_z V_y)] = M_z.
\end{array}
\right. \tag{11.1}
$$

The forces F_x, F_y, F_z and moments M_x, M_y, M_z are subdivided into three components:

- forces and moments caused by gravity effects,
- hydrodynamic forces and moments,
- forces and moments arising on propellers.

$$
\begin{array}{l}
F_x = mg\cos\alpha_1 + F_{xn} + F_{xp}, \\
F_y = mg\cos\alpha_2 + F_{yn} + F_{yp}, \\
F_z = mg\cos\alpha_3 + F_{zn} + F_{zp}, \\
M_x = mg(\cos\alpha_3 y_g - \cos\alpha_2 z_g) + M_{xn} + M_{xp}, \\
M_y = mg(\cos\alpha_1 z_g - \cos\alpha_3 x_g) + M_{yn} + M_{yp}, \\
M_z = mg(\cos\alpha_2 x_g - \cos\alpha_1 y_g) + M_{zn} + M_{zp}.
\end{array} \tag{11.2}
$$

Here α_i are the angles between the corresponding axis and the vector of the ship gravity force. In principle the hydrodynamic forces and propeller forces can be calculated as the total force in CFD. In some works (see, for instance, [16]) the propeller contribution to forces and moments are calculated separately using a simple model.

11.2.2 URANS equations in ship fixed coordinate system

The hydrodynamic forces are calculated by direct integration of normal and shear stresses over the wetted ship area. The stresses are found from the fluid dynamics equations which are written in the ship fixed coordinate system.

The Reynolds averaged equations are supplemented by additional terms taking the acceleration, translation and rotation of the reference frame into account.

Let us $\vec{i}, \vec{j}, \vec{k}$ is a triad of orthogonal unit vectors fixed in the moving frame. Any vector $\vec{W}$ can be written through the projections $\vec{W} = W_1\vec{i} + W_2\vec{j} + W_3\vec{k}$. The change of $\vec{W}$ occurs as a result of both change of components W_1, W_2, W_3 in the moving frame and change of the unit vectors $\vec{i}, \vec{j}, \vec{k}$

$$\begin{aligned}
\left.\frac{d\vec{W}}{dt}\right|_0 &= \frac{dW_1}{dt}\vec{i} + \frac{dW_2}{dt}\vec{j} + \frac{dW_3}{dt}\vec{k} + W_1\frac{d\vec{i}}{dt} + W_2\frac{d\vec{j}}{dt} + W_3\frac{d\vec{k}}{dt} = \\
&= \frac{dW_1}{dt}\vec{i} + \frac{dW_2}{dt}\vec{j} + \frac{dW_3}{dt}\vec{k} + W_1(\vec{\Omega} \times \vec{i}) + W_2(\vec{\Omega} \times \vec{j}) + W_3(\vec{\Omega} \times \vec{k}) = \\
&= \frac{d\vec{W}}{dt} + \vec{\Omega} \times \vec{W}
\end{aligned} \tag{11.3}$$

The derivative $\frac{d\vec{W}}{dt}$ is calculated in the frame of reference rotating with angular velocity $\vec{\omega}$ whereas $\left.\frac{d\vec{W}}{dt}\right|_0$ is determined in the inertial reference system.
Let us consider the vector $\vec{x}$ determining the position of a moving element with respect to the moving frame of reference.
The speed of this element in the inertial frame of reference is:

$$\left.\frac{d\vec{x}}{dt}\right|_0 = \underbrace{\vec{V}}_{\substack{\text{velocity of the moving} \\ \text{frame of reference (m.r.f)}}} + \underbrace{\vec{\omega} \times \vec{x}}_{\substack{\text{contribution due to} \\ \text{rotation of m.r.f}}} + \underbrace{\frac{d\vec{x}}{dt}}_{\substack{\text{velocity of element} \\ \text{in m.r.f.}}} \tag{11.4}$$

The acceleration of the moving element in the inertial frame of reference is:

$$\begin{aligned}\left.\frac{d^2\bar{x}}{dt^2}\right|_0 &= \frac{d}{dt}\left(\left.\frac{d\vec{x}}{dt}\right|_0\right) + \vec{\omega}\times\left(\left.\frac{d\vec{x}}{dt}\right|_0\right) = \\ &= \frac{d\vec{\mathrm{v}}}{dt} + \frac{d\vec{\omega}}{dt}\times\vec{x} + \vec{\omega}\times\frac{d\vec{x}}{dt} + \frac{d^2\vec{x}}{dt^2} + \vec{\omega}\times\vec{V} + \vec{\omega}\times(\vec{\omega}\times\vec{x}) + \vec{\omega}\times\frac{d\vec{x}}{dt} = \\ &= \frac{d\vec{V}}{dt} + \frac{d\vec{\omega}}{dt}\times\vec{x} + 2\vec{\omega}\times\frac{d\vec{x}}{dt} + \frac{d^2\vec{x}}{dt^2} + \vec{\omega}\times\vec{V} + \vec{\omega}\times(\vec{\omega}\times\vec{x})\end{aligned} \tag{11.5}$$

$\frac{d\vec{x}}{dt}$ is the velocity of a fluid particle $\vec{u} = \frac{d\vec{x}}{dt}$, $\frac{d\vec{u}}{dt} = \frac{d^2\vec{x}}{dt^2}$. Here $\vec{u}$ is the velocity of the particle in m.r.f.

$$\frac{d\vec{u}}{dt} = \frac{\partial\vec{u}}{\partial t} + (\vec{u}\nabla)\vec{u} \tag{11.6}$$

The equation of Navier Stokes takes the form

$$\begin{aligned}\frac{d\vec{u}}{dt} + \frac{d\vec{V}}{dt} + \frac{d\vec{\omega}}{dt}\times\vec{x} + 2\vec{\omega}\times\vec{u} + \vec{\omega}\times\vec{V} + \vec{\omega}\times(\vec{\omega}\times\vec{x}) = \\ = \vec{f} - \frac{1}{\varrho}\nabla p + \nu\Delta\vec{u}\end{aligned}$$

or

$$\begin{aligned}\frac{\partial\vec{u}}{\partial t} + (\vec{u}\nabla)\vec{u} = \vec{f} - \frac{1}{\varrho}\nabla p + \nu\Delta\vec{u} - \frac{d\vec{V}}{dt} - \frac{d\vec{\omega}}{dt}\times\vec{x} - \\ - 2\vec{\omega}\times\vec{u} - (\vec{\omega}\times\vec{V}) - \vec{\omega}\times(\vec{\omega}\times\vec{x})\end{aligned} \tag{11.7}$$

The equation (11.7) is the Navier Stokes equation in a moving frame of reference. Additional body forces are referred to as: $-\frac{d\vec{V}}{dt}$ apparent body force compensating the translational acceleration of the frame, $-2\vec{\omega}\times\frac{d\vec{x}}{dt} - \vec{\omega}\times\vec{\mathrm{V}} = -2\bar{\omega}\times\bar{u} - \vec{\omega}\times\vec{\mathrm{V}}$ is the Coriolis force, $-\vec{\omega}\times(\vec{\omega}\times\vec{x})$ is the centrifugal force.

The unsteady Reynolds averaged equations in the ship fixed reference system have the same additional terms:

$$\begin{aligned}&\varrho\frac{\partial\bar{u}_i}{\partial t} + \varrho\frac{\partial\bar{u}_i\bar{u}_j}{\partial x_j} = \varrho\bar{f}_i + \frac{\partial}{\partial x_j}(\bar{\tau}_{ij} - \overline{u_i'u_j'}) - \frac{\partial\bar{p}}{\partial x_i} - \\ &- \frac{dV_i}{dt} - 2\varepsilon_{ijk}\omega_j\bar{u}_k - \varepsilon_{ijk}\frac{d\omega_j}{dt}x_k - \\ &- \varepsilon_{ijk}\omega_j\varepsilon_{kmn}\omega_m x_n - \varepsilon_{ijk}\omega_j V_k\end{aligned} \tag{11.8}$$

where V_i, ω_i are ship velocities and ε_{ijk} is the tensor of Levi-Civita. Derivation of (11.8) can be found in [23] (see also [16]). The viscous shear stresses $\bar{\tau}_{ij}$ are determined from the Newton hypothesis

$$\bar{\tau}_{ij} = \varrho\nu \left(\frac{\partial \bar{u}_i}{\partial x_j} + \frac{\partial \bar{u}_j}{\partial x_i} \right). \tag{11.9}$$

The Reynolds stresses are approximated with an eddy viscosity model proposed by Boussinesq:

$$-\overline{u_i' u_j'} = \nu_t \left(\frac{\partial \bar{u}_i}{\partial x_j} + \frac{\partial \bar{u}_j}{\partial x_i} \right) - \frac{2}{3}\delta_{ij} k \tag{11.10}$$

where ν_t is the turbulent kinematic viscosity and $k = \frac{1}{2}\overline{u_i' u_i'}$ is the turbulent kinetic energy. The overline in (11.8) - (11.10) stands for the time or ensemble averaging.
The turbulent viscosity is determined from any turbulence closure models, for instance, from $k - \varepsilon, k - \omega$, or from $k - \omega$ SST models.
Note that the transport equations for scalar quantities k, ω and the continuity equation

$$\frac{\partial \bar{u}_i}{\partial x_i} = 0 \tag{11.11}$$

remain without changes valid in the ship fixed coordinate system.
The vector of gravitational forces $\bar{F}_i$ is

$$\vec{F} = (\cos\alpha_1 \vec{i} + \cos\alpha_2 \vec{j} + \cos\alpha_3 \vec{k})g \tag{11.12}$$

11.2.3 Calculation of steady yaw ship motion

The steady yaw ship motion (see 11.1) is calculated to determine the dependence of forces on Ω. The ship rotation is considered in two ways. First, the incident flow has at the component of the speed $\vec{\omega} \times \bar{r}$ at the inlet of the computational domain. Second, URANS equations have additional forces:

$$\begin{aligned} \varrho\frac{\partial \bar{u}_i}{\partial t} + \varrho\frac{\partial \bar{u}_i \bar{u}_j}{\partial x_j} &= \varrho\bar{F}_i + \frac{\partial}{\partial x_j}(\bar{\tau}_{ij} - \overline{u_i' u_j'}) - \frac{\partial \bar{p}}{\partial x_i} - \\ &- 2\varepsilon_{ijk}\omega_j \bar{u}_k - \varepsilon_{ijk}\omega_j V_k - \varepsilon_{ijk}\omega_j \varepsilon_{kmn}\omega_m x_n \end{aligned}$$

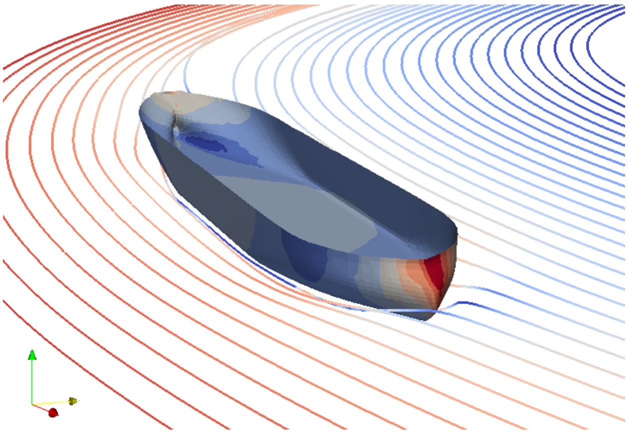

Figure 11.1: The ship at a yaw motion. Calculations of M. Haase, University of Rostock

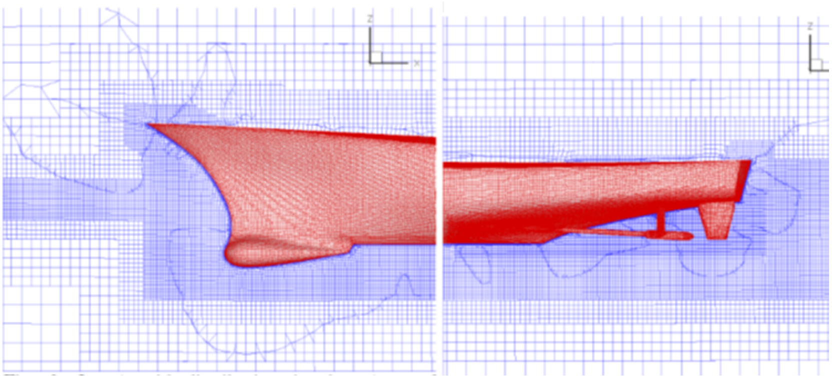

Figure 11.2: The Cartesian grid for the combatant ship [19]

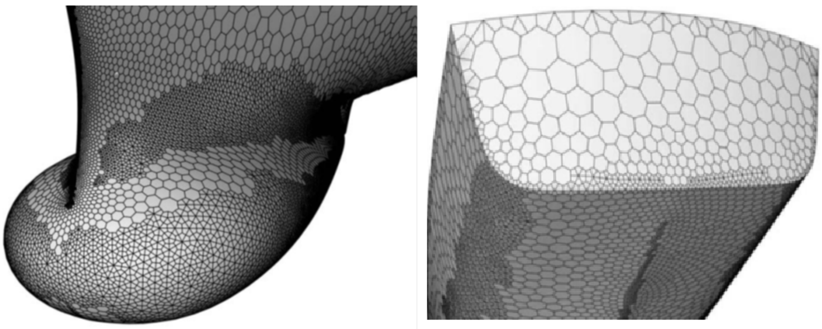

Figure 11.3: Unstructured grid for the combatant ship [28]

11.3 Computational grids

The quality of the grid has a strong impact on the accuracy of numerical prediction. The change of the cell topology within the computational domain

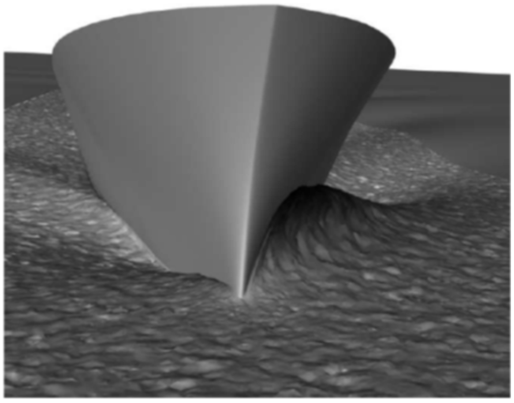

Figure 11.4: Unstructured grid for the combatant ship with the free surface [28]

should be smooth especially at the border between different grid blocks. The grid resolution should be high especially in areas of boundary layers and close to the free surface. For this sake the special refinement is used in these areas. To increase the accuracy of the computations in boundary layers one uses special grid boundary layers close to walls. Some samples of the grid for the combatant ship are presented in Fig.11.2 (cartesian block structured grid) and Fig.11.3 and 11.4 (unstructured grid) .

To get impression on sizes of the computational domain, we presents typical data taken from a CFD calculation of manoeuvrability [19]: in X direction the computational domain is from -2L to 3L (L is the ship length), the ship is from -0.5L to 0.5L, in the transversal direction from -L to 2L, in vertical direction from 0.2L to -1.5L. The resolution is chosen from the condition $y^+ \approx 1$ for the model scale and $y^+ \approx 100$ for the full scale.

11.3.1 Overset or Chimera grids

For complicated ship forms one uses overset or Chimera grids. The idea of chimera or overset grids is to generate the grids separately around each geometrical entity in the computational domain. After that the grids are combined together in such a way that they overlap each other where they meet. The crucial operation is an accurate transfer of quantities between the different grids at the overlapping region. The most important advantage of the overset or Chimera grid is the possibility to generate high quality structured particular grids separately for hull, rudder, propeller, appendages completely independent of each other, without having to take care of the interface between grids (Fig.11.5 and 11.6). The experience shows that the grid number necessary for rudder and propeller models is approximately as large as for the whole hull.

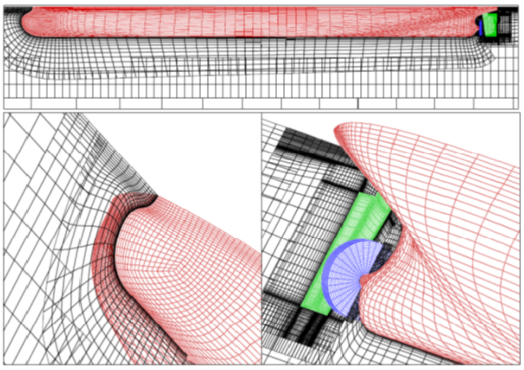

Figure 11.5: Chimera grid for tanker KVLCC2 [12]. Propeller is modeled using body forces distributed along the propeller disc

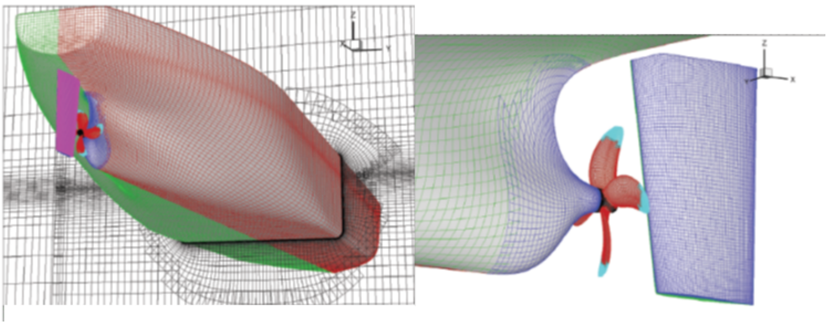

Figure 11.6: Chimera grid for a container ship with propeller and rudder [13]

11.3.2 Morphing grids

Very efficient way of complicated ship motion modeling is the use of moving or morphing grids [34]. The idea is the computational grid is moved in accordance with the displacement of the body by using an analytical weighted regridding which is a type of extrapolation of rigid transformation. For instance, in order to replicate the sway motion produced in the experimental PMM tests the ship geometry moves within the domain, deforming the mesh. The possible problem of morphing grid is poor quality caused by its motion. Consequently if the mesh surrounding the vehicle is allowed to deform the elements around the vehicle deform. This can quickly lead to poor quality elements if care is not taken. An alternative method is to replicate the motion of the vessel with the fluid domain split into an inner and outer region. The outer domain remains fixed in space while the inner domain containing the hull moves laterally to replicate the motion induced by a PMM. The mesh in the inner sub domain remains locked in position relative to the lateral motion of the vessel. This prevents deformation of the detailed mesh around the vessel. The outer mesh is deformed due to the motion of the inner region.

If moving grids are used the Navier Stokes should be transformed to take the velocity of grid faces $\vec{U}_g$ into account,

$$\frac{\partial \vec{u}}{\partial t} + \left\{ \left(\vec{u} - \vec{U}_g \right) \nabla \right\} \vec{u} = \vec{f} - \frac{1}{\rho} \nabla p + \nu \Delta \vec{u} \tag{11.13}$$

Thomas and Lombard have shown that the function $\vec{U}_g$ can not be arbitrary rather than they have to be found from the Geometric Conservation Law

$$\frac{\partial}{\partial t} \int\limits_U dU - \int\limits_S \vec{U}_g \vec{n} dS = 0 \tag{11.14}$$

Where U and S are respectively volume and surface of cells. The equation (11.14) is derived from the condition that the computation of the control volumes or of the grid velocities must be performed in a such a way that the resulting numerical scheme preserves the state of the uniform flow, independently of the deformation of the grid. The equation (11.14) is satisfied automatically if the control volumes don't change their shape. The Geometric conservation law (11.14) should solve coupled with other fluid flow equations using the same discretizations schemes.

A sample of calculation of the catamaran NPL performed by M. Haase using the OpenFoam code is presented in Fig.11.7 [20].

11.4 Exercises

Using the Code OpenFoam calculate the wigley ship at the drift angle 10 degrees. The Calculation case can be downloaded from http://www.lemos.uni-rostock.de/cfd-software/.

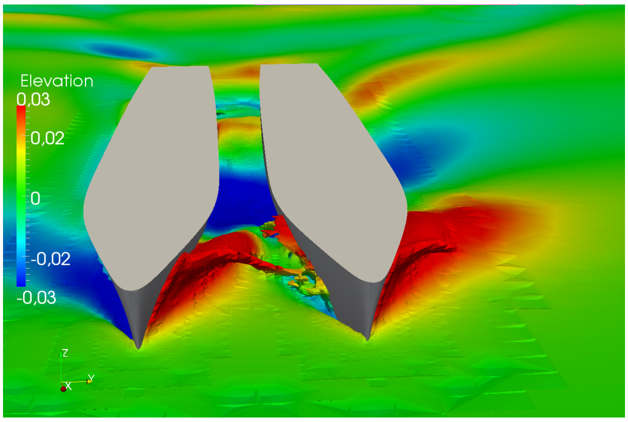

Figure 11.7: Bow wave and free surface elevation at $\beta = 15°$ and $Fn = 0.4$

Chapter 12

Dynamics and Stability of Wing in ground effect craft (WIG)

Summary: The chapter is optional. The subject is the aerodynamics, dynamics and stability of wing in ground effect craft (WIG). General six degree of freedom (6DOF) motion equations are derived. Hurwitz linear analysis is applied for derivation of criterion of the longitudinal stability. WIG static stability is analysed using the criterion proposed by Irodov. The WIG design requirements are formulated.

12.1 Introduction

The Wing-In-Ground craft (WIG) , called also ekranoplan and Ground Effect Machine (GEM), is a high-speed low-altitude flying vehicle that utilizes a favourable ground effect. This effect appears at about one wing chord distance from the ground and results in an enhanced lift-drag ratio. As a means for transportation, WIG is positioned in the niche between ships and aircraft: speeds of WIG are much higher than those of ships, and operational expenses are much lower than those of airplanes. Another advantage of most WIG vehicles is their amphibious properties; moreover, they can take off and land on any relatively flat surface, such as land, water, snow, and ice. Military WIG craft fly below the air defence radars' zone, and are invulnerable to mine-torpedo weapons. The usage of the ground effect has also been discovered in nature: birds and flying fish spend less energy moving in the vicinity of water surfaces [8].
The most significant contribution to the progress of the WIG concept was

made in Russia by the Central Hydrofoil Design Bureau under the guidance of R.E. Alekseev, who developed a number of unique test craft (the series SM and the famous Caspian Monster KM), as well as the first serial vehicles of Orlyonok (Fig. 12.1) and Lun types. Two generations of ekranoplans were constructed and successfully tested [29]. Due to a low commercial potential of these craft designed for the Navy and a high cost of the development, large ekranoplans did not find practical application in the new economic and political situation of the last decade. At the present time, more attention is paid to the development of manually controlled small craft (Amphistar, FS8, Hoverwing, Hydrowing, TAF and Chinese craft) [3]. The ground effect, resulting in the considerable increase of the lift and the lift-drag ratio, makes the efficiencies of these WIG vehicles higher than those of the other transportation means in the speed range from 60 mph to 300 mph. The recent success of the FS8 vehicle, designed by German firm AFD [18], raises a hope that WIG craft will find their niche in the transportation system in the near future.
Unique characteristics of the WIG concept make it a suitable platform for various tasks. The use of WIG craft has been studied for rescue operations in the ocean and as a first stage in the sea-based launch of reusable aerospace planes [6] [33]. Boeing Phantom Works has recently announced a project to develop a high-capacity cargo plane using ground effect for military and commercial purposes [14].[1]

Figure 12.1: Ekranoplan Orlyonok

[1] The introduction is taken from [24]

12.2 Criterion of the static stability of WIG craft and hydrofoils

Let us the position 1 of the wing in ground effect craft is the equilibrium state. The hight of flight is h_1 and the trim angle ψ_1. Due to perturbations the trim angle increases and attains the value ψ_2 (position 2). The increase of the trim angle results in the increase of the lift what, in its turn, leads to the growth of the height of flight. The WIG runs to the new position 3 which is equilibrium state for the lift force, but not for the moment. If the moment in the position 3 is negative, the trim angle can decrease and the WIG craft is able to return to the original position 1. The WIG is statically stable, otherwise statically unstable. The criterion of the statical stability can in this case derived from these considerations.

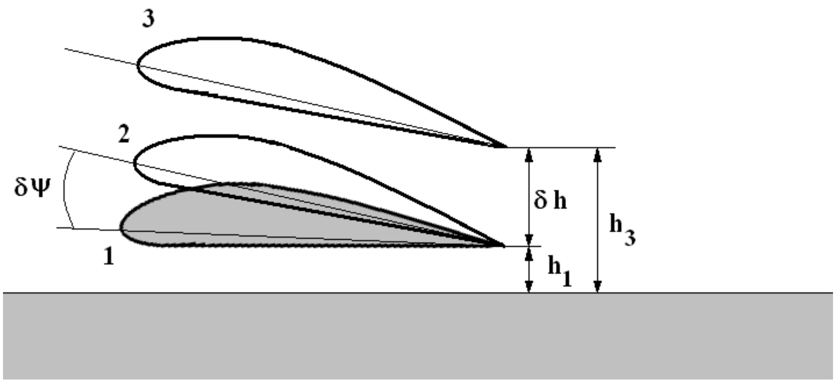

Figure 12.2: Illustration to derivation of the criterion of the WIG statical stability

Generally, the lift coefficient and the moment coefficient have the following representations neglecting nonlinear terms:

$$C_l = C_{l1} + C_l^{\psi}(\psi - \psi_1) + C_l^h(h - h_1) \tag{12.1}$$

$$m_z = m_z^{\psi}(\psi - \psi_1) + m_z^h(h - h_1) \tag{12.2}$$

where C_{l1} is the lift coefficient at the position 1. Since the position 3 is the force balance state, the force increment due to trim increase is counterbalanced by the force decrease due to growth of the height of flight

$$\begin{aligned} &C_l^{\psi}\left(\psi_2 - \psi_1\right) + C_l^h\left(h_3 - h_1\right) = 0 \\ &C_l^{\psi}\delta\psi + C_l^h\delta h = 0 \end{aligned} \tag{12.3}$$

We have to estimate the moment at the position 3. If

$$m_z^\psi \delta\psi + m_z^h \delta h < 0 \tag{12.4}$$

the WIG is statically stable. Expressing $\delta\psi$ from (12.3) $\delta\psi = -C_l^h/C_l^\psi \delta h$ and substituting into (12.4) yields the formula

$$C_l^h m_z^\psi / C_l^\psi - m_z^h > 0$$

Dividing the last formulae by C_l^h which is usually negative $C_l^h < 0$ one gets the criterion of the static stability

$$m_z^\psi / C_l^\psi - m_z^h / C_l^h < 0 \Rightarrow \frac{m_z^h}{C_l^h} > \frac{m_z^\psi}{C_l^\psi} \tag{12.5}$$

The arm of forces arising due to change of the height of flight is located in front of the arm of forces arising due to change of the trim angle:

$$X^h > X^\psi$$

The arm of forces due to h change is referred as to the aerodynamic center in height, whereas the arm due to change of the trim is referred as to the aerodynamic center in pitch. The same form has the criterion of the static stability of the hydrofoil ship.

12.3 Basic nomenclature and indices used in WIG dynamics theory

12.3.1 Basic nomenclature

$g[m/sec^2]$	- acceleration of gravity ;
$\rho[kg/m^3]$	- air density;
h_c	- non dimensional cruise flight height of air wings;
h	- non dimensional current flight height of air wings ;
ϑ_c	- cruise angle of pitch ;

ϑ	- current angle of pitch of air wings ;
$(\vartheta, \beta, \gamma, \psi)$	- angles of pitch, slip angle of roll and angle of course ;
$(\omega_x, \omega_y, \omega_z)\,[sec^{-1}]$	- angle rates;
$U[m/sec]$	- speed of motion;
$h_{cg}[m]$	- height of the center of mass;
$S[m^2]$	- area(characteristic);
$b[m]$	- AAC - averaged aerodynamic chord (characteristic linear dimension in longitudinal motion);
$l[m]$	- span(characteristic dimension in lateral motion);
ϑ_0	- adjusted angle of attack ;
$m_0[kg]$	- mass;
$(J_x, J_y, J_z, J_{xy})\,[kg \cdot m^2]$	- moments of inertia;
$\overline{x}_{cg}, \overline{y}_{cg}$	- ordinates of the center of gravity , as fraction of AAC;
$T_{b(s)}[n], n_{b(s)}, \Theta_{jb(s)}, y_{jb(s)}[m], \varepsilon_{b(s)}$	- thrust, number, installation angle, arm of thrust, mode of operation of engines of the front (b) and rear (s)

power plants;

$(\delta_e, \delta_f, \delta_r, \delta_{ai})$	- angles of deflection of elevators, flap, rudders of course, flaps-ailerons ;
$K_{\vartheta}^{\delta_e}, K_{\dot\vartheta}^{\delta_e}[s], K_h^{\delta_f}[m]$	- transfer coefficients of the system

$K_{\dot{h}}^{\delta_f}[m \cdot s], K_{\gamma}^{\delta_{ai}}, K_{\omega_x}^{\delta_{ai}},$ $K_{\psi}^{\delta_r}, K_{\psi_h}^{\delta_r}, K_{\psi_{\omega_y}}^{\delta_r}$	of automatic control
$\Delta\delta_e(t), \Delta\delta_f(t), \Delta\delta_{ai}(t), \Delta\delta_r(t)$	- perturbed deflections of control devices ;
$C_x(t), C_y(t), m_z(t),$ $C_z(t), m_x(t), m_y(t)$	- perturbations in forms of forces and moments;
$\Delta T_{b(s)}(t)$	- variation of thrust of the front (rear) engine;
$w_x(t), w_y(t), w_z(t)\,[m/s]$	- components of the speed of wind in coordinate system connected with boat;
$t[sec]$	- time;
$\dot{F}$	- dF/dt;
$x_\vartheta = {m_z}^\vartheta/{c_y}^\vartheta$	- aerodynamic center in pitch angle;
$x_h = {m_z}^h/{c_y}^h$	- aerodynamic center in height ;
C_T	- thrust coefficient of the engine ;
SAC	- system of automatic motion control;
$Fr = \frac{U_0}{\sqrt{gb}}$	- Froude number;
λ	- aspect ratio of air wing;

12.3.2 Indices

d	– course;
a	– air;
ai	– aileron($aileron$);

e – elevator ($elevator$);

r – course rudder($rudder$);

cg – center of mass;

tr – trailing edge;

cs – system of automatic control;

s – rear;

b – front;

f – flap ;

md – maximal distance ;

c – cruise regime of motion;

$nominal$ – nominal regime of operation of engines;

per – perturbation;

dec – decay ;

sm – light throttle operation of the engine;

$hydr$ – hydrodynamic;

12.3.3 Designations of dimensions

$[m]$ – meter;

$[kg]$ – kilogram ;

$[n]$ – newton ;

$[deg]$ – degree;

$[sec]$ – second;

12.4 Representation of forces in WIG aerodynamics

Classical aerodynamics is based on the representation of forces and moments in form of Taylor series. For instance the force C_y can be represented for airplanes as:

$$C_y(\alpha, t) = C_y^0(\alpha_0) + \frac{\partial C_y}{\partial \alpha}(\alpha_0)(\alpha(t) - \alpha_0) + \frac{\partial C_y}{\partial \dot{\alpha}}(\alpha_0)\frac{\dot{\alpha}(t)b}{U_a} + ... \qquad (12.6)$$

Here $\alpha = \alpha(t)$ is the angle of attack, $U_a = const$ is the relative speed, $\dot{\alpha} = \frac{d\alpha(t)}{dt}$ and b is the mean aerodynamic chord. Details can be found in any textbooks on airplane aerodynamics. This representation can formally be extended to the case of flight near the ground:

$$C_y(\alpha, h, t) = C_y^0(\alpha_0, h_0) + \frac{\partial C_y}{\partial \alpha}(\alpha_0, h_0)(\alpha(t) - \alpha_0) + \frac{\partial C_y}{\partial h}(\alpha_0, h_0)(h(t) - h_0) +$$

$$\frac{\partial C_y}{\partial \dot{\alpha}}(\alpha_0, h_0)\frac{\dot{\alpha}(t)b}{U_a} + \frac{\partial C_y}{\partial \dot{h}}(\alpha_0, h_0)\frac{\dot{h}(t)}{U_a} + ... \qquad (12.7)$$

As shown by Prof. Treshkov in the late of sixties (see, for instance, [25]) the representation (12.7) is not convenient for the ground effect aerodynamics. He proposed to replace the angle of attack α by the pitch angle ϑ. The force representation (12.7) takes the form:

$$C_y(\vartheta, h, t) = C_y(\vartheta, h) + \frac{\partial C_y}{\partial \dot{\vartheta}}(\vartheta, h)\frac{\dot{\vartheta}(t)b}{U_a} + \frac{\partial C_y}{\partial \dot{h}}(\vartheta, h)\frac{\dot{h}(t)}{U_a} + ... \qquad (12.8)$$

Using the common designation for the derivatives the last equation can be rewritten in the form:

$$C_y(\vartheta, h, t) = C_y(\vartheta, h) + C_y^{\dot{\vartheta}}\frac{\dot{\vartheta}(t)b}{U_a} + C_y^{\dot{h}}(\vartheta, h)\frac{\dot{h}(t)}{U_a} + ... \qquad (12.9)$$

12.5 WIG motion equations

12.5.1 Input data for calculation of dynamics of WIG

1. Geometric characteristics

$$S, b, l, \vartheta_0, n_{b(s)}, \Theta_{jb(s)}, Y_{b(s)}$$

2. Mass–inertial characteristics

$$m_0, J_x, J_y, J_z, J_{xy}, \overline{x}_{cg}, \overline{y}_{cg}$$

3. Characteristics of engines

$$T_{b(s)} = f\left(U, \varepsilon_{b(s)}, \varepsilon_{b(s)_0}\right)$$

For determination of speed characteristics of engines it is necessary to specify the table of speeds of motion (within expected range of motion speed); the table of regimes of operation (degree of throttling of engines). The table should be given in the range from $\varepsilon_{s.m}$ to ε_{max}, where $\varepsilon_{s.m}$ – regime of " light throttle "(usually $\varepsilon_{s.m} = 0.4$); ε_{max} – maximal regime of operation ($\varepsilon_{max} = 1.1 \div 1.2$); There exist $\varepsilon_{nominal} = 1$ and $\varepsilon_{max.dist} = \varepsilon_{md} = 0.85 \div 1.0$

4. Aerodynamic characteristics

$$(C_x, C_y, m_z, C_x^{\dot{h}}, C_x^{\dot{\vartheta}}, C_y^{\dot{h}}, C_y^{\dot{\vartheta}}, m_z^{\dot{h}}, m_z^{\dot{\vartheta}}, m_z^{\ddot{h}}, C_z^{\beta}, m_x^{\beta}, m_y^{\beta}, C_z^{\gamma}, m_x^{\gamma}, m_y^{\gamma}, C_{z'}^{\omega_x},$$

$$m_{x'}^{\omega_x}, m_{x'}^{\omega_y}, m_{y'}^{\omega_y}, C_{z'}^{\delta_{ai}}, m_{x'}^{\delta_{ai}}, m_{y'}^{\delta_{ai}}, C_{z'}^{\delta_r}, m_{x'}^{\delta_r}, m_{y'}^{\delta_r}, m_z^{\beta}) = f\left(\vartheta, h, \delta\right)$$

$$C_x, C_y, m_z = f\left(\delta_e\right)$$

Moments and forces are given in semi-connected (moving) coordinate system (differs from connected coordinate system by the angle ϑ).

5. Transfer coefficients of the system of automatic control (SAC)

$$K_{\vartheta}^{\delta_e}, K_{\dot{\vartheta}}^{\delta_e}, K_h^{\delta_f}, K_{\dot{h}}^{\delta_f}, K_{\gamma}^{\delta_{ai}}, K_{\omega_x}^{\delta_{ai}}, K_{\psi}^{\delta_h}, K_{\psi_d}^{\delta_h}, K_{\omega_y}^{\delta_h}$$

6. Perturbations

The following types of perturbations are considered:

6.1 Deflection of control devices:

$$\Delta\delta_e\left(t\right), \Delta\delta_f\left(t\right), \Delta\delta_{ai}\left(t\right), \Delta\delta_r\left(t\right)$$

6.2 Variation of thrust of engines : $\Delta T_{b(s)}\left(t\right)$

6.3 Gusts of the wind : $w_x\left(t\right), w_y\left(t\right), w_z\left(t\right)$

6.4 Drop of weight : $\Delta m[kg]$

6.5 Action of forces and moments:
$C_x\left(t\right), C_y\left(t\right), m_z\left(t\right), C_z\left(t\right), m_x\left(t\right), m_y\left(t\right)$

7. Initial conditions: $U_0, h_0, \delta_{f_0}, \beta_0, \gamma_0, \omega_{x_0}, \omega_{y_0}, \omega_{z_0}, \psi_0, U_{y_0}$ – initial regime of motion.

12.5.2 Equations of dynamics of three-dimensional motion (6DOF) of WIG

Equations, describing three-dimensional dynamics of ekranoplan, can be obtained directly from the second law of Newton and can be stated in earth fixed, speed, WIG fixed or semi-fixed coordinate system [31] (Figure 12.3).

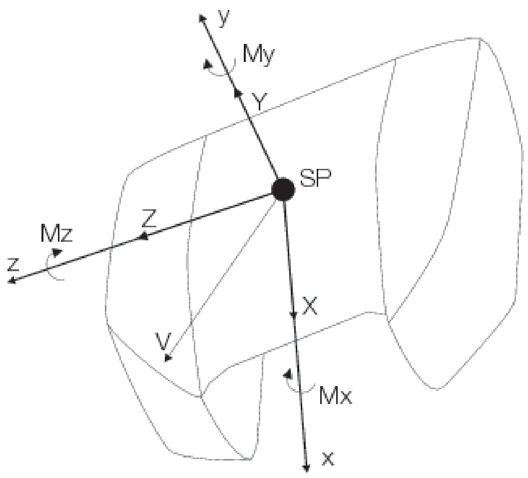

Figure 12.3: Coordinate systems

The choice of coordinate system for formulation of equation of dynamics is defined by requirements of simplicity of form and convenience in presentation of forces. Most appropriate in this sense is the semi-fixed system of coordinates. In what follows a general complete system is presented of equations of three-dimensional motion

$$\dot{U}_d = f_1 \left(T_{s_2} + T_{b_2}\right) - f_2 {U_a}^2 \left(C_x - C_z \beta_a\right) \tag{12.10}$$

$$\dot{U}_{ycg} = f_2 {U_a}^2 C_y \cos\gamma + f_1 \left(T_{b_2} \vartheta_b + T_{s_2} \vartheta_s\right) - 9.81 \tag{12.11}$$

$$\dot{\beta}_d = f_2 U_a \left(C_z + C_y \sin\gamma + C_x \beta_a\right) + \omega_y - \left(T_{b_2} + T_{s_2}\right) \beta_a \tag{12.12}$$

$$\dot{\omega}_x = f_3 {U_a}^2 \left(m_x + f_4 m_y\right) \tag{12.13}$$

$$\dot{\omega}_y = f_5 {U_a}^2 \left(m_y - f_6 m_x\right) \tag{12.14}$$

$$\dot{\omega}_z = \left(f_7 {U_a}^2 m_z - f_8 T_{b_2} - f_9 T_{s_2}\right) \tag{12.15}$$

$$\dot{h}_{cg} = U_{y_{cg}}, \dot{\gamma} = \omega_x - \omega_y \left(\vartheta - \vartheta_0\right), \dot{\psi} = \omega_y, \dot{\vartheta} = \omega_z$$

$$\beta_a = \beta_d - \frac{w_z(t)}{U_a}, U_y = U_{y_{cg}} - w_y(t), U_a = U_d + w_x(t)$$

$$\psi_d = \psi - \beta_d, h = \frac{h_{cg}}{b} - \left(1 - \overline{x}_{cg}\right) \vartheta - \overline{y}_{cg}$$

$$\vartheta_b = \vartheta + \Theta_{jb} - \vartheta_0, \vartheta_s = \vartheta + \Theta_{js} - \vartheta_0$$

$$f_1 = \frac{1}{m}, f_2 = \frac{\rho S}{2m}, f_3 = \frac{\rho S l}{2J_{xc}}, f_5 = \frac{\rho S l}{2J_{yc}}, f_7 = \frac{\rho S b}{2J_z}, f_8 = \frac{y_{jb}}{J_z}, f_9 = \frac{y_{js}}{J_z}$$

$$f_4 = \left[1 - \frac{J_{xc}}{J_{yc}}\right] \tan\left(\vartheta + \varphi_c - \vartheta_0\right), f_6 = \left[1 - \frac{J_{yc}}{J_{xc}}\right] \tan\left(\vartheta + \varphi_c - \vartheta_0\right)$$

$$\varphi_c = \frac{1}{2} \arctan\left[\frac{2J_{xy}}{J_y - J_x}\right]$$

$$J_{xc} = J_x \cos^2\varphi_c + J_y \sin^2\varphi_c - 2J_{xy} \cos\varphi_c \sin\varphi_c$$

$$J_{yc} = J_y \cos^2\varphi_c + J_x \sin^2\varphi_c - 2J_{xy} \cos\varphi_c \sin\varphi_c$$

The coefficients of aerodynamic forces can be represented as

$$C_x = C_x\left(\vartheta, h, \delta_f\right) + C_x^{\dot{\vartheta}}\left(\vartheta, h, \delta_f\right)\omega_z \frac{b}{U_a} + C_x^{\dot{h}}\left(\vartheta, h, \delta_f\right)\frac{U_y}{U_a} + C_{x_{per}}$$

$$C_y = C_y\left(\vartheta, h, \delta_f\right) + C_y^{\dot{\vartheta}}\left(\vartheta, h, \delta_f\right)\omega_z \frac{b}{U_a} + C_y^{\dot{h}}\left(\vartheta, h, \delta_f\right)\frac{U_y}{U_a} + C_{y_{per}}$$

$$\begin{gathered} C_z = \left\{\left[C_z^{\beta}\left(\vartheta, h, \delta_f\right)\beta_a + C_z^{\gamma}\left(\vartheta, h, \delta_f\right)\gamma\right] + \right. \\ \left. + 0.5U_a\left[C_z^{\omega_x}\left(\vartheta, h, \delta_f\right)\omega_x + C_z^{\omega_y}\left(\vartheta, h, \delta_f\right)\omega_y\right]\right\} + C_{z_{per}} \end{gathered}$$

$$\begin{gathered} m_x = \left\{\left[m_x^{\beta}\left(\vartheta, h, \delta_f\right)\beta_a + m_x^{\gamma}\left(\vartheta, h, \delta_f\right)\gamma\right] + \right. \\ \left. + 0.5U_a\left[m_x^{\omega_x}\left(\vartheta, h, \delta_f\right)\omega_x + m_x^{\omega_y}\left(\vartheta, h, \delta_f\right)\omega_y\right]\right\} + m_{x_{per}} \end{gathered}$$

$$\begin{gathered} m_y = \left\{\left[m_y^{\beta}\left(\vartheta, h, \delta_f\right)\beta_a + m_y^{\gamma}\left(\vartheta, h, \delta_f\right)\gamma\right] + \right. \\ \left. + 0.5U_a\left[m_y^{\omega_x}\left(\vartheta, h, \delta_f\right)\omega_x + m_y^{\omega_y}\left(\vartheta, h, \delta_f\right)\omega_y\right]\right\} + m_{y_{per}} \end{gathered}$$

$$\begin{gathered} m_z = m_z\left(\vartheta, h, \delta_f\right) + m_z^{\dot{\vartheta}}\left(\vartheta, h, \delta_f\right)\omega_z \frac{b}{U_a} + m_z^{\dot{h}}\left(\vartheta, h, \delta_f\right)\frac{U_y}{U_a} + \\ + m_z^{\ddot{h}}\left(\vartheta, h, \delta_f\right)\ddot{h}_{cg}\left[\frac{b}{U_a}\right]^2 + m_z^{\beta}\left(\vartheta, h, \delta_f\right)[\beta] + m_{z_{per}} \end{gathered}$$

Components of perturbing forces are due to wind perturbations and operation of control devices:

$$C_{x_{per}} = C_x\left(t\right) + C_x\left(\delta_e\right)$$

$$C_{y_{per}} = C_y\left(t\right) + C_y\left(\delta_e\right)$$

$$C_{z_{per}} = C_y\left(t\right) + {C_z}^{\delta_{ai}}\delta_{ai} + {C_z}^{\delta_r}\delta_r$$

$$m_{x_{per}} = m_x\left(t\right) + {m_x}^{\delta_{ai}}\delta_{ai} + {m_x}^{\delta_r}\delta_r$$

$$m_{y_{per}} = m_y\left(t\right) + {m_y}^{\delta_{ai}}\delta_{ai} + {m_y}^{\delta_r}\delta_r$$

$$m_{z_{per}} = m_z\left(t\right) + m_z\left(\delta_e\right)$$

Deflection of control surfaces in general case is determined by three components: mean deflection of control surfaces securing design regime, response of the pilot and response of the system of automatic motion control (SAC)

$$\delta_f = \delta_{f_0} + \Delta\delta_f\left(t\right) + \Delta\delta_{f_{cs}}\left(t\right)$$

$$\delta_e = \delta_{e_0} + \Delta\delta_e\left(t\right) + \Delta\delta_{e_{cs}}\left(t\right)$$

$$\delta_{ai} = \Delta\delta_{ai}\left(t\right) + \Delta\delta_{ai_{cs}}\left(t\right)$$

$$\delta_r = \Delta\delta_r\left(t\right) + \Delta\delta_{r_{cs}}\left(t\right)$$

The following law of operation of SAC is considered (PD control):

$$\delta_{f_{cs}} = -K_h^{\delta_f}\Delta h - K_{\dot{h}}^{\delta_f}\dot{h}_{cg}, \Delta h = h - h_c$$

$$\delta_{e_{cs}} = K_\vartheta^{\delta_e}\Delta\vartheta + K_{\dot{\vartheta}}^{\delta_e}\dot{\vartheta}, \Delta\vartheta = \vartheta - \vartheta_c$$

$$\delta_{ai_{cs}} = -K_\gamma^{\delta_{ai}}\gamma - K_{\omega_x}^{\delta_{ai}}\omega_x,$$

$$\delta_{r_{cs}} = -K_\psi^{\delta_r}\Delta\psi - K_{\psi_d}^{\delta_r}\Delta\psi_d + K_{\omega_y}^{\delta_r}\Delta\omega_y, \Delta\psi = \psi - \psi_0, \Delta\psi_d = \psi_d - \psi_0$$

Thrust of the engines is represented as a sum of a mean thrust and additional thrust due to work of the pilot:

$$T_{b_2} = T_b n_b + \Delta T_b\left(t\right),$$

$$T_{s_2} = T_s n_s + \Delta T_s\left(t\right),$$

The problem of determination of transfer coefficients is a separate problem. These coefficients are selected depending on aerodynamic configuration and design particulars.
It is assumed here that the efficiency of control surfaces is the same in manual and automatic modes. In case this efficiency is different the above equations are easily modified.
Thrust of the front and rear engines T_b and T_s is determined from functions $T_s\left(U,\varepsilon\right)$ and $T_b\left(U,\varepsilon\right)$ for $U = U_a$, $\varepsilon = \varepsilon_{b_0}$ and $\varepsilon = \varepsilon_{s_0}$ (so called speed characteristics). Determination of aerodynamic characteristics of air wings in semi-fixed coordinate system can be performed using the program Autowing [4]. The second derivative $m_z^{\ddot{h}}$ can be approximately assumed equal $m_z^{\dot{\alpha}}$ of horizontal tail plane.

12.5.3 Evaluation of longitudinal stability

Additional input data are derivatives of aerodynamic characteristics C_x, C_y and m_z with respect to parameters $\vartheta, h, \delta_f, \delta_e$, as well as derivatives of thrust force with respect to speed T_b^U, T_s^U.
Stability is determined through analysis of roots of characteristic equation of linearized system describing longitudinal perturbed motion.
The linearized system of longitudinal motion can be represented in the following form [36]:

$$\Delta\dot{\overline{U}} + a_{11}\Delta\overline{U} + b_{12}\Delta\dot{h} + a_{12}\Delta h + a_{13}\Delta\vartheta = 0$$

$$a_{21}\Delta\overline{U} - c_{22}\Delta\ddot{h} + b_{22}\Delta\dot{h} + a_{22}\Delta h + c_{23}\Delta\ddot{\vartheta} + b_{23}\Delta\dot{\vartheta} + a_{23}\Delta\vartheta = 0$$

$$a_{31}\Delta\overline{U} + c_{32}\Delta\ddot{h} + b_{32}\Delta\dot{h} + a_{32}\Delta h - c_{33}\Delta\ddot{\vartheta} + b_{33}\Delta\dot{\vartheta} + a_{33}\Delta\vartheta = 0$$

where

$$\Delta\overline{U} = \frac{\Delta U}{U_0}; \overline{U} = \frac{U}{U_0}; \dot{\vartheta} = \frac{b\omega_z}{U_a}; \dot{h} = \frac{U_y}{U_a}; \ddot{h} = \frac{b}{U_0}\frac{d\dot{h}}{dt}; \ddot{\vartheta} = \frac{b}{U_0}\frac{d\dot{\vartheta}}{dt}$$

The coefficients in the equation are:

$$a_{11} = 2C_W\frac{\rho_W}{\rho} - C_T^{\overline{U}}\frac{\rho_W}{\rho} + 4\frac{\rho_W}{\rho}k\left(\beta\right)\frac{b^2}{S}\widetilde{l_0}^2\vartheta_0^3 + 2c_x^0$$

$$b_{12} = \left(C_x^{\dot{h}} - 4\frac{\rho_W}{\rho}k\left(\beta\right)\frac{b^2}{S}\widetilde{l_0}^2\vartheta_0^3\right)\frac{1}{\mu}$$

$$a_{12} = C_x^h - 4\frac{\rho_W}{\rho}k\left(\beta\right)\frac{b^2}{S}\widetilde{l_0}\vartheta_0^3$$

$$a_{13} = C_x^\vartheta + 4\frac{\rho_W}{\rho}k\left(\beta\right)\left(\frac{\widetilde{l_0}}{2} - \widetilde{\xi_0}\right)\frac{b^2}{S}\widetilde{l_0}\vartheta_0^3 + 2\frac{\rho_W}{\rho}k\left(\beta\right)\widetilde{l_0^2}\frac{b^2}{S}\vartheta_0^3$$

$$a_{21} = \left(2C_y^0 + C_T^{\overline{U}}\frac{\rho_W}{\rho}\vartheta_T + \kappa\vartheta_0\right)\mu$$

$$c_{22} = 1 + \frac{1}{3}\left(2 - \cos\beta\right)\widetilde{l_0}\kappa\frac{1}{\mu}$$

$$b_{22} = C_y^{\dot{h}} - 2\kappa$$

$$a_{22} = \left(C_y^h - 2\kappa \frac{1}{\widetilde{l_0}}\right)\mu$$

$$c_{23} = -\left(2 - \cos\beta\right)\kappa \frac{\widetilde{l_0}}{3}\left(\frac{\widetilde{l_0}}{4} - \widetilde{\xi_0}\right)\frac{1}{\mu}$$

$$b_{23} = C_y^{\dot{\vartheta}} + 2\kappa\widetilde{\xi_0}$$

$$a_{23} = \left(C_y^{\vartheta} + 2\kappa\left(\frac{\widetilde{l_0}}{2} + \widetilde{\xi_0}\right)\frac{1}{\widetilde{l_0}}\right)\mu$$

$$a_{31} = \left(-\widetilde{y_T}\frac{\rho_W}{\rho}C_T^{\overline{U}} + 2\left(C_T^0\frac{\rho_W}{\rho} - 2\frac{\rho_W}{\rho}k\left(\beta\right)\left(\frac{\widetilde{l_0}}{3} - \widetilde{\xi_0}\right)\widetilde{l_0}\frac{b^2}{S}\vartheta_0^3 + \right.\right.$$
$$\left.\left. + C_W\frac{\rho_W}{\rho}\frac{S_0}{S}\left(\widetilde{\eta_0} - \widetilde{H_0}\right)\right)\right)\frac{\mu}{i_z}$$

$$c_{32} = \left(m_z^{\ddot{h}} - \frac{1}{3}\kappa\left(2 - \cos\beta\right)\left(\frac{\widetilde{l_0}}{4} - \widetilde{\xi_0}\right)\widetilde{l_0}\right)\frac{1}{\mu i_z}$$

$$b_{32} = \left(m_z^{\dot{h}} - 2\kappa\left(\frac{\widetilde{l_0}}{3} - \widetilde{\xi_0}\right)\right)\frac{1}{i_z}$$

$$a_{32} = \left(m_z^h - 2\kappa\left(\frac{\widetilde{l_0}}{2} - \widetilde{\xi_0}\right)\frac{1}{\widetilde{l_0}} + 2C_W\frac{\rho_W}{\rho}\frac{S_0}{S}\frac{\widetilde{\eta_0} - \frac{3}{2}\widetilde{H_0}}{\widetilde{H_0}}\right)\frac{\mu}{i_z}$$

$$c_{33} = 1 + \kappa\left(2 - \cos\beta\right)\frac{\widetilde{l_0}}{3}\left(\frac{\widetilde{l_0^2}}{10} - \frac{\widetilde{l_0}\widetilde{\xi_0}}{2} + \widetilde{\xi_0^2}\right)\frac{1}{\mu i_z}$$

$$b_{33} = \left(m_z^{\dot{\vartheta}} - 2\kappa\left(\frac{\widetilde{l_0^2}}{12} - \frac{\widetilde{l_0}\widetilde{\xi_0}}{3} + \widetilde{\xi_0^2}\right)\right)\frac{1}{i_z}$$

$$a_{33} = \left(m_z^{\vartheta} - \kappa\frac{\widetilde{\xi_0}}{\widetilde{l_0}} + C_x\frac{\rho_W}{\rho}\frac{S_o}{S}\frac{2\widetilde{H_0} - \widetilde{\eta_0}}{\vartheta_0}\right)\frac{\mu}{i_z}$$

$$\mu = \frac{2m_0}{\rho S b}, i_z = \frac{J_z}{mb^2}, C_{T_b}^{\overline{U}} = \frac{2T_b^U}{\rho U S}, C_{T_s}^{\overline{U}} = \frac{2T_s^U}{\rho U S}$$

$$\kappa = 2\frac{\rho_W}{\rho}k\left(\beta\right)\widetilde{l_0^2}\frac{b^2}{S}\vartheta_0^2$$

Introduce differentiation operators:

$$p = \frac{d}{dt}, p^2 = \frac{d^2}{dt^2}$$

Replacing derivatives of flight parameters p and grouping terms proportional to flight parameters, obtain the system of algebraic equations with respect to U, h, ϑ.
Determinant of this system is :

$$\begin{vmatrix} p + a_{11} & b_{12}p + a_{12} & a_{13} \\ a_{21} & -c_{22}p^2 + b_{22}p + a_{22} & c_{23}p^2 + b_{23}p + a_{23} \\ a_{31} & c_{32}p^2 + b_{32}p + a_{32} & -c_{33}p^2 + b_{33}p + a_{33} \end{vmatrix}$$

Calculating this determinant obtain characteristic equation of the system in the form:

$$D_5p^5 + D_4p^4 + D_3p^3 + D_2p^2 + D_1p + D_0 = 0$$

This equation is quintic and has 5 roots.
Necessary and sufficient conditions of stability are [36]:

$$D_i > 0, (i = 1, 2, 3, 4, 5) ; D_1D_2 - D_3 > 0;$$
$$R_5 = (D_1D_2 - D_3)(D_3D_4 - D_2D_5) - (D_1D_4 - D_5)^2 > 0$$

The boundary of dynamic (oscillatory) stability is determined by equation $R_5 = 0$, and the boundary of static (aperiodic) stability $D_5 = 0$ with other conditions of stability being fulfilled.

12.5.4 Requirements for aerodynamic design of WIG craft

From condition of static stability the difference in position of aerodynamic center in height and aerodynamic center in pitch $\Delta x = x_h - x_\vartheta$ should be positive which determines the lower bound Δx. The upper bound is determined by requirements of dynamic stability.
Stability is considerably dependent upon reciprocal position of aerodynamic centers and center of mass of the vehicle (see [24]). Consider static equations, determining design regime of motion :

$$C_y(h, \vartheta) \frac{\rho {U_0}^2}{2} S = m_0 g;$$

$$m_z(h, \vartheta) \frac{\rho {U_0}^2}{2} Sb = 0;$$

Let U,h and ϑ have small increments $\delta U, \delta h$ and $\delta\vartheta$ and suppose that the vehicle passes over to a new position close to the previous state of equilibrium. Using expansions:

$$C_y = C_y^0\,(h,\vartheta) + {C_y}^h \delta h + {C_y}^\vartheta \delta\vartheta$$

$$m_z = m_z^0\,(h,\vartheta) + {m_z}^h \delta h + {m_z}^\vartheta \delta\vartheta$$

we can obtain after some simple calculations the criterion of binding to the ground:

$$\frac{dh}{dU} = -\frac{2}{U_0}\frac{C_y^0}{{C_y}^h}\frac{x_\vartheta}{x_\vartheta - x_h}$$

For a statically stable ekranoplan the following equation is valid:

$$\mathrm{sign}\frac{dh}{dU} = -\mathrm{sign} x_\vartheta$$

When the engine thrust is increased it is required that boat be increasing the flight height. The latter is possible only if the aerodynamic center in pitch is behind the center of mass. Performing similar calculations we obtain the following criterion:

$$\frac{d\vartheta}{dU} = -\frac{2}{U_0}\frac{C_y^0}{{C_y}^\vartheta}\frac{x_h}{x_h - x_\vartheta}$$

wherefrom it follows that, if the aerodynamic center in height is located behind the center of mass, then the increase of thrust would result in decrease of pitch angle.When under action of wind the vehicle should not significantly change flight height and pitch angle. This requirement can be fulfilled if we restrict value of criterion of "binding" to the ground .
Thus, accounting for dynamic criteria we can formulate the following requirements to design of air wing configuration in cruise:

- Securing of a given C_y^0,
- Ensuring of maximal lift to drag ratio,
- Ensuring of positive difference of aerodynamic centers bounded from above,
- Aerodynamic center in pitch should be located behind the center of mass at a small distance which minimizes the criterion of binding to the ground

- Satisfaction of conditions of dynamic (oscillatory) stability, which for a small value of difference in position of aerodynamic centers can be written as follows: $D_3 D_4 - D_2 D_5 > 0$.

Detailed analysis of WIG dynamics and stability can also be found in [24].

12.6 Exercises

Investigate the static and dynamic stability of the WIG craft Seawing using the code Autowing. The results should be represented as function of the flight height and pitch angle.
The program Autowing and the file seawing10.win can be downloaded from http://www.lemos.uni-rostock.de/cfd-software/.

Bibliography

[1] [n.d.a]. *www.oceaniccorp.com* .

[2] [n.d.b]. *www.becker-marine-systems.com* .

[3] [n.d.c]. *The WIG Page, http://www.se-technology. com/* .

[4] [n.d.d]. *http://www.lemos.uni-rostock.de/cfd-software/* .

[5] Abkowitz, M. A. [1964]. Lectures on ship hydrodynamics - steering and manoeuvrability, *Hydro- and Aerodynamic Laboratory, Lyngby, Denmark, Technical Report Hy-5* .

[6] Aframeev, E. (ed.) [1998]. *Conceptual bases of WIG craft building: ideas, reality and outlooks*, RTO AVT Symposium on Fluid Dynamics Problems of Vehicles Operating Near or in the Air-Sea Interface, Amsterdam.

[7] Artjuschkov, L., Achkinadse, A. and Russetsky, A. [1988]. *Schiffsantriebe*, Sudostroenie, Leningrad, (in Russian).

[8] Belavin, N. [1977]. Ekranoplans, *Sudostroenie, Leningrad, (in Russian)* .

[9] Bertram, V. [2000]. *Practical ship hydromechanics*, Butterworth-Heinemann.

[10] Bishop, R. and Parkinson, A. [1970]. *On the planar motion mechanism used in ship model testing*, Vol. 266 of *Series A*, Phil. Transactions of the Royal Society of London, Mathematical and Physical Sciences, pp. 35–61.

[11] Brix, J. [1993]. *Manoeuvring technical manual*, Seehafen Verlag.

[12] Broglia, R., Muscari, R. and Di Mascio, A. (eds) [2008]. *Numerical simulations of the pure sway and pure yaw motion of the KVLCC-1 and KVLCC2 tankers*, Proceedings of the SIMMAN workshop, F2-F9.

[13] Carrica, P. and Stern, F. (eds) [2008]. *DES simulations of KVLCC1 in turn and zigzag manoeuvers with moving propeller and rudder*, Proceedings of the SIMMAN workshop, F10-F15.

[14] Cole, W. [2002]. The pelican: a big bird for the long haul, *Boeing Frontiers Online, http://www.boeing.com/news/frontiers/* **1**(05).

[15] Committee, M. S. [2002]. Resolution msc.137(76), *Technical report*, IMO.

[16] Cura Hochbaum, A. and Vogt, M. [2003]. Towards the simulation of seakeeping and manoeuvring based on the computation of the free surface viscous ship flow, *Twenty-Fourth Symposium on Naval Hydrodynamics*, p. 268.

[17] Fedayevsky, K. and Sobolev, G. [1963]. Control and stability in ship design, *State Union Shipbuilding Publishing House, Leningrad, USSR* .

[18] Fischer, H. and Matjasic, K. [1998]. From airfisch to hoverwing, *Workshop WISE up to ekranoplan GEMs*, The University New South Wales, pp. 69–89.

[19] Guilmineau, E., Queutey, P., Visonneau, M., Leroyer, A. and Deng, G. (eds) [2008]. *RANS simulation of a US navy frigate with PMM motions*, Proceedings of the SIMMAN workshop, F28-F33.

[20] Haase, M., Kornev, N., Bronsart, R. and Krüger, C. (eds) [2011]. *Validation of Viscous Free-Surface Flows around NPL Catamarans in Oblique Motion at Moderate Froude Number*, Proceedings of the 14th Numerical Towing Tank Symposium, Southampton.

[21] Kleinau, D. [2001]. *Theorie des Schiffes-Manuskript*, University of Rostock, (in German).

[22] Kornev, N. [2009a]. *Propellertheorie*, Shaker Verlag, (in German).

[23] Kornev, N. [2009b]. *Schiffstheorie I*, Shaker Verlag, (in German).

[24] Kornev, N. and Matveev, K. [2003]. Numerical modeling of dynamics and crashes of wing-in-ground vehicles, *AIAA Paper 2003-600* pp. 1–9. AIAA.

[25] Kornev, N. and Treshkov, V. [1992]. Numerical investigation of nonlinear unsteady aerodynamics of the wig vehicle, *Proc. Intersociety High Performance Marine Vehicle Conference, Arlington, VA, USA* pp. ws38–ws48.

[26] Korotkin, A. [2008]. Added masses of ship structures, *Springer* .

[27] Lewandowski, E. [2004]. *The dynamics of marine craft*, World scientific.

[28] Maki, K. and Wilson, W. [2008]. Steady drift force calculation on the naval destroyer hull 5415, *Proceedings of the SIMMAN workshop* pp. F34–F39.

[29] Maskalik, A., Rozhdestvensky, K. and Synitsin, D. [1998]. A view of the present state of research in aero- and hydrodynamics of ekranoplans, RTO AVT Symposium on Fluid Dynamics Problems of Vehicles Operating Near or in the Air-Sea Interface, Amsterdam.

[30] Norrbin, N. [1971]. Theory and observations on the use of a mathematical model for ship manoeuvring in deep and conned water, *Swedish State Shipbuilding Experimental Tank, Gothenburg, Technical Report 63* .

[31] Plisov, N., Rozhdestvensky, K. and Treshkov, V. [1991]. Aerohydrodynamics of ships with dynamic principles of support, *Sudostroenie, Leningrad, (in Russian)* p. 248.

[32] Schneekluth, H. [1988]. *Hydromechanik zum Schiffsentwurf*, Herford-Koehler.

[33] Tomita, N., Nebylov, A., Sokolov, V., Tsumrumaru, D., Saotome, T. and Ohkami, Y. (eds) [1996]. *Feasibility Study of Rocket Powered HTHL-SSTO with Ekranoplane as Takeoff Assist*, AIAA-96-4517.

[34] Turnock, S., Phillips, A. and Furlong, M. (eds) [2008]. *URANS simulations of static drift and dynamic manouveres of the KVLCC2 tanker*, Proceedings of the SIMMAN workshop.

[35] Voitkunsky [1985]. *Handbook of the ship theory*, (in Russian).

[36] Zhukov, V. (ed.) [1997]. *Peculiarities of the wig's aerodynamics and stability*, TSAGI Press, (in Russian).

Appendix A

Theory of irrotational flow

Definitions. If the vorticity is zero $\vec{\omega} = \nabla \times \vec{u} = 0$ and the flow is inviscid the velocity can be expressed through the gradient of the scalar function φ called the potential:

$$\vec{V} = grad\varphi = \nabla\varphi \tag{A.1}$$

In Cartesian coordinate system the velocities are:

$$V_x = \frac{\partial\varphi}{\partial x}; \quad V_y = \frac{\partial\varphi}{\partial y}; \quad V_z = \frac{\partial\varphi}{\partial z}. \tag{A.2}$$

Such flow is called as the irrational or potential flow. The potential has to satisfy the Laplace equation

$$\Delta\varphi = \frac{\partial^2\varphi}{\partial x^2} + \frac{\partial^2\varphi}{\partial y^2} + \frac{\partial^2\varphi}{\partial z^2} = 0. \tag{A.3}$$

which is derived by substitution of formulae (A.2) into the continuity equation

$$div\vec{V} = 0 \tag{A.4}$$

$$div\vec{V} = divgrad\varphi = \nabla\nabla\varphi = \Delta\varphi = 0 \Rightarrow \Delta\varphi = 0. \tag{A.5}$$

The boundary conditions for the Laplace equation (A.3) are as follows:

- no penetration on the ship surface S

$$V_n = \left.\frac{\partial\varphi}{\partial n}\right|_S = V_{n\_body}. \tag{A.6}$$

  where $\vec{n}$ is the normal vector to the ship surface S, V_{n_body} is the local normal component of the body velocity at the surface point.

- decay of perturbations far from the ship

$$\nabla\varphi \to 0 \quad when \quad R = \sqrt{x^2 + y^2 + z^2} \to \infty \tag{A.7}$$

Kinetic energy of the fluid surrounding the body. Let us consider the body with the surface S (see Fig.A.1). Ambient fluid is located between two surfaces S and $\sum$ with the radius $R = \sqrt{x^2 + y^2 + z^2}$. The fluid volume is W_∞. The case $R \to \infty$ corresponds to the unbounded flow. According to definition, the kinetic energy of the fluid is

$$E_{\mathrm{F1}} = \frac{\rho}{2} \int\limits_{W_\infty} \left[\left(\frac{\partial\varphi}{\partial x} \right)^2 + \left(\frac{\partial\varphi}{\partial y} \right)^2 + \left(\frac{\partial\varphi}{\partial z} \right)^2 \right] dW \tag{A.8}$$

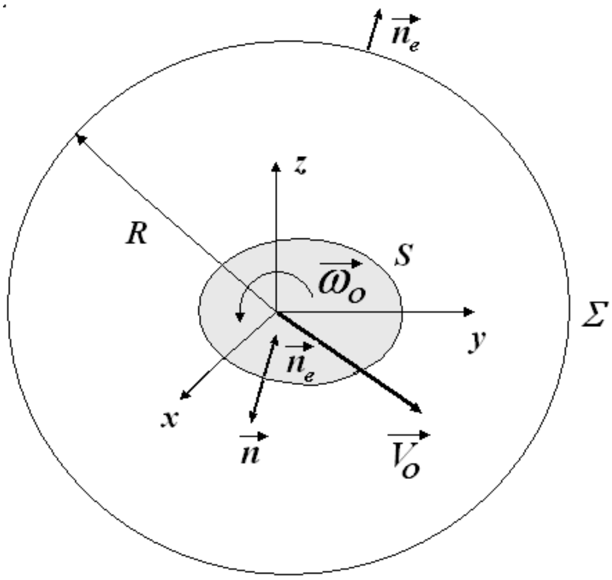

Figure A.1: Illustration to derivation of fluid energy

The sum $\left(\frac{\partial\varphi}{\partial x}\right)^2 + \left(\frac{\partial\varphi}{\partial y}\right)^2 + \left(\frac{\partial\varphi}{\partial z}\right)^2$ can be calculated using the following identities:

$$\left(\frac{\partial\varphi}{\partial x} \right)^2 = \frac{\partial}{\partial x} \left(\varphi \frac{\partial\varphi}{\partial x} \right) - \varphi \frac{\partial^2\varphi}{\partial x^2};$$
$$\left(\frac{\partial\varphi}{\partial y} \right)^2 = \frac{\partial}{\partial y} \left(\varphi \frac{\partial\varphi}{\partial y} \right) - \varphi \frac{\partial^2\varphi}{\partial y^2};$$
$$\left(\frac{\partial\varphi}{\partial z} \right)^2 = \frac{\partial}{\partial z} \left(\varphi \frac{\partial\varphi}{\partial z} \right) - \varphi \frac{\partial^2\varphi}{\partial z^2}.$$

i.e.

$$\left(\frac{\partial\varphi}{\partial x}\right)^2+\left(\frac{\partial\varphi}{\partial y}\right)^2+\left(\frac{\partial\varphi}{\partial z}\right)^2=$$
$$=\left[\frac{\partial}{\partial x}\left(\varphi\frac{\partial\varphi}{\partial x}\right)+\frac{\partial}{\partial y}\left(\varphi\frac{\partial\varphi}{\partial y}\right)+\frac{\partial}{\partial z}\left(\varphi\frac{\partial\varphi}{\partial z}\right)\right]-\varphi\left(\frac{\partial^2\varphi}{\partial x^2}+\frac{\partial^2\varphi}{\partial y^2}+\frac{\partial^2\varphi}{\partial z^2}\right). \tag{A.9}$$

The last term disappears because of the Laplace equation $\frac{\partial^2\varphi}{\partial x^2}+\frac{\partial^2\varphi}{\partial y^2}+\frac{\partial^2\varphi}{\partial z^2}=0$:

$$\left(\frac{\partial\varphi}{\partial x}\right)^2+\left(\frac{\partial\varphi}{\partial y}\right)^2+\left(\frac{\partial\varphi}{\partial z}\right)^2=\left[\frac{\partial}{\partial x}\left(\varphi\frac{\partial\varphi}{\partial x}\right)+\frac{\partial}{\partial y}\left(\varphi\frac{\partial\varphi}{\partial y}\right)+\frac{\partial}{\partial z}\left(\varphi\frac{\partial\varphi}{\partial z}\right)\right]$$

and

$$E_{\mathrm{F1}}=\frac{\rho}{2}\int\limits_{W_\infty}\left[\frac{\partial}{\partial x}\left(\varphi\frac{\partial\varphi}{\partial x}\right)+\frac{\partial}{\partial y}\left(\varphi\frac{\partial\varphi}{\partial y}\right)+\frac{\partial}{\partial z}\left(\varphi\frac{\partial\varphi}{\partial z}\right)\right]dW \tag{A.10}$$

Use of the Gauss theorem gives

$$E_{Fl}=\frac{\rho}{2}\oint\limits_{S+\sum}\left[\varphi\frac{\partial\varphi}{\partial x}\cos(n_e,x)+\varphi\frac{\partial\varphi}{\partial y}\cos(n_e,y)+\varphi\frac{\partial\varphi}{\partial z}\cos(n_e,z)\right]dS=$$
$$=\frac{\rho}{2}\oint\limits_{S}\varphi\frac{\partial\varphi}{\partial n_e}dS+\frac{\rho}{2}\oint\limits_{\sum}\varphi\frac{\partial\varphi}{\partial n_e}dS \tag{A.11}$$

where $\vec{n_e}$ is outer normal vector to the surfaces S and $\sum$, $\vec{n_e}=-\vec{n}$ (see Fig.A.1). The normal derivative of the potential is

$$\frac{\partial\varphi}{\partial n_e}=\vec{n}_e\nabla\varphi=\frac{\partial\varphi}{\partial x}\cos(n_e,x)+\frac{\partial\varphi}{\partial y}\cos(n_e,y)+\frac{\partial\varphi}{\partial z}\cos(n_e,z).$$

The second integral (in A.11) is zero because of the decay condition (A.7)

$$E_{Fl}=\frac{\rho}{2}\int\limits_{S}\varphi\frac{\partial\varphi}{\partial n_e}dS=-\frac{\rho}{2}\int\limits_{S}\varphi\frac{\partial\varphi}{\partial n}dS, \tag{A.12}$$

The no penetration condition (A.6) at a point $\vec{z}$

$$\left.\frac{\partial\varphi}{\partial n}\right|_S=V_{n\_body}=\left(\overrightarrow{V_0}+\overrightarrow{\omega_0}\times\overrightarrow{r}\right)\overrightarrow{n}, \tag{A.13}$$

with account for the identity

$$\vec{V}_0 \cdot \vec{n} + (\vec{\omega}_0 \times \vec{r}) \cdot \vec{n} = \vec{V}_0 \cdot \vec{n} + (\vec{\omega}_0 \times \vec{n}) \cdot \vec{r}$$

can be rewritten in the form

$$\begin{aligned} \left.\frac{\partial \varphi}{\partial n}\right|_S = V_{0x}\cos(n,x) + V_{0y}\cos(n,y) + V_{0z}\cos(n,z) + \\ + \omega_{0x}\left[y\cos(n,z) - z\cos(n,y)\right] + \\ + \omega_{0y}\left[z\cos(n,x) - x\cos(n,z)\right] + \\ + \omega_{0z}\left[x\cos(n,y) - y\cos(n,x)\right] \end{aligned} \tag{A.14}$$

Since the Laplace equation is linear, the solution can be sought in the form of a superposition

$$\varphi = V_{0x}\varphi_1 + V_{0y}\varphi_2 + V_{0z}\varphi_3 + \omega_{0x}\varphi_4 + \omega_{0y}\varphi_5 + \omega_{0z}\varphi_6 \tag{A.15}$$

where φ_1 are potentials of the flow when the ship is moved in i-th direction with unit speed. They depend only on coordinates and on the ship geometry. They don't depend on time. In (A.14) $V_1 = V_{0x}, V_2 = V_{0y}, V_3 = V_{0z}, V_4 = \omega_{0x}, V_5 = \omega_{0y}, V_6 = \omega_{0z}$ are components of linear and angular velocities. Substituting (A.15) into (A.14) one obtains:

$$\frac{\partial \varphi}{\partial n} = V_{0x}\frac{\partial \varphi_1}{\partial n} + V_{0y}\frac{\partial \varphi_2}{\partial n} + V_{0z}\frac{\partial \varphi_3}{\partial n} + \omega_{0x}\frac{\partial \varphi_4}{\partial n} + \omega_{0y}\frac{\partial \varphi_5}{\partial n} + \omega_{0z}\frac{\partial \varphi_6}{\partial n}$$

$$\Downarrow$$

$$\left.\begin{aligned} &\frac{\partial \varphi_1}{\partial n} = \cos(n,x); \ \frac{\partial \varphi_2}{\partial n} = \cos(n,y); \ \frac{\partial \varphi_3}{\partial n} = \cos(n,z); \\ &\frac{\partial \varphi_4}{\partial n} = y\cos(n,z) - z\cos(n,y); \\ &\frac{\partial \varphi_5}{\partial n} = z\cos(n,x) - x\cos(n,z); \\ &\frac{\partial \varphi_6}{\partial n} = x\cos(n,y) - y\cos(n,x). \end{aligned}\right\} \tag{A.16}$$

The functions φ_i satisfy the Lapalce equation $\Delta\varphi_i = 0$, decay condition $\varphi_i \to 0$ if $r \to \infty$ and no penetration conditions in corresponding form (A.16).

Using the designations $V_1 = V_{0x}, V_2 = V_{0y}, V_3 = V_{0z}, V_4 = \omega_{0x}, V_5 = \omega_{0y}$, $V_6 = \omega_{0z}$ the potential of the flow at arbitrary ship motion is written in the form

$$\varphi(x, y, z, t) = \sum_{i=1}^{6} V_i(t)\varphi_i(x, y, z) = \sum_{i=1}^{6} V_i\varphi_i. \tag{A.17}$$

Substituting (A.17) in (A.12) one obtains:

$$\frac{\partial\varphi}{\partial n} = \sum_{k=1}^{6} V_k \frac{\partial\varphi_k}{\partial n}$$

$$E_{F1} = -\frac{\rho}{2} \int\limits_S \sum_{i=1}^{6} V_i\varphi_i \sum_{k=1}^{6} V_k \frac{\partial\varphi_k}{\partial n} dS = \frac{1}{2} \sum_{i=1}^{6} \sum_{k=1}^{6} V_i V_k \left(-\rho \oint\limits_S \varphi_i \frac{\partial\varphi_k}{\partial n} dS \right). \tag{A.18}$$

The term in brackets

$$m_{ik} = -\rho \oint\limits_S \varphi_i \frac{\partial\varphi_k}{\partial n} dS \tag{A.19}$$

is called the added mass. The kinetic energy then reads

$$E_{\mathrm{Fl}} = \frac{1}{2} \sum_{i=1}^{6} \sum_{k=1}^{6} V_i V_k m_{ik} \tag{A.20}$$

The number of added mass is 36. In unbounded flows this number is reduced to 21 due to the symmetry condition

$$\oint\limits_S \varphi_i \frac{\partial\varphi_k}{\partial n} dS = \oint\limits_S \varphi_k \frac{\partial\varphi_i}{\partial n} dS \tag{A.21}$$

or

$$m_{ik} = m_{ki} \tag{A.22}$$

Appendix B

Mirror principle

If the free surface deformation is small at small Fn number the free surface can be considered as a rigid wall. If can be demonstrated using the mixed boundary condition

$$\frac{\partial^2 \varphi}{\partial t^2} + g \frac{\partial \varphi}{\partial z} = 0$$

in the nondimensional form:

$$\frac{UL}{T^2} \quad \frac{\partial^2 \tilde{\varphi}}{\partial \tilde{t}^2} + \frac{UL}{L} g \quad \frac{\partial \tilde{\varphi}}{\partial \tilde{z}} = 0 \Rightarrow \left(\frac{L}{UT} \right)^2 \quad \frac{U^2}{gL} \quad \frac{\partial^2 \tilde{\varphi}}{\partial \tilde{t}^2} + \frac{\partial \tilde{\varphi}}{\partial \tilde{z}} = 0$$

where $\tilde{\varphi} = \varphi / UL$, $\tilde{z} = z/L$, $\tilde{t} = t/T$.

Introducing the Strouhal number $Sh = \frac{L}{UT}$ and Fn number $Fn = V/\sqrt{gL}$ we obtain:

$$Sh_{\phi}^2 \quad Fn_{\phi}^2 \quad \frac{\partial^2 \tilde{\varphi}}{\partial \tilde{t}^2} + \frac{\partial \tilde{\varphi}}{\partial \tilde{z}} = 0$$

For restricted $Sh < \infty$ and small $Fn \to 0$ we get the condition

$$\frac{\partial \tilde{\varphi}}{\partial \tilde{z}} = 0$$

on the free surface.

The last equation is the no-trough condition satisfied at rigid walls in inviscid flows. This condition can easily be satisfied for plane wall using the mirror principle which is illustrated in Fig. B.1.

The flow around the cylinder alone is presented in Fig. B.1(left). If an additional cylinder is placed below at the height $y = -h$ the line $y = 0$ is then a streamline Fig. B.1(right) and can be considered as a rigid wall within the inviscid flow theory.

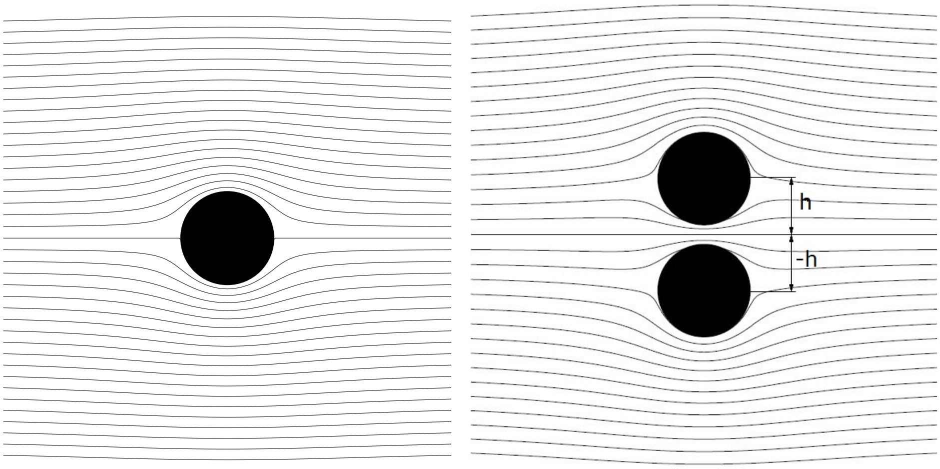

Figure B.1: Illustration of the mirror principle

Index